

**Innovative, Platy Nano-Additives as Efficient Flame
Retardants for Polymer Nanocomposites**

Dissertation

zur Erlangung des akademischen Grades eines

Doktors der Naturwissenschaften (Dr. rer. nat)

im Fach Chemie

an der Fakultät für Biologie, Chemie und Geowissenschaften

der Universität Bayreuth

vorgelegt von

Bashar Diar Bakerly

geboren in Aleppo - Syria

Bayreuth

2013

Die vorliegende Arbeit wurde in der Zeit von Oktober 2009 bis September 2013 in Bayreuth am Lehrstuhl Anorganische Chemie I unter Betreuung von Herrn Prof. Dr. Josef Breu angefertigt.

Vollständiger Abdruck der von der Fakultät für Biologie, Chemie und Geowissenschaften der Universität Bayreuth genehmigten Dissertation zur Erlangung des akademischen Grades eines Doktors der Naturwissenschaften (Dr. rer. nat.).

Dissertation eingereicht am: 08.10.2013

Zulassung durch die Prüfungskommission: 16.10.2013

Wissenschaftliches Kolloquium: 12.12.2013

Amtierender Dekan: Prof. Dr. Rhett Kempe

Prüfungsausschuss:

Prof. Dr. Josef Breu (Erstgutachter)

Prof. Dr. Andreas Greiner (Zweitgutachter)

Prof. Dr. Peter Strohriegl (Vorsitz)

Prof. Dr. Georg Papastavrou

This dissertation is dedicated to my parents

“If you are trying to achieve, there will be roadblocks. I’ve had them; everybody has had them. But obstacles don’t have to stop you. If you run into a wall, don’t turn around and give up. Figure out how to climb it, go through it, or work around it”

Michael Jordan

Contents

1. Summary – Zusammenfassung.....	1
2. Introduction	5
2.1. Polymer composite materials.....	5
2.1.1. General remarks.....	5
2.1.2. Development of fire.....	6
2.1.3. Flammability tests	7
2.1.4. Flame retardants (FRs): Mechanisms of action.....	8
2.2. Inorganic layered materials as nano-additives.....	10
2.2.1. 2:1 Layered silicates	10
2.2.2. 1:1 Layered silicates	11
2.2.3. Selective surface modification by catechols.....	12
2.2.4. Layered double hydroxides (LDHs).....	13
2.2.5. Graphite-based compounds	14
2.2.6. Combined FRs	15
3. Synopsis.....	16
3.1. Motivation.....	16
3.2. Selective modification of μ -hydroxy (gibbsite-like) surfaces	17
3.3. PS-LDH nanocomposite with enhanced flame retardancy.....	19
3.4. Combination of high aspect ratio LDH and graphene oxide	21
3.5. Combining anionic and cationic clays: ‘Trojan horse’ concept	23
4. Bibliography.....	26
5. Individual contributions to the joint publications/manuscripts	29
5.1. Appendix 1: Modification of Kaolinite by Grafting of Siderophilic Ligands to the External Octahedral Surface.....	31
5.2. Appendix 2: Significance of Aspect Ratio on Efficiency of Layered Double Hydroxide Flame Retardants	50

5.3. Appendix 3: Superior Flame Retardant by Combining High Aspect Ratio Layered Double Hydroxide and Graphene Oxide.....	70
5.4. Appendix 4: Multi-Component Flame Retardants: Combining Anionic and Cationic Clays as Trojan Horses for Molecular Flame Retardants	90
6. List of publications/manuscripts	110
6.1. Publications/manuscripts.....	110
6.2. Conferences	110
7. Acknowledgment	111
8. Declaration – Erklärung	113

Abbreviations

AEC	Anion exchange capacity
ATH	Aluminum trihydroxide
Aspect ratio	α
BET	Brunauer, Emmett, and Teller
CEC	Cation exchange capacity
DBP	3,4-dihydroxybenzophenone
DDA	1-Dodecylamine
DSC	Differential scanning calorimetry
F ⁻ -ISE	Fluoride ion selective electrode
FRs	Flame retardants
GO	Graphene oxide
Hectorite	hect
HFRs	Halogenated flame retardants
HRR	Heat release rate
IR	Infrared
LDH	Layered double hydroxide
MDH	Magnesium dihydroxide
Me	Melaminium
MMT	Montmorillonite
OS	Octahedral surface
PFRs	Phosphorus flame retardants
PHRR	Peak of heat release rate
PP	Phenyl phosphate
PS	Polystyrene
PSD	Particle size distribution
PXRD	Powder X-ray diffraction
Qu	Quercetin
SEM	Scanning electron microscope
SLs	Siderophilic ligands

Abbreviations

SLS	Static light scattering
TEM	Transmission electron microscope
THR	Total heat release
TRM	Three-roll mil
t_{ig}	Time to ignition
TISAB	Total ionic strength adjustment buffer
UV-Vis	Ultraviolet – Visible

1. Summary – Zusammenfassung

Summary

The objective of this work was to explore inorganic layered materials (nano-additives) as innovative flame retardants for polymer nanocomposites. In particular, polystyrene (PS) nanocomposites were prepared with a variety of nano-additives including layered double hydroxides (LDHs), hectorite (hect), graphite oxide (GO), or a combination of these.

The maximum flame retardant (FR) efficiency can be achieved when these nano-additives are perfectly dispersed in the polymer matrix yielding a maximum specific interface area. Good dispersion is most efficiently achieved by appropriate surface modification lowering the surface tension. Due to the unique 1:1 layered structure of kaolinite that represents two different kinds of external basal surfaces, kaolinite was used as a model to investigate selective surface modification of μ -hydroxy (gibbsite-like) surfaces. The surface modification was achieved by siderophilic ligands such as catechol derivatives. The catechol functional group (1,2-dihydroxyphenyl) forms stable chelate-complexes with the aluminum cation of the octahedral surface (OS). Modification was confirmed by bathochromic shifts of the reflection maxima of the adsorbed catechols. Furthermore, forced sedimentation measurements proved a better stability of the modified kaolinite in an organic solvent (e.g. THF). Later on, this kind of surface modification was applied to modify the structurally related materials with similar surface functionalities such as LDHs.

CO_3^{2-} -LDHs with high aspect ratio (α : 20-40) were either directly synthesized via the urea hydrolysis method at low concentration or by a two-step method including post-synthesis milling in a stirred media mill. Selective surface modification was applied using a siderophilic ligand (3,4-dihydroxybenzophenone). Consequently, suspensions of surface modified LDHs showed a better stability in THF as compared to the pristine LDH. Furthermore, surface modification restricted to the external surface diminishes the mass of the easy flammable modifier, expressly, reducing the fire load of the nano-additives.

Moreover, the intercalation of LDHs was investigated following the synthesis of anion-exchangeable NO_3^- -LDHs using a modified urea hydrolysis method. As a result, anions having FR properties such as phosphorus-containing organic anions were intercalated.

Additionally, LDHs were used in combination with other FRs such as GO to investigate possible synergism. In order to prevent heterocoagulation and to achieve stable dispersion in

an organic solvent, GO was also surface modified using 1-dodecylamine leading to a reversal of the surface charge (“Umladung”). Furthermore, the ion exchange properties of cationic/anionic clays were harnessed to design multi-component FR systems. Combinations of LDHs and hect having ions with FR properties adsorbed in the interlayer or on the external surfaces were investigated. For instance, LDH intercalated with phenyl phosphate while hectorite modified with melaminium were used to introduce an additional intumescent FR system.

In order to maximize the dispersion of nano-additives in PS, all mentioned PS nanocomposites were compounded via solution blending in THF utilizing a three-roll mill (TRM). Thereby, shear forces were sufficient to break aggregates, which were monitored by measuring the particle size distributions (PSDs).

The cone calorimeter results highlighted the importance of the aspect ratio and the interlayer anion of LDHs on flame retardancy. This was confirmed by large reductions of peak heat release rates (PHRR). Moreover, synergisms of combined systems of FRs were achieved indicated by enhanced reductions in PHRR ($\approx 50\%$) at relatively low loadings ($\approx 5\text{ wt}\%$) for both combinations LDH/hect and LDH/GO.

Zusammenfassung

Ziel dieser Arbeit war es, anorganische Schichtmaterialien (Nano-Additive) als neuartige Flammenschutzmittel für Polymeranokomposite zu erproben. Es wurden Polystyrol Nanokomposite mit einer Reihe von Nano-Additiven hergestellt, darunter schichtartige gemischtvalente Hydroxide (LDHs), Hectorit (hect), Graphitoxid (GO) und Kombinationen dieser.

Der maximale Flammschutzeffekt kann nur erzielt werden, wenn diese Nano-Additive perfekt in der Polymermatrix dispergiert sind und die spezifische Grenzfläche maximiert wird. Eine gute Dispergierung wird am besten erzielt, indem man die Oberfläche des Additivs passend modifiziert, sodass eine Reduktion der Grenzflächenspannung resultiert. Kaolinit bietet aufgrund seiner 1:1 Schichtstruktur zwei chemisch unterschiedlich beschaffene externe Basalflächen an. Es wurde daher als Modellverbindung verwendet, um die selektive Oberflächenmodifikation von μ -hydroxy (hier: gibbsitische) Flächen zu untersuchen. Siderophile Liganden, wie Catechol, die über ihre Catechol-Gruppe (1,2-dihydroxyphenyl) stabile Chelat-Komplexe mit dem Aluminiumkation der Oktaederschicht bilden, wurden erfolgreich zur Oberflächenmodifikation eingesetzt. Die Adsorption von Catecholderivaten

wurde über bathochrome Verschiebungen der Lichtabsorption der adsorbierten Liganden überprüft. Desweiteren wurde die Dispersionsstabilität in organischen Lösungsmitteln (z.B. THF) mittels Sedimentationskinetik in einer Lumifuge bestätigt. Diese Art von Oberflächenmodifikation wurde im Weiteren auf die strukturell verwandten LDHs (brucitische Flächen) übertragen.

CO₃²⁻-LDHs mit hohem Aspektverhältnis (α : 20-40) wurden einerseits direkt über die Harnstoff-Hydrolyse-Synthese bei niedriger Konzentration erhalten und andererseits über einen zweistufigen Prozess erhalten, der aus Synthese und anschließendem Mahlen in einer Rührwerkskugelmühle besteht. Erneut wurden siderophile Liganden (hier: 3,4-dihydroxybenzophenon) für die Oberflächenmodifikation herangezogen, wodurch sich wiederum die Dispersionsstabilität verbessern ließ. Diese Art von Oberflächenmodifikation ist auf die externen Oberflächen beschränkt, die im Vergleich zu den internen Oberflächen verschwindend gering sind. Dies mindert die Brandlast, die andernfalls vom Additiv zum Komposit hinzugefügt wird, wenn wie hier leicht entflammbare Modifikatoren verwendet werden.

Weiterhin wurde über eine Variation der Harnstoff-Hydrolyse-Synthese ein NO₃⁻-LDH hergestellt, mit dem ein Anionenaustausch möglich ist. Es konnten phosphorhaltige organische Anionen intercaliert werden, die selbst schon Flammenschutzqualitäten besitzen.

LDHs wurden auch mit anderen Flammenschutzmitteln wie GO kombiniert um mögliche synergistische Effekte zu untersuchen. Dabei musste Heterocoagulation der beiden Additive verhindert werden, um eine stabile Dispersion in organischen Lösungsmitteln zu erhalten. Aus diesem Grund wurde GO mit 1-Dodecylamin modifiziert, was eine Umkehr der Oberflächenladung (Umladung) zur Folge hat. Andererseits wurde die Fähigkeit zum Ionenaustausch bei kationischen und anionischen Tonmineralen dazu verwendet um Mehrkomponenten-Flammschutz-Systeme zu entwickeln. Diese Idee wurde anhand einer Kombination von LDH und hec erprobt. Ionen mit eigener Flammenschutzqualität wurden bei LDHs sowohl auf interne als auch auf externe Oberflächen adsorbiert (kompletter Ionenaustausch) und bei Hectoriten aus praktischen Gründen nur auf die externen Oberflächen. Dabei wurden LDH mit Phenylphosphat intercaliert und Hectorit mit Melaminium modifiziert um einen zusätzlichen Intumeszenzeffekt zu erreichen.

Um die Nano-Additive optimal in Polystyrol zu dispergieren, wurde „solution blending“ in THF mithilfe eines Dreiwalzwerks angewendet. Die dabei auftretenden Scherkräfte waren

ausreichend um Aggregate aufzubrechen, was über die Partikelgrößenverteilung verfolgt werden konnte.

Die Flammtests im „Cone-Calorimeter“ zeigten die besondere Rolle von Aspektverhältnis und Zwischenschichtanion der LDHs für den Flammenschutz auf, was sich an deutlichen Reduktionen des Spitzenwerts der Wärmefreisetzungsrate (Peak of Heat Release Rate; PHRR) erkennen ließ. Solch eine Reduktion des PHRR ($\approx 50\%$) konnte bei den Kombinationen LDH/hect und LDH/GO bereits bei relativ niedrigen Füllstoffgehalten ($\approx 5\%$) erreicht werden, was auf einen Synergismus der Additive hindeutet.

2. Introduction

2.1. Polymer composite materials

2.1.1. General remarks

Biopolymers were widely used by our ancestors as cotton, natural rubber and silk for thousands of years. During the last decades, however, usage of polymeric materials has been rapidly growing and polymers are now found as essential parts in almost all objects that surround us. In modern life, polymers are found everywhere in the household such as in electrical devices, furniture, clothing, and even in construction (1). In addition, polymers represent an essential component of packaging, toys, automotive, and aircraft industries. Therefore, it is not surprising that the global production of plastic is expected to increase annually by 5 % to reach approximately 300 million tons in the year 2015, with Europe being the second largest producer with 21.5 % behind China with 23.5 % (2).

Despite the unique properties of polymers, such as viscoelasticity, there are still some limitations for certain applications. Consequently, numerous studies focused on preparing polymer composite materials with enhanced mechanical and physical properties (3-7). One of the crucial limitations of polymers is their flammability, especially for aliphatic polymers that even have a higher heat of combustion as compared to the related hydrocarbons (8). Particularly, in electrical devices where cables face a high risk to get in direct contact with an electrical spark, flammability is a key issue. Generally, with the increasing mass of polymers acting as potential fire fuel in our environment, the requirements for flame retardants must become increasingly severe. In order to overcome the flammability problems, polymers are usually mixed with flame retardants (FRs). These FRs are chemicals that resist or stop the spread of fires, ideally, even prevent the ignition of fires. Thus, FRs play a key role to reduce fire risk and diminish human casualties and economic losses. For instance, the number of deaths caused by fire in 2010 was 4400 and 3120 in Europe and USA, respectively (9). The benefits of FRs can be clearly followed by the steep descent of casualties seen upon introduction of FRs which decreased by 54 % between 1990-2006 in Germany and by 66 % between 1979-2007 in USA (9). Thus, development of more fire-safe polymers represents a real need that helps reducing the fire risks and decreasing properties and human damages caused by fire.

2.1.2. Development of fire

Developing suitable FRs for certain polymer requires a detailed understanding of the fire event and the mechanism by which FRs work. Fire is considered as a complex superposition of different oxidation reactions. Therefore, it is complicated to simulate a real fire, which hampers predicting the behavior of a material under real conditions (8).

Generally, creation of fire requires heat, fuel, and oxygen. However, as a fire breaks out, it goes through different stages: i) ignition, ii) fire growth (spreading and flashover), iii) fully developed fire, and finally iv) extinguishing (Figure 1).

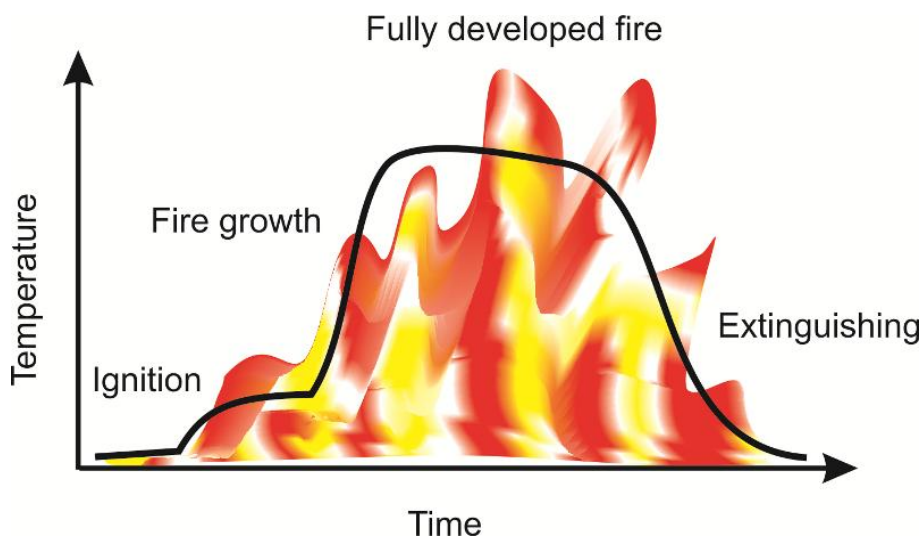


Figure 1. Stages of development of fire (adapted from (10))

Ignition occurs subsequent to the exposure to an ignition source, which could be an electrical spark or a human failure such as a dropped candle or cigarette. The ignition source increases the temperature ($\approx 350\text{ }^{\circ}\text{C}$) which eventually results in the decomposition of the material to flammable gases (pyrolysis) followed by creation of a flame. While the temperature keeps increasing (around $500\text{ }^{\circ}\text{C}$), the fire will then spread (“flashover”). The increased temperature during flashover results in igniting any possible fire fuel nearby the original fire. The maximum temperature (higher than $600\text{ }^{\circ}\text{C}$) is reached when the fire is fully developed and carries on to burn till all the fuel is consumed, hence, extinguishing will occur (11). Therefore, it is essential to characterize the fire stages and their temperatures to facilitate designing an effective FRs.

The fire danger can be divided into two subgroups, direct (heat) and indirect (toxicity, suffocation). In household fires, most of the deaths are outside of the room of fire origin, therefore, an important factor to minimize fire risk is to delay, or even to prevent, flashover (12).

2.1.3. Flammability tests

In order to explore the fire behavior of polymers while developing new FRs, several laboratory tests are available. Generally, these tests provide information about a particular fire scenario and do not simulate the situation in a real fire. Nevertheless, choosing an appropriate test is related to the standards to be matched for certain application. The commonly utilized tests are: i) underwriter's laboratories 94 (UL-94), ii) limiting oxygen index (LOI), and iii) cone calorimetry. These tests can be quickly done (few minutes), moreover, they require only samples with small/medium size, which is an advantage for FRs researchers.

For UL-94 test, a sample bar is placed vertically and its response to an ignition source is measured. According to ignition time, dripping, and extinguishing, different classification could be obtained (13). In LOI a sample bar is placed vertically in a chimney. The sample is continuously ignited in a mixture of O₂ and N₂. Then the O₂ fugacity is gradually increased until the fire no longer extinguishes. In other words, LOI is the minimum (limiting) concentration of O₂ that a flame requires to survive (14).

Cone calorimetry (Figure 2) is the most meaningful method to evaluate the flammability of polymer composite materials. It provides several data including i) time to ignition (t_{ig}), ii) burn out time, iii) heat release rate (HRR), iv) peak of heat release rate (PHRR), and v) total heat release (THR). For an ideal FR, the t_{ig} and burn out time should be increased, while the HRR, PHRR, and THR should be decreased (15). A standard plaque with dimensions of 10 cm × 10 cm × (0.3 - 0.6 cm) is required. The sample is placed horizontally on the sample holder and then it is heated by a cone heater at a certain heat flux (typically 35-50 kW/m²). Increasing surface temperature leads to the evolution of combustible gases produced by pyrolysis. By means of an electrical spark generator the released gases will ignite. The combustion products are collected in the cone hood while passing through an exhaust by a blower (15). From the reduction of oxygen concentration in the exhaust gases, the HRR can be calculated based on the oxygen consumption principle. No clear correlations between these different tests were found, in some cases, only rough correlations were proved (16).

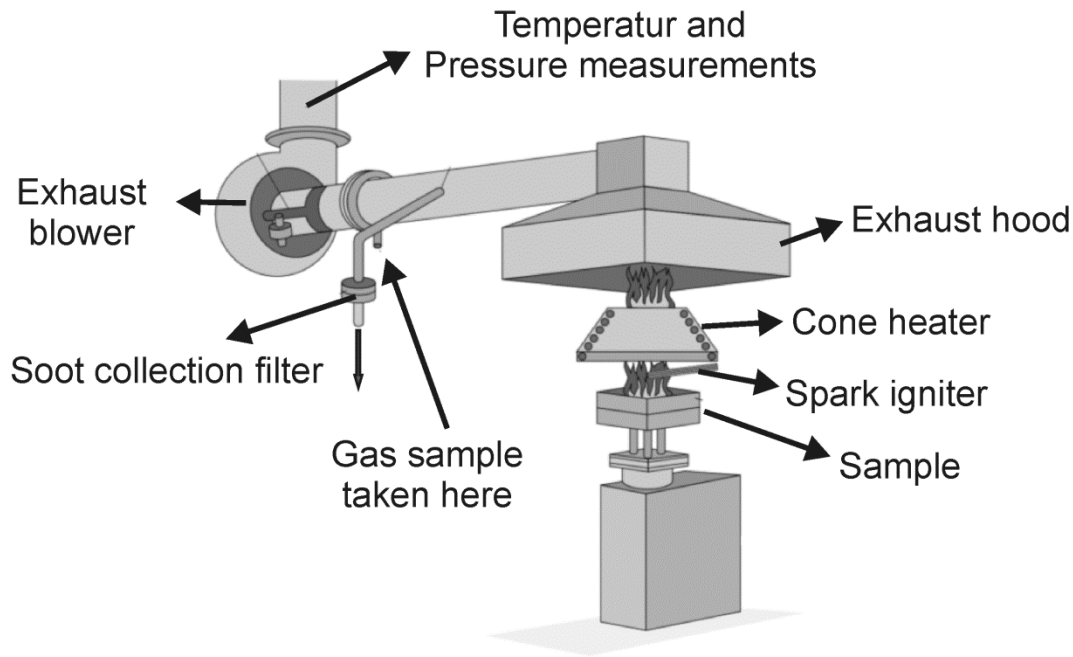


Figure 2. Schematic presentation of a cone calorimeter (17)

2.1.4. Flame retardants (FRs): Mechanisms of action

The global consumption of FRs was around 2 million tons worth 5 billion USD in 2011. The demand for FRs is expected to rise 5.4 % per year to reach 2.6 million tons in 2016 (18). A wide range of organic and inorganic compounds are commercially available as FRs (Figure 3). In the literature, there are numerous studies that describe the interaction between FRs and polymers (19,20). Generally, these interactions are classified to be physical or chemical interactions, which may take place either in the condensed phase or in the gas phase (20). Nevertheless, it is still intricate to suggest one mechanism since mostly a certain FR could introduce several interactions at the same time. The physical interactions include:

- Cooling by endothermic degradation
- Dilution of the combustible gases by inert gases
- Formation a protective layer (carbonaceous (char) or ceramic-like)

While the chemical interactions include:

- Catalysis of the degradation route of the polymer.
- Radicals scavenging.

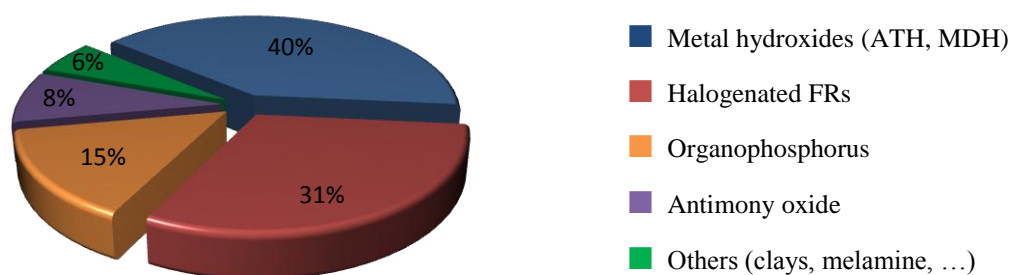


Figure 3. Global Consumption of Flame Retardants in Plastics (2011) (21)

Metal hydroxides are represented by aluminum trihydroxide (ATH) and magnesium dihydroxide (MDH). The endothermic thermal degradation of metal hydroxide is considered as the main mechanism by which they retard the fire (20). At the moment ATH is the most used commercial FR (Figure 3). High loadings (40-65 wt%) are, however, required to get sufficient flame retardancy which in turn deteriorate the physical and processing properties of the polymer. Additional limitation of utilizing ATH appears when compounding at temperatures higher than the dehydroxylation ($> 200^{\circ}\text{C}$). To overcome this problem, MDH is used (dehydroxylation around 300°C). Recently, layered double hydroxides (LDHs), which are structurally comparable to ATH and MDH, were widely investigated as an alternative FRs (22).

Halogenated FRs (HFRs) include brominated and chlorinated organic compounds such as decabromodiphenyl oxide and chlorinated paraffins. The general role of HFRs is radical quenching through interrupting the free radical oxidation chain of fire. Subsequent to degradation of halogen-rich organic compounds, HCl and HBr are released. Soon after, they react with the highly reactive radicals OH^{\cdot} and O^{\cdot} to give H_2O and the less reactive radicals Cl^{\cdot} and Br^{\cdot} . Moreover, HFRs are usually combined with other FRs such as antimony trioxide (20). Although HFRs provide sufficient flame retardancy for a wide spectrum of polymers, the main drawback is their toxicity. Due to increased concerns of environmental and humane contamination with combustion products of HFRs, such as halogenated dioxins and furans, HFRs will be eventually banned (23). Therefore, interest for alternative and halogen-free FRs has been growing.

Phosphorous FRs (PFRs) such as ammonium polyphosphate are in particular used in oxygen containing polymers such as polyurethanes. PFRs promote char formation through release of phosphoric acid that attacks the polymer chain leading to char. Furthermore, phosphoric acid acts as thermal shield and radical scavenger by the PO^{\cdot} and HPO^{\cdot} (20).

For non-charring polymers, PFRs are usually combined with nitrogenous compounds such as melamine, resulting in the formation of intumescent systems (24). In such systems, PFRs act as an acid generator while nitrogenous compounds act as blowing agent. Besides, the endothermic dissociation of melamine cools the combusted polymer (25).

2.2. Inorganic layered materials as nano-additives

The nano-additives such as cationic clays (hectorite), anionic clays (LDHs) and graphite-based compounds (graphene oxide) represent an emerging class of FRs (4,6,26). These additives are non-combustible materials and consume heat retarding the start of polymer burning (20). To prepare polymer nanocomposites with such nano-additives, the inorganic additives should be well dispersed on the nano-level in the polymer matrix. The surface tension of polymer and hydrophilic fillers are, however, quite different (27). Therefore, compounding hydrophilic additives with hydrophobic polymers is challenging. Surface modification of the additives is always essential to decrease surface tension, increase interface area, and to prevent phase segregation (26).

2.2.1. 2:1 Layered silicates

2:1 layered silicates (Figure 4) such as montmorillonite (MMT) and hectorite, consists of layers of edge-shared metal-octahedra (e.g. Mg^{2+} , Al^{3+}) sandwiched between two layers of corner-shared SiO_4 -tetrahedra. However, the isomorphous substitution of higher valent cations by lower valent cations in the octahedral layer or/and of Si^{4+} by $M(III)$ in the tetrahedral layer introduces negative charges, which are counterbalanced by interlayer cations (Na^+ , Cs^+ , Li^+ , Mg^{2+} , ...) (27). Depending on the layer charge, the type of interlayer cation, and the relative humidity, different hydration states, and accordingly, different d-spacings were reported (28). This is an important feature to tune the swellability and to switch between shear-labile and shear-stiff forms, which facilitate the fine tuning of the aspect ratio (29).

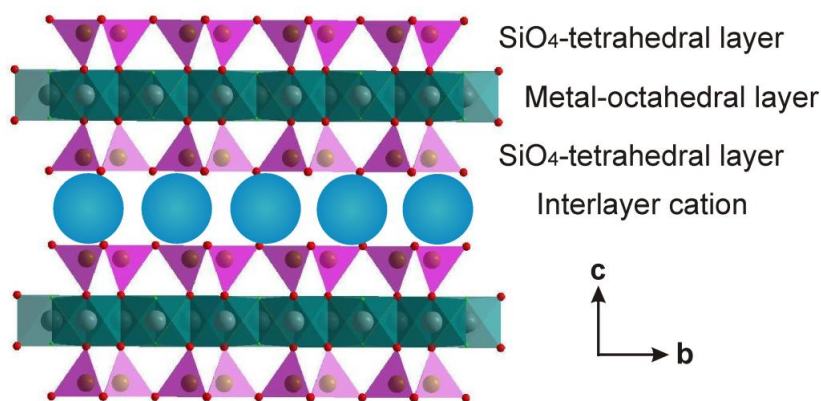


Figure 4. Structure of 2:1 layered silicates (hectorite) (30)

The basal surface of 2:1 layered silicates is presented by negatively charged oxygen atoms. In addition, edge surfaces that are resulted from defect sites are pH-dependant and correlated to the aspect ratio (31). The basal surfaces (external and internal), with permanent negative charge, are usually modified through ion exchange using cationic modifiers such as quaternary ammonium salts or polyelectrolytes (32). This was in most cases sufficient to achieve good dispersibility in the polymer. However, it also introduces a high amount of the easy flammable organics, which increase the fire load of the nano-additives.

2.2.2. 1:1 Layered silicates

The most abundant 1:1 layered silicate (Figure 5) is kaolinite [$\text{Al}_2\text{Si}_2\text{O}_5(\text{OH})_4$]. Although the structure of kaolinite is polar, usually no twinning has been observed (33). Consequently, polar basal planes dominate the external surface area which exhibit two chemically different types of external basal surfaces: i) a siloxane surface formed from the basal oxygen atoms of the tetrahedral layers of SiO_4 (tetrahedral surface, TS) and ii) a gibbsite surface formed from μ -hydroxy groups of the octahedral layers of $\text{Al}_2(\text{OH})_4$ (octahedral surface, OS) (27).

In addition, the edge surfaces of kaolinite exhibit two different kinds of hydroxyl functional groups i) silanols ($\equiv\text{Si-OH}$) and ii) aluminols ($\equiv\text{Al-OH}$), where \equiv represents the edge of the kaolinite. The degree of hydrolysis of hydroxyl groups at edges is pH-dependant, the acidity is, however, be higher as compared to the μ -hydroxyl groups at the basal surface (34).

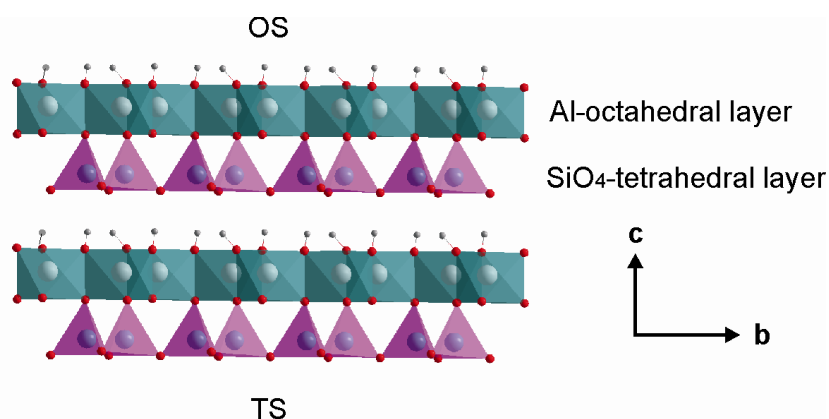


Figure 5. Structure of 1:1 layered silicates (kaolinite) (35)

Natural kaolinite, though formally neutral in charge, possesses a small cation exchange capacity (CEC) due to an isomorphous substitution of Si^{4+} by Al^{3+} in the tetrahedral layers. Therefore, it can only be counterbalanced at the outer TS by hydrated cations. The TS, can therefore be modified by simple cation exchange similar to 2:1 layered silicates. This cation exchange does not affect the non-charged OS which remains unmodified.

Selective modification of the OS by covalent grafting is more challenging as compared to TS modification. It is nevertheless required to fine-tune the so-called ``Janus-character`` of the kaolinite particles. Hence, the unique 1:1 structure of kaolinite was used as a model to selectively modifying gibbsite-like surfaces.

2.2.3. Selective surface modification by catechols

As stated before, though conventional surface treatment of nano-additives provides good dispersion, at the same time, it increases the content of flammable organic mass. Therefore, it is advantageous to find low molecular weight modifiers that are selective towards the external surfaces only. The most stable complexes of trivalent metal cations are formed by so-called siderophilic ligands (SLs) that, in the sense of the HSAB concept, are hard chelate ligands of the catechol type (36-37). Catechols having 1,2-dihydroxyphenyl functional group (Figure 6) are considered as extremely reactive compared to the related alcohol or phenols. The two ortho-hydroxyl groups are part of a larger conjugated planar π -system which increases the electron density at the coordinating oxygen atoms (Lewis base; electron donor), and hence, improves the reactivity towards metal cations (Lewis acid; electron acceptor). In addition, the distance between the two oxygen atoms in 1,2-dihydroxyphenyl group is similar to the distance ($\approx 2.8 \text{ \AA}$) between two adjacent μ -hydroxy groups located at the OS of kaolinite. Therefore, catechols are suitable candidates for modification of this type of non-charged, gibbsite-like surfaces. Furthermore, the complexation behavior of Al-cations located in the surface of a layered inorganic material was found to be similar to solution (38).

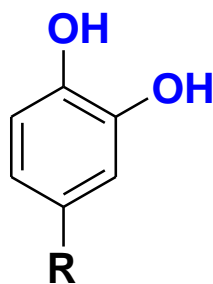


Figure 6. Chemical structure of simple catechol

It was found that catechols are selective towards the OS of kaolinite. This was achieved by adsorption of ^{31}P -labeled catechol on kaolinite followed by solid-state ^{31}P -NMR. Moreover, selective modification could be proven by secondary ion mass spectrometry (SIMS) analysis of oriented platelets (39). It was also unequivocally proven that intercalated ethylene glycol was covalently grafted to the μ -hydroxy groups by probing the chemical environment of aluminum nuclei using solid-state NMR techniques (40).

However, the external surface area (SA) is very small (typically $< 4 \text{ m}^2/\text{g}$) compared to the huge total internal area of the basal surfaces (typically over $1000 \text{ m}^2/\text{g}$) that is available for intercalates. Consequently, most sensitive analytics are required to follow adsorption purely on OS.

2.2.4. Layered double hydroxides (LDHs)

LDHs are anionic clays, also known as hydrotalcite-like compounds, that are structurally related to brucite $[\text{Mg}(\text{OH})_2]$ with edge-sharing layers of octahedrally coordinated cations (Figure 7). Partial isomorphous substitution of the divalent cation by trivalent cations in the octahedral layer renders the layers to carry a permanent positive charge. A variety of interlayer anions are possible that balance the layer charge resulting in the general formula of $[\text{M}(\text{II})_{1-x} \text{M}(\text{III})_x (\text{OH})_2]^{x+} [\text{A}^{n-}_{x/n}]^{x-} \cdot m\text{H}_2\text{O}$, where M(II) and M(III) are divalent and trivalent metal cations, respectively, A^{n-} is the charge balancing interlayer anion, while x determines the layer charge and ranges between 0.20 and 0.33 and m refers to the number of interlayer water molecules (41). A very wide spectrum of compositions, and hence properties, could be produced by tuning M(II); Mg^{2+} , Mn^{2+} , Cu^{2+} , Fe^{2+} , Co^{2+} , Ni^{2+} or Zn^{2+} , M(III); Al^{3+} , Fe^{3+} , Cr^{3+} , the M(II)/M(III) ratio and A^{n-} ; Cl^- , Br^- , NO_3^- , CO_3^{2-} , SO_4^{2-} , or even organic anions. A complex network of hydrogen bonds exists in the interlayer due to interaction between interlayer water and anions, and the hydroxyl group of the layers. Therefore, LDHs are difficult to exfoliate compared to cationic clays.

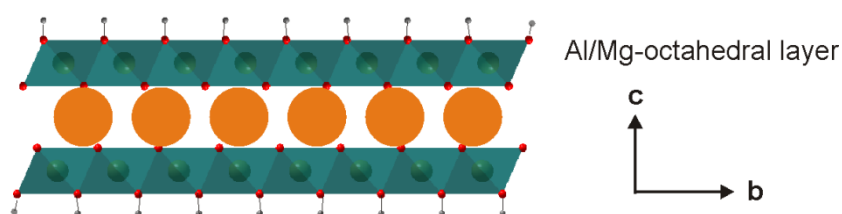


Figure 7. Structure of LDHs (42)

Depending on the required properties of LDHs such as crystallinity, particle size, aspect ratio, M(II)/M(III) ratio, and interlayer anion, various synthesis routes could be utilized for LDHs. The commonly used methods are: i) co-precipitation, ii) reconstruction, and iii) precipitation from homogeneous solution (43). The co-precipitation method includes titration of a solution of a mixed metal salt to a solution of sodium hydroxide at controlled $\text{pH} \approx 10$. This produces low aspect ratio, disordered and badly crystalline LDHs. The reconstruction method includes calcinations of LDH at 500C° followed by re-dispersion in a solution containing the desired anion which is claimed to be intercalated by a so-called “memory effect”.

This method leads to a deteriorated crystallinity, and moreover, may introduce some morphological changes. Nevertheless, for both methods a variety of interlayer anions such as Cl^- , NO_3^- or organic anions could be incorporated in the interlayer.

Contrary to co-precipitation, precipitation from homogeneous solution, also called the urea hydrolysis method, is well known to produce high charge density, well ordered, and well crystalline CO_3^{2-} containing LDHs (44). The thermally induced hydrolysis of urea increases the pH that facilitates precipitation of LDHs. Due to the high charge density and the low hydration enthalpy of carbonate, CO_3^{2-} -LDHs, however, cannot be directly anion exchanged with other organic/inorganic anions, in contrast to the Cl^- or NO_3^- containing LDHs obtained by the co-precipitation method. Few studies reported the deintercalation of CO_3^{2-} from LDH produced by the urea method, e.g. using acid/salt mixed solution (45). Recently, the urea hydrolysis method was successfully extended for the direct synthesis of well crystallized Zn/Al- NO_3^- -LDH (46).

As a result of the various possible formulations of LDHs (metal cations, interlayer anions), LDHs have a wide range of potential application such as catalyst, pharmaceuticals, photochemistry, and ion adsorption/exchange (41). LDHs were recently also investigated as FR in polymer nanocomposites. The mechanism of flame retardancy is expected to be comparable to that of ATH. Due to the endothermic degradation (dehydroxylation, decarbonation) of LDHs, they are used as heat sink additives. Moreover, released CO_2 (an inert gas; in case of CO_3^{2-} -LDHs) dilutes the volatiles. Furthermore, the residual metal oxides may act as a protective layer that separates the underlying polymer from the flame.

2.2.5. Graphite-based compounds

Graphite-based materials are different allotropes of carbon that consist of hexagonal sheets of carbon atoms. Due to their remarkable thermal and mechanical properties, these materials have a wide range of potential applications such as in batteries, pencils, and carbon fibers. Graphite-based compounds are prepared starting from graphite, for instance, by intercalation of nitric or sulfuric acid, expandable graphite is obtained. Moreover, by flash heating expandable graphite, expanded graphite can be obtained. In addition, graphite could be oxidized through e.g. the Hummers/Offeman method to graphite oxide (GO) (47). The oxidation introduces epoxy and hydroxyl functional groups at the surface and carboxyl functional groups at the edges and at defects, yielding hydrophilic GO with a considerable cation exchange capacity (≈ 500 meq/100g) (48).

Moreover, due to the interlayer cations, at low ionic strength GO can be delaminated based on osmotic swelling. Depending on the lateral extension of the pristine graphite flakes used, huge α up to 10^4 can be achieved.

2.2.6. Combined FRs

As stated previously, a synergistic effect might be achieved by combining appropriate FRs. Moreover, synergism would provide sufficient flame retardancy at much lower loadings. As a result, costs might be lowered while mechanical and processing properties of the pristine polymers may be preserved.

Combinations of graphite-based materials with different clays were reported in the literature (49-50) where compounding was mostly achieved by melt blending. However, it was proven that compounding by solution blending is more effective to achieve better dispersion qualities. Nevertheless, even with solution blending the problem of heterocoagulation (“flocculation”) of the oppositely charged platelets arises (Figure 8). To overcome this problem, at least one of the combined FRs should be neutralized or even “umgeladen”. Therefore, a proper surface modification should be applied prior to compounding to limit heterocoagulation.

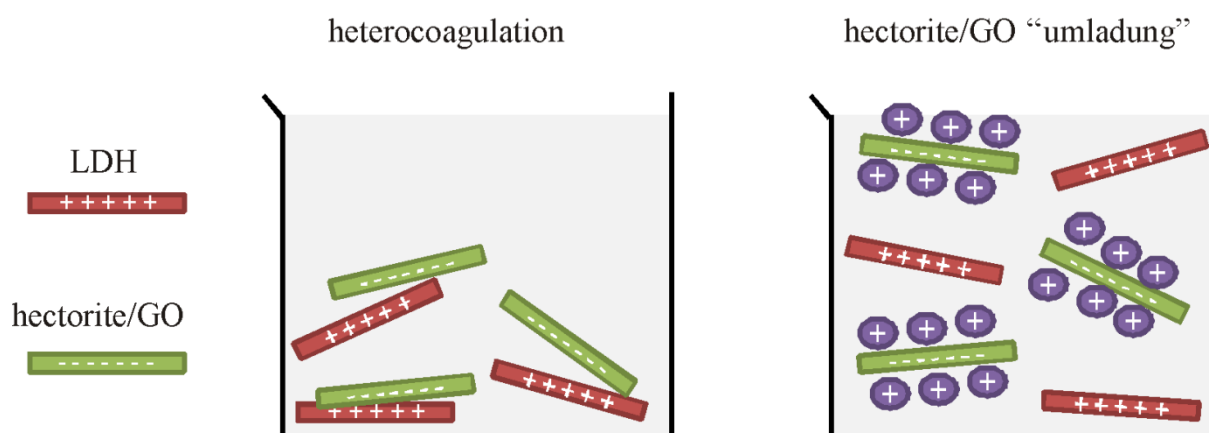


Figure 8. Schematic presentation of possible situation while mixing two additives of surface charges of opposite sign

Furthermore, by taking advantage of the ion exchange capacity of anionic (LDH) and cationic (e.g. hectorite) clays additionally molecular FRs may be incorporated rising hope for even larger synergistic effects. For instance, intercalation of organic phosphate and melamine in LDH and hectorite, respectively, may provide an additional intumescent effect. In such intumescent systems the phosphate acts as an acid generator while the melamine acts as a blowing agent (51).

3. Synopsis

3.1. Motivation

The objective of this work was the development of polymer nanocomposites with enhanced flame retardant properties. This is an urgent demand, since most of the commercially available FRs have critical limitations. For this reason, inorganic layered materials (nano-additives) including layered double hydroxides (LDHs), hectorite (hect), and graphite oxide (GO) were synthesized and tested as FRs. The key factors in achieving the maximum potential of these nano-additives are the aspect ratio (α) and the quality of dispersion in the polymer matrix. Optimization of α was established either by controlling the synthesis conditions (e.g. concentration) or by a post-synthesis milling in a ball mill. Combinations of different nano-additives were used to explore possible synergistic effects.

Selective surface modification of the nano-additives is of highest priority to decrease the surface tension with the polymer. Moreover, selective modification that is restricted to external surfaces lowers the mass of organics introduced via the nano-additives. Commonly used organic modifiers like ammonium salts are easy flammable due to Hofmann elimination reactions and increase the fire load. The selective modification was investigated on kaolinite (as a model) using siderophilic ligands.

LDHs represent a potential alternative for the structurally comparable and widely used aluminum trihydroxide FR. While the influence of α of hectorite on flame retardancy is already established, a similar correlation is expected for LDHs. This effect was systematically investigated after tailoring α of LDHs. Prior to prepare PS nanocomposites, the selective surface modification mentioned above was applied to stabilize LDH in THF.

To maximize flame retardancy, combined FR systems were established. For instance, a combination of LDH and GO was explored. The challenge was to combine these nano-additives without triggering heterocoagulation in a suspension containing both of these platelets carrying surface charges of opposite sign. This requires neutralization or even reversion (“Umladen”) of the surface charge of one of the two components, which was achieved by appropriate surface modifiers. Furthermore, a combination of LDH with hect was also explored. For this combination, the ion exchange capacities of both LDH and hect were taken in advantage to incorporate thermally stable molecular FRs. It is expected that the thermal stability and the flame retardancy of such multi-component systems will be superior.

A synergism of combined FR systems is of the highest importance, because it has the potential to assure FR requirements while preserving physical properties of the polymer and ease of processing.

3.2. Selective modification of μ -hydroxy (gibbsite-like) surfaces

Kaolinite has a unique 1:1 layered structure that represents two different kinds of external basal surfaces; octahedral surface (μ -hydroxy, OS) and tetrahedral surface (TS). Therefore, kaolinite was used as a model to investigate selective surface modification of μ -hydroxy (gibbsite-like) surfaces. Additionally, the edge surfaces of kaolinite exhibit two different kinds of hydroxy functional groups, silanols and aluminols (27). The TS, because of the permanent negative charge, may be modified through simple ion exchange using cationic modifiers, during which the non-charged OS maintains unmodified. The most stable complexes of trivalent metal ions are formed by so-called siderophilic ligands that are hard chelate ligands of the catechol type (40). Furthermore, the distance between the two oxygen atoms in 1,2-dihydroxyphenyl group ($\approx 2.8 \text{ \AA}$) is similar to the distance between two adjacent μ -hydroxy groups located at the OS of kaolinite (Figure 9). Therefore, the modification of OS of kaolinite was investigated using siderophilic ligands having 1,2-dihydroxyphenyl group such as 3,4-dihydroxybenzophenone and quercetin. The reaction time and temperature were optimized, adsorption isotherms were obtained colorimetrically, and adsorption capacities were determined.

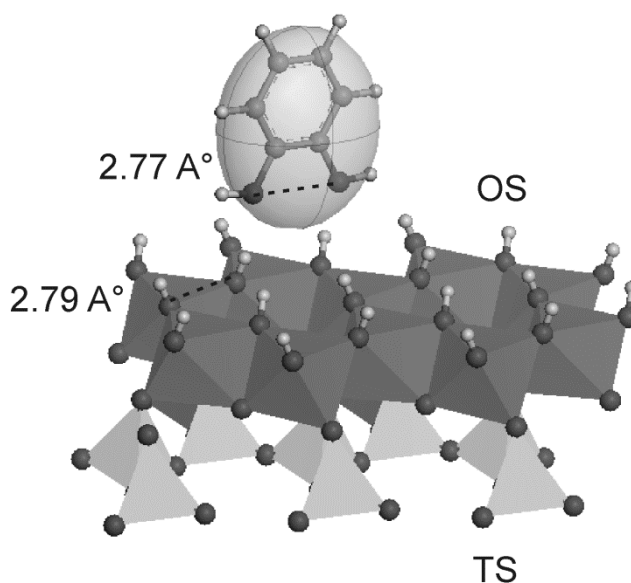


Figure 9. Kaolinite basal surface showing the perfect match between μ -hydroxy groups of the OS and the ortho-oxygen atoms of a simple catechol molecule (1,2-dihydroxybenzene).

The terminal aluminol groups at the edges are expected to be more reactive as compared to the μ -hydroxy groups at the OS and will be complexed first (34). Therefore, the adsorption of fluoride ions was applied to quantify the non- μ -hydroxy groups of the edges and derive the surface area of edges. This facilitates the estimation of the maximum adsorption capacity of edges, and hence the minimum adsorption capacity of OS. Comparing maximum adsorption capacities with edge areas as indirectly determined by ion exchange of fluoride ions, it was concluded that ligands with a 1,2-dihydroxyphenyl group are indeed capable to coordinate to the aluminol basal surface of kaolinite.

After surface modification, the PXRD patterns did not indicate any shift in the d-spacing values, confirmed that the SLs were not adsorbed on the internal surfaces (intercalated), rather they selectively modified the external surfaces. Moreover, a significant bathochromic shifts upon adsorption of the ligands was recorded that confirms the formation of a surface complex with exposed Al^{3+} . As a result of the surface modification, the hydrophilic nature of the kaolinite is rendered more hydrophobic. Consequently, the stability of suspensions of kaolinite in organic solvents is expected to improve upon modification (Figure 10).

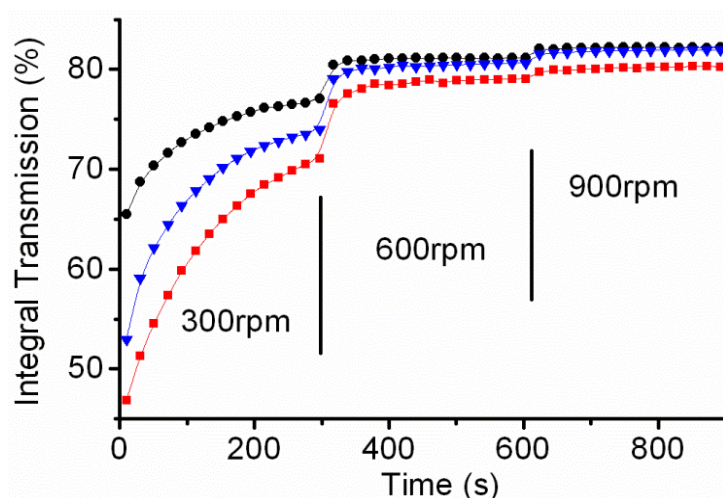


Figure 10. Sedimentation kinetics of pristine kaolinite (●) and the modified; kao-DBP (■) and kao-Qu (▼) in THF as determined by centrifugation forced sedimentation using a Lumifuge. Vertical lines indicate times when the centrifugal velocity was increased stepwise.

This kind of surface modification can be applied to organophilize kaolinite-related material (such as LDH) for the utilization as filler in polymer composite materials.

For further details and discussions please see Appendix 1: *Modification of Kaolinite by Grafting of Siderophilic Ligands to the External Octahedral Surface.*

3.3. PS-LDH nanocomposite with enhanced flame retardancy

The influence of smectites, like hectorite and montmorillonite, on the flame retardant properties of polymer nanocomposites is fairly well understood. While the crucial role of α of hectorite has been elucidated (7,26), the mechanism by which LDHs influence flame retardant properties is not yet clear. In an attempt to elucidate the mechanism of flame retardancy of LDHs, the effect of specific surface area and α of different LDHs on flame retardant properties of PS/LDH nanocomposites was systematically investigated. LDHs were synthesized by the precipitation from homogeneous solution (urea hydrolysis method), which produces well crystalline LDHs (44). Due to precipitation from a highly concentrated solution, LDHs with rose-like aggregates were obtained (Figure 11). Disaggregation of these rose-like aggregates was established by means of controlled ball milling.

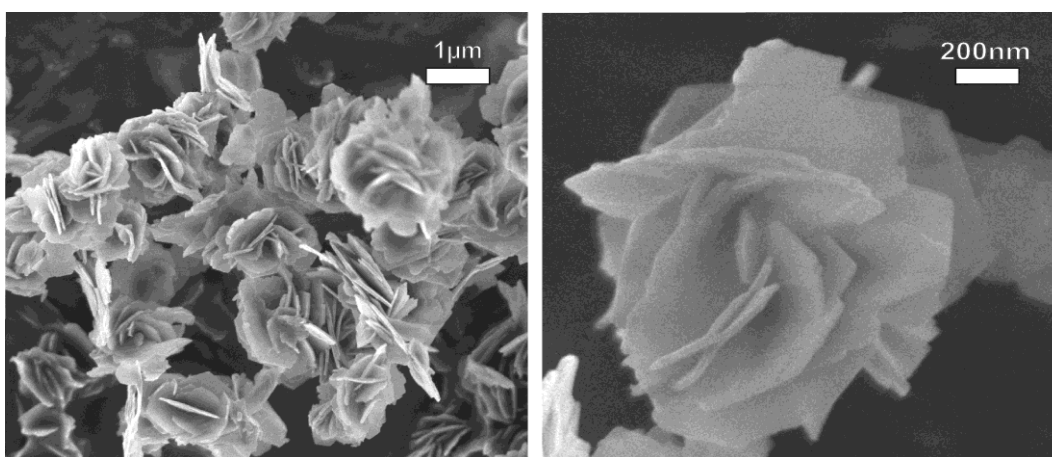


Figure 11. SEM images of LDH synthesized by the homogeneous precipitation method showing the rose-like aggregate morphology at low (left) and high (right) magnification.

LDHs are highly hydrated and cannot be dispersed effectively in hydrophobic polymer matrices without surface modification. Since we confirmed (section 3.2) the success of the selective modification of gibbsite-like surfaces using catechols, this kind of modification was applied to modify the external basal surface of LDH.

PXRD pattern proved that the surface modification was restricted to the external surfaces of LDH. This surface modification minimizes the content of the highly flammable organic mass, which could deteriorate the FR properties by increasing the fire load. The efficiency of this surface modification was confirmed by studying the sedimentation kinetics in an organic solvent (THF), where surface modified LDH showed enhanced stability as compared to pristine LDH. The modified LDHs were used to prepare PS/LDH nanocomposites.

PS/LDH nanocomposites were prepared by solution blending in a three-roll mill (Figure 12), which provides homogenization and disaggregation of LDHs by applying high shear forces of the highly viscous polymer. Afterwards, PS/LDH suspensions were dried, ground into a powder, and hot pressed to obtain plaques for cone calorimetry.



Figure 12. Photograph of the three three-roll mill utilized for compounding PS nanocomposites

Cone calorimetry (Figure 13) revealed little influence of specific surface areas but a pronounced influence of α on flame retardancy. Optimizing α yielded a significant reduction of the peak of heat release rate. Interestingly, more carbonaceous char was formed by increasing LDH loadings, which suggests that LDHs somehow promoted char formation.



Figure 13. Cone calorimeter during burning of a PS nanocomposite sample

These LDHs showed much higher FR efficiency than the widely used aluminum trihydroxide (structurally related to LDH), and therefore, they can be used as promising alternatives.

For further details and discussions please see Appendix 2: *Significance of Aspect Ratio on Efficiency of Layered Double Hydroxide Flame Retardants*.

3.4. Combination of high aspect ratio LDH and graphene oxide

We proved (section 3.3) the significance of α of LDHs on the flame retardancy of PS/LDH nanocomposites. In this work, high- α LDH and delaminated GO were combined to prepare PS/LDH/GO nanocomposites, and hence, to explore a possible synergism.

High- α LDH (Figure 14) that was directly synthesized starting from a diluted solution of metal salts is comparable to LDHs used in (section 3.3) that have been disaggregated by ball milling. Thus, much less rose-like aggregates were observed and disaggregation may indeed be avoided by modifying the synthesis concentration.

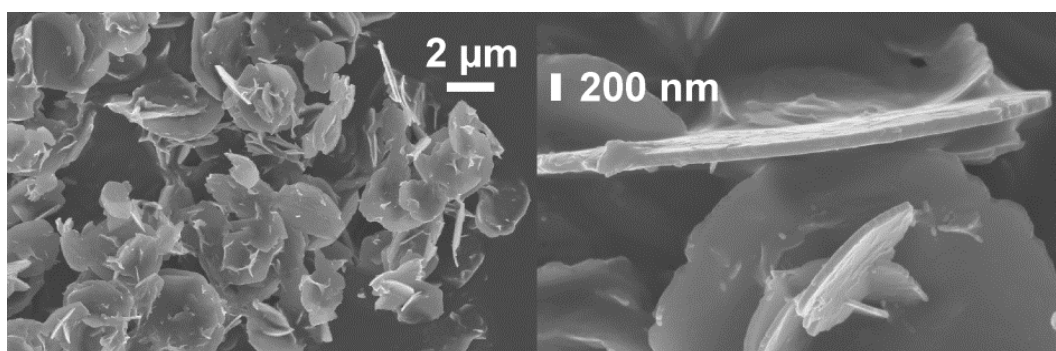


Figure 14. SEM images of high- α LDH synthesized by the urea hydrolysis method (0.05 M) at low (left) and high (right) magnification

GO was prepared by a modified Hummers/Offeman method (47). Due to the presence of interlayer cations, at low ionic strength GO was delaminated based on osmotic swelling. Combining LDH with GO in a suspension, however, is still not trivial due to surface charges of opposite sign of anionic LDH and cationic GO. As a consequence heterocoagulation will arise if failing to reverse (“Umladen”) one of the two nano-additives by appropriate surface modification. Therefore, GO, with a large cation exchange capacity, was surface modified by an ion exchange using dodecylammonium where the organic cation was adsorbed in excess of the CEC. LDH was modified using catechol (analog to the modification applied in section 3.3). Subsequent to surface modifications, stable suspensions in THF of singular and combined nano-additives were obtained.

Forced sedimentation measurements, particle size distributions, and TEM (Figure 15) confirmed the good dispersion and suggested that heterocoagulation between the two types of oppositely charged colloids could be prevented by the appropriate combination of surface modifiers. The surface charges of GO might indeed have been reversed upon surface modification. PS nanocomposites were prepared via solution blending analog to section 3.3. Cone calorimetry was used to evaluate the flame retardancy of the tested nanocomposites.

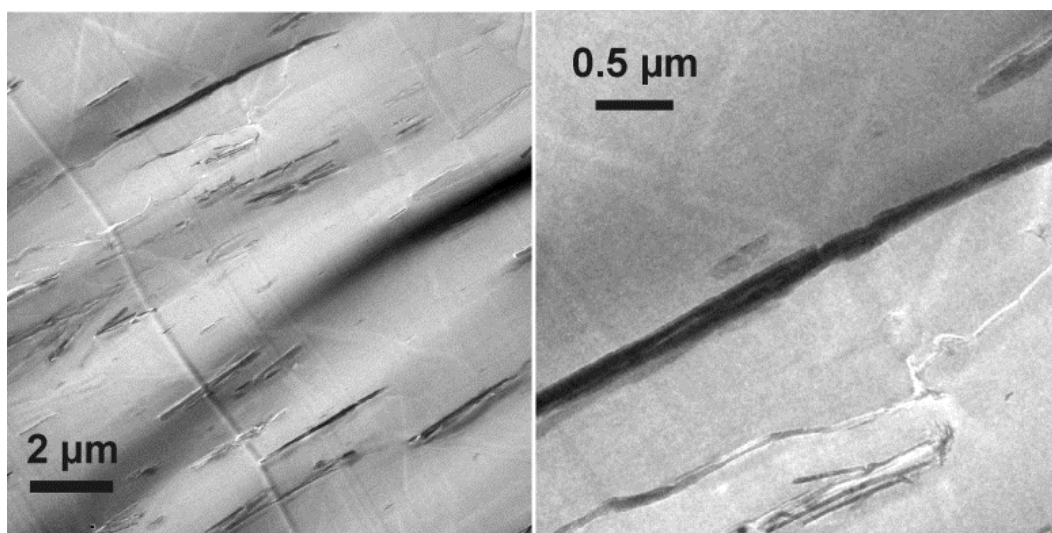


Figure 15. TEM images of PS/LDH-DBP-5wt%-GO-DDA-0.5wt% at low (left) and high (right) magnification.

Significant enhancement of flame retardancy was indicated for the PS with combined nano-additives as a result of a considerable synergism. Besides, an intumescent effect was observed for these combined nano-additives (Figure 16). More interestingly, the formation of a protective layer isolating the burning polymer from the flame led to a dramatically prolonged burn out time.



Figure 16. A PS nanocomposite with a combination of LDH and GO showing an intumescent behavior

This superior flame retardancy of this combination of nano-additives underlines the potential of utilizing LDHs with graphite-based compounds as synergistic FRs in polymer nanocomposites.

For further details and discussions please see Appendix 3: *Superior Flame Retardant by Combining High Aspect Ratio Layered Double Hydroxide and Graphene Oxide*.

3.5. Combining anionic and cationic clays: ‘Trojan horse’ concept

In the previous section (3.4), the synergism of two nano-additives (LDH/GO) was proved resulting in superior flame retardancy of PS nanocomposites. In this work, a multi-component FR system was tested using a combination of two synthetic clays; LDH and high- α K-*hect*. The intrinsic ion exchange properties of these nano-additives were employed for organophilization with thermally stable molecular FRs. LDH was synthesized by a modified urea hydrolysis method that directly produces well crystalline NO_3^- -LDHs (Figure 17, left). The LDH obtained by this route can be completely and quickly ion-exchanged. The high- α K-*hect* (Figure 17, right) was synthesized starting from Na-*hect* (29,52). The interlayer space of K-*hect* is cross-linked by the perfect fit of K-ions and therefore only the external cations can be replaced by organic cations allowing the surface tension to be modified. Thermally stable ions with FR properties were used for organophilization; LDH was intercalated with phenyl phosphate (LDH-PP) while high- α K-*hect* was organophilized with melaminium (*hect*-Me).

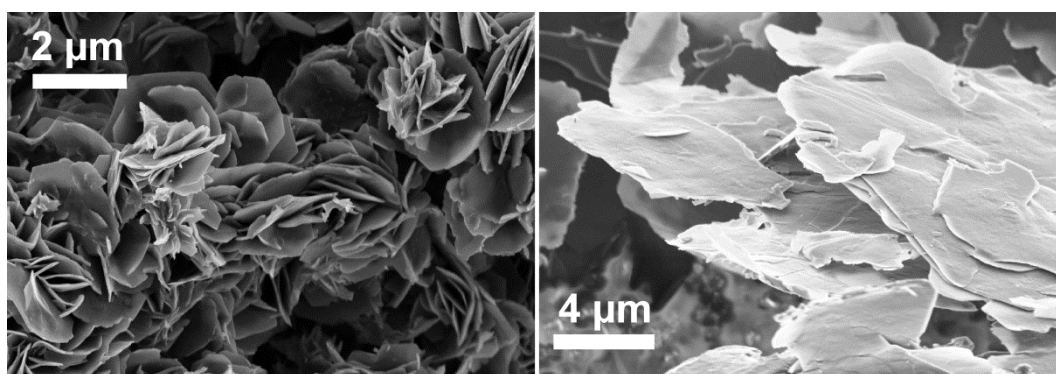


Figure 17. SEM images of (left) the directly synthesized NO_3^- -LDH by the modified urea method and (right) the milled K-*hect*

XRD patterns of the modified nano-additives confirmed that in the case of K-*hect* only the external basal surfaces were accessible, while for LDH a complete intercalation was achieved. As a consequence of this organophilization, both LDH-PP and *hect*-Me flocculated and were then centrifuged and re-suspended in THF.

Unfortunately, neither LDH-PP nor hectorite-Me formed stable suspensions in THF rather they tended to aggregate. In an attempt to nevertheless achieve the best possible dispersion of the tow clays in the PS matrix, compounding utilizing a three-roll mill was applied. This process is expected to break aggregates by providing shear forces in the highly viscose polymer dispersion. Hence, this will assist in maximizing the specific interface area between the nano-additives and the polymer to get the maximum flame retardancy. Particles size distribution measurements confirmed that for both PS/LDH-PP and PS/hect-Me, three-roll mill provided sufficient shear forces to establish a decent dispersion of theses clays in the PS matrix. For PS/LDH-PP/hect-Me, additional aggregation is actually expected because the two types of clay have surface charges of opposite sign and heterocoagulation will be triggered. However, a large portion of the aggregates were destroyed upon mechanical agitation as indicated by a shift of the maxima of Particles size distribution (Figure 18). TEM images confirmed, despite the aggregation, that the nano-additives are homogeneously distributed in the polymer matrix. Samples for cone calorimetry were prepared analog to section 3.3. Moreover, thermal stabilities of the nanocomposites were explored by a thermogravimetric analysis.

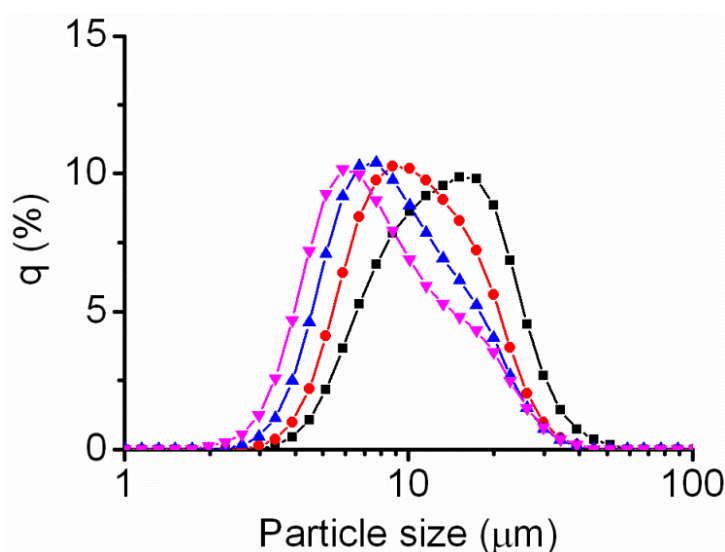


Figure 18. Particle size distributions of PS/LDH-PP/hect-Me after increasing number of cycles of three-roll milling (■) 0 (●) 2 (▲) 4, and (▼) 6. All measurements were done in THF suspension.

For all PS nanocomposites, superior enhancements of thermal stabilities were recorded as indicated by a significant shift in the $T_{0.5}$. We suggest that the thermally stable modifiers, Me and PP passed on their thermal stability to the nanocomposites.

Cone calorimetry recorded a maximum reduction of PHRR for PS/LDH-PP/hect-Me, which was significantly higher than reductions achieved by a singular nano-additive (Figure 19).

This corroborates a synergistic effect which may be explained by the intumescent effect as resulting from the combination of the two organic modifiers; Me and PP. The intumescent type of FR was corroborated a comparison of the photographs of the residues. Interestingly, the lowest THR was recorded for PS/hect-Me.

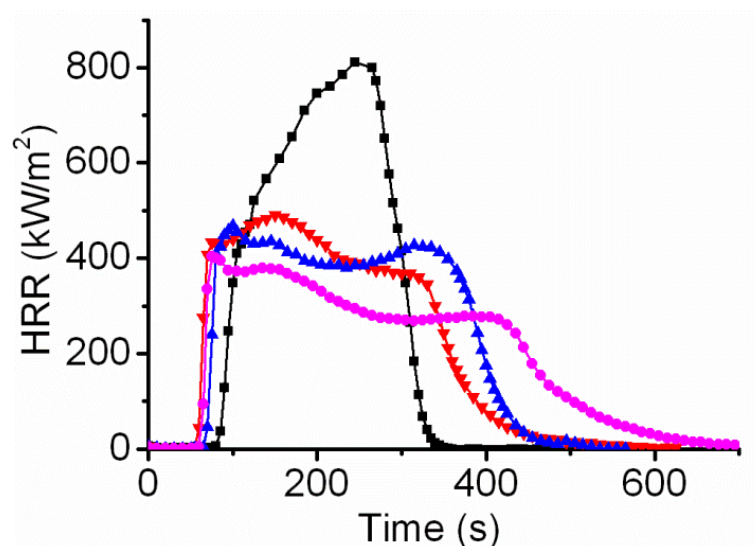


Figure 19. Heat release rate curves for PS nanocomposites with (■) PS (▲) LDH-PP (▼) hect-Me and (●) LDH-PP/hect-Me.

The reduction of THR could be explained by promotion of char formation by the hectorite that lead to an incomplete combustion of the polymer and the conversion of a portion of the polymer to residual char.

For further details and discussions please see Appendix 4: *Multi-Component Flame Retardants: Combining Anionic and Cationic Clays as Trojan Horses for Molecular Flame Retardants.*

4. Bibliography

1. www.polyplastics.com/en/pavilion/life/index_t.html, **6/2013**
2. www.studymode.com/essays/Global-Plastics-Industry-139-4013.html, **7/2013**
3. Fischer, B.; Ziadeh, M.; Pfaff, A.; Breu, J.; Altstädt, V. *Polymer*, **2012**, *53*, 3230-3237.
4. Dittrich, B.; Wartig, K. A.; Hofmann, D.; Mülhaupt, R.; Schartel, B. *Polymer Degradation and Stability*, **2013**, *98*, 1495-1505.
5. Kotal, M.; Srivastava, S. K.; Bhowmick, A. K.; Chakraborty, S. K. *Polymer International*, **2011**, *60*, 772-780.
6. Nyambo, C.; Songtipya, P.; Manias, E.; Jimenez-Gasco, M. M.; Wilkie, C. A. *Journal of Materials Chemistry*, **2008**, *18*, 4827-4838.
7. Schütz, M. R.; Kalo, H.; Lunkenbein, T.; Groschel, A. H.; Muller, A. H. E.; Wilkie, C. A.; Breu, J. *Journal of Materials Chemistry*, **2011**, *21*, 12110-12116.
8. Edward, D. W.; Sergei, V. L. Flame Retardants in Commercial Use or Development for Polyolefins, in *Flame Retardants for Plastics and Textiles*, Carl Hanser Verlag GmbH & Co. KG: Munich, **2009**; pp. 3-34.
9. Fire Death Rate Trend: An International Perspective, Topical Fire Report Series, FEMA, **2011**, *12*, 1-8
10. Schartel, B.; Hull, T. R. *Fire and Materials*, **2007**, *31*, 327-354.
11. http://www.nist.gov/fire/fire_behavior.cfm, **5/2013**
12. Gordon, L. N.; Alexander, B. M.; Charles, A. W. Fire Retardancy in 2012, in *Fire and Polymers VI: New Advances in Flame Retardant Chemistry and Science*, American Chemical Society: Washington, DC, **2012**; pp. 1-13.
13. www.boedeker.com/bpi-ul94.htm, **7/2013**
14. Edward, D. W.; Sergei, V. L. Comments on Flammability and Smoke Tests, in *Flame Retardants for Plastics and Textiles*, Carl Hanser Verlag GmbH & Co. KG: Munich, **2009**; pp. 227-240.
15. Babrauskas, V. *Fire and Materials*, **1984**, *8*, 81-95.
16. Morgan, A. B.; Bundy, M. *Fire and Materials*, **2007**, *31*, 257-283.
17. Beyer, G. *Plastics, Additives and Compounding*, **2002**, *4*, 22-28.
18. www.giiresearch.com/press/7717.shtml, **6/2013**

19. Gilman, J. W. Flame Retardant Mechanism of Polymer – Clay Nanocomposites, in *Flame Retardant Polymer Nanocomposites*, John Wiley & Sons, Inc.: Hoboken, NJ, **2007**; pp. 67-87.
20. Edward, D. W.; Sergei, V. L. Overview of Modes of Action and Interaction of Flame Retardants, in *Flame Retardants for Plastics and Textiles*, Carl Hanser Verlag GmbH & Co. KG: Munich, **2009**; pp. 241-251.
21. www.townsend-solutions.com/-Townsend_Published_Reports.html, **7/2013**
22. Chen, W.; Qu, B. *Journal of Materials Chemistry*, **2004**, *14*, 1705-1710.
23. Birnbaum, L. S.; Staskal, D. F. *Environmental Health Perspectives*, **2003**, *112*, 9-17.
24. Bourbigot, S.; Le Bras, M.; Duquesne, S.; Rochery, M. *Macromolecular Materials and Engineering*, **2004**, *289*, 485.
25. Weil, E. D.; Choudhary, V. *Journal of Fire Sciences*, **1995**, *13*, 104-126.
26. Schütz, M. R.; Kalo, H.; Lunkenbein, T.; Breu, J.; Wilkie, C. A. *Polymer*, **2011**, *52*, 3288-3294.
27. Brigatti, M. F.; Galan, E.; Theng, B. K. G. Chapter 2 Structures and Mineralogy of Clay Minerals, in *Developments in Clay Science Handbook of Clay Science*, Volume 1 ed.; Faiza Bergaya, B. K. G., editor; Elsevier: Amsterdam, **2006**; pp. 19-86.
28. Morodome, S.; Kawamura, K. *Clays and Clay Minerals*, **2011**, *59*, 165-175.
29. Ziadeh, M.; Chwalka, B.; Kalo, H.; Schütz, M. R.; Breu, J. *Clay Minerals*, **2012**, *47*, 341-353.
30. Breu, J.; Seidl, W.; Stoll, A. *Zeitschrift für anorganische und allgemeine Chemie*, **2003**, *629*, 503-515.
31. Schoonheydt, R. A.; Johnston, C. T. Chapter 3 Surface and Interface Chemistry of Clay Minerals, in *Developments in Clay Science Handbook of Clay Science*, Faiza Bergaya, B. K. G., editor; Elsevier: Amsterdam, **2006**; pp. 87-113.
32. Mittal, V. *Applied Clay Science*, **2012**, *56*, 103-109.
33. Kogure, T.; Elzea-Kogel, J.; Johnston, C. T.; Bish, D. L. *Clays and Clay Minerals*, **2010**, *58*, 62-71.
34. Weiss, A.; Mehler, A.; Koch, G.; Hofmann, U. *Zeitschrift für norganische und allgemeine Chemie*, **1956**, *284*, 247-271.
35. Bish, D. L. *Clays and Clay Minerals*, **1993**, *41*, 738-744.

36. Golounin, A. V.; Shchedrin, Y.; Fedorov, V. A. *Russian Journal of Organic Chemistry*, **2001**, *37*, 1266-1269.
37. Sedo, J.; Saiz-Poseu, J.; Busque, F.; Ruiz-Molina, D. *Advanced Materials*, **2013**, *25*, 792.
38. Kummert, R.; Stumm, W. *Journal of Colloid and Interface Science*, **1980**, *75*, 373-385.
39. Hirsemann, D.; Shylesh, S.; De Souza, R. A.; Diar-Bakerly, B.; Biersack, B.; Müller, D. N.; Martin, M.; Schobert, R.; Breu, J. *Angewandte Chemie International Edition*, **2011**, *51*, 1348-1352.
40. Hirsemann, D.; Köster, T. K. J.; Wack, J.; van Wüllen, L.; Breu, J.; Senker, J. *Chemistry of Materials*, **2011**, *23*, 3152-3158.
41. Evans, D.; Slade, R. Structural Aspects of Layered Double Hydroxides, in *Layered Double Hydroxides*, Duan, X.; Evans, D., editors; Springer: Berlin, **2006**; pp. 1-87.
42. Nagai, T.; Hattori, T.; Yamanaka, T. *American Mineralogist*, **2000**, *85*, 760-764.
43. Chibwe, M.; Valim, J. B.; Jones, W. The Synthesis, Characteristics and Applications of Layered Double Hydroxides, in *Multifunctional Mesoporous Inorganic Solids*, Sequeira, C.; Hudson, M., editors; Springer: Netherlands: **1993**; pp. 191-206.
44. Costantino, U.; Marmottini, F.; Nocchetti, M.; Vivani, R. *European Journal of Inorganic Chemistry*, **1998**, *1998*, 1439-1446.
45. Iyi, N.; Sasaki, T. *Journal of Colloid and Interface Science*, **2008**, *322*, 237-245.
46. Inayat, A.; Klumpp, M.; Schwieger, W. *Applied Clay Science*, **2011**, *51*, 452-459.
47. Hummers, W. S.; Offeman, R. E. *Journal of the American Chemical Society*, **1958**, *80*, 1339.
48. Hofmann, U.; Holst, R. *Berichte der deutschen chemischen Gesellschaft (A and B Series)*, **1939**, *72*, 754-771.
49. Gao, F.; Beyer, G.; Yuan, Q. *Polymer Degradation and Stability*, **2005**, *89*, 559-564.
50. Han, Y.; Wu, Y.; Shen, M.; Huang, X.; Zhu, J.; Zhang, X. *Journal of Materials Science*, **2013**, *48*, 4214-4222.
51. Bourbigot, S.; Duquesne, S. *Journal of Materials Chemistry*, **2007**, *17*, 2283-2300.
52. Kalo, H.; Müller, M. W.; Ziadeh, M.; Dolejs, D.; Breu, *Applied Clay Science*, **2010**, *48*, 39-45.

5. Individual contributions to the joint publications/manuscripts

The publications/manuscripts were obtained in cooperation with other co-workers at different departments. My contributions to each publication are specified below and the asterisk denotes the corresponding author.

Appendix 1:

This work was submitted to Applied Clay Science under the title “**Modification of Kaolinite by Grafting of Siderophilic Ligands to the External Octahedral Surface**”. By Bashar Diar-Bakerly, Dunja Hirsemann, Hussein Kalo, Rainer Schobert, Josef Breu* .

- I performed the modification and characterization of kaolinite, F⁻ potentiometric titration, in addition to writing the manuscript.
- Dr. Dunja Hirsemann and Dr. Hussein Kalo assisted by establishing CPK-models of the surface modification.
- Prof. Dr. Rainer Schobert contributed to the scientific discussion about the surface modifier.
- Prof. Josef Breu contributed to proofreading the manuscript and the scientific discussion.

My contribution to this work was ca. 80%.

Appendix 2:

This work was published in American Chemical Society (DOI: 10.1021/bk-2012-1118.ch026) under the title “**Significance of Aspect Ratio on Efficiency of Layered Double Hydroxide Flame Retardants**”. By Bashar Diar-Bakerly, Günter Beyer, Rainer Schobert, Josef Breu* .

- I performed the synthesis, milling and modification of LDH, preparation of PS nano-composites, in addition to writing the manuscript.
- Dr. Günter Beyer performed the cone calorimetry measurements and contributed to the scientific discussion.
- Prof. Rainer Schobert contributed to the scientific discussion regarding the modifier.
- Prof. Josef Breu contributed to proofreading the manuscript and the scientific discussion.

My contribution to this work was ca. 85%.

Appendix 3:

This work will be submitted to Polymer under the title “**Superior Flame Retardant by Combining High Aspect Ratio Layered Double Hydroxide and Graphene Oxide**”. By Bashar Diar-Bakerly, Patrick Feicht, Andreas Edenharter, Günter Beyer, Josef Breu^{*}

- I performed the synthesis of LDH, preparation of PS nanocomposites, in addition to writing the manuscript.
- Patrick Feicht synthesized and modified graphite oxide, helped by compounding, and also contributed to the scientific discussion.
- Andreas Edenharter helped by compounding and proofreading the manuscript.
- Dr. Günter Beyer performed the cone calorimetry measurements and contributed to the scientific discussion.
- Prof. Josef Breu contributed to proofreading the manuscript and the scientific discussion.

My contribution to this work was ca. 50%.

Appendix 4:

This work will be submitted to Polymer under the title “**Multi-Component Flame Retardants: Combining Anionic and Cationic Clays as Trojan Horses for Molecular Flame Retardants**”. By Bashar Diar-Bakerly, Josef Hausner, Hussein Kalo, Andreas Edenharter, Mazen Ziadeh, Günter Beyer, Josef Breu^{*}

- I performed the synthesis and intercalation of LDH, preparation of PS nanocomposites, in addition to writing the manuscript.
- Josef Hausner modified the hectorite, helped by compounding, and also contributed to the scientific discussion.
- Dr. Hussein Kalo provided the Na-hectorite.
- Andreas Edenharter helped by compounding and proofreading the manuscript.
- Mazen Ziadeh helped by milling and proofreading the manuscript.
- Dr. Günter Beyer performed the cone calorimetry measurements and contributed to the scientific discussion.
- Prof. Josef Breu contributed to proofreading the manuscript and the scientific discussion.

My contribution to this work was ca. 60%

5.1. Appendix 1: Modification of Kaolinite by Grafting of Siderophilic Ligands to the External Octahedral Surface

Bashar Diar-Bakerly¹, Dunja Hirsemann¹, Hussein Kalo¹, Rainer Schobert², Josef Breu^{1,*}

¹) Department of Inorganic Chemistry I, University of Bayreuth, Universitaetsstr. 30, 95447 Bayreuth, Germany

²) Department of Organic Chemistry I, University of Bayreuth, Universitaetsstr. 30, 95447 Bayreuth, Germany

Corresponding author: Prof. Dr. Josef Breu, Universitaetsstr. 30, 95440 Bayreuth, Germany

* E-mail: josef.breu@uni-bayreuth.de

Abstract

The modification of the external octahedral surface of kaolinite was investigated using two siderophilic ligands (SLs): 3,4-dihydroxybenzophenone (DBP) and quercetin (Qu). These SLs have a 1,2-dihydroxyphenyl group that forms chelate-complexes with aluminum cations. Adsorption isotherms were obtained colorimetrically. PXRD patterns proved that the adsorption was attributed only to the external surfaces. Furthermore, adsorption of fluoride ions was applied to quantify the non- μ -hydroxy groups of the edges and derive the surface area of edges.

Comparing maximum adsorption capacities with surface area of edges, it can be safely concluded that SLs are indeed capable to coordinate to the aluminol basal surface of kaolinite. This conclusion is corroborated by significant bathochromic shifts upon adsorption of the ligands that indicate the formation of a surface complex with exposed Al^{3+} . Thus, even small amounts of adsorbed SLs changed the surface tension of kaolinite significantly. Consequently, forced sedimentation experiments showed the modified kaolinite to be rendered hydrophobic enough to form stable suspensions in organic solvents fostering preparation of polymer composite materials.

Keywords: kaolinite; catechol; surface modification; fluoride adsorption; surface-complex.

1. Introduction

Kaolinite [$\text{Al}_2\text{Si}_2\text{O}_5(\text{OH})_4$] is the main component of the wide spread rock kaolin and thus is an abundant, ubiquitous, and inexpensive (200 €/tonne) mineral. Although the structure of the

dioctahedral 1:1 layered silicate is polar, usually no twinning has been observed (Kogure et al., 2010). Kaolinite is found as strongly anisometric platelets with large aspect ratios that are typically in the range of 10-40. Consequently, polar basal planes dominate the external surface area which exhibit two chemically different types of external basal surfaces i) a siloxane surface formed by basal oxygen atoms of the tetrahedral layers of SiO_4 (tetrahedral surface, TS) and ii) a gibbsite surface formed by μ -hydroxy groups of octahedral layers of $\text{Al}_2(\text{OH})_4$ (octahedral surface, OS). The interlayer space of kaolinite is tightly bridged by strong hydrogen bonds between opposing tetrahedral and octahedral layers (Brigatti et al., 2006). Consequently, direct intercalation is restricted to guest capable of forming strong hydrogen bonds (Elbokl and Detellier 2008). Natural kaolinite, though formally neutral in charge, possesses a small cation exchange capacity (CEC) due to some isomorphous substitution in the tetrahedral layers, which can only be counterbalanced at the outer TS by hydrated cations (Brady et al., 1996). The TS, because of the permanent negative charge, may be modified through simple ion exchange using cationic modifiers such as metal cation complexes or polyelectrolytes, during which the non-charged OS maintains unmodified. Selective modification of the OS by covalent grafting (Hirseman et al., 2011a; Letaief and Detellier 2007; Murakami et al., 2004; Tunney and Detellier 1994) is more challenging as compared to TS modification. It is nevertheless required to fine-tune the intrinsic so-called ``Janus-character`` of the kaolinite particles (Hirseman et al., 2011b; Weiss et al., 2013). Janus particles in general have been shown to have a wide range of promising industrial application e.g. as a catalyst (Perro et al., 2005; Walther and Müller 2008).

Moreover, the organic modification introduces organophilization of the initially hydrophilic nature of the OS, and hence, improves the suspension quality in organic solvents or even in hydrophobic polymer matrices which helps manufacturing polymer-clay nanocomposites (Gardolinski et al., 2000).

There are various studies that investigated adsorption and surface complexation of different organic ligands on a wide range of clays and metal oxides surfaces (Blesa et al., 2000; guez et al., 1996; Talbot et al., 2003). Most of these studies focused on the uptake of humic acid, catechols, and phenols, from waste water using clays and other metal oxides. Fewer studies investigated neutral organic ligands as potential surface modifiers for these materials (Diar-Bakerly et al., 2012). Kummert and Stumm (1980) found that the adsorption of catechol on $\gamma\text{-Al}_2\text{O}_3$ surfaces is related to the pK_a value of the ligand and its affinity towards the Al-cations, which is in turn comparable with complex building constants in solution.

Haderlein and Schwarzenbach (1993) proved that the adsorption of catechol on kaolinite is not related to the adsorption of nitrophenols, which adsorb on the tetrahedral surface of kaolinite. We proved in our previous work (Hirseman et al., 2011b; Weiss et al., 2013) that catechols are selective towards the OS of kaolinite. This was achieved by adsorption of ^{31}P -labeled catechol on kaolinite followed by solid-state ^{31}P -NMR. Moreover, selective modification could be proven by SIMS analysis of oriented platelets. We also unequivocally proved (Hirseman et al., 2011a) that intercalated ethylene glycol was covalently grafted to the μ -hydroxy groups by probing the chemical environment of aluminum nuclei using solid-state NMR techniques. However, the external surface area (SA) is very small (typically $< 9 \text{ m}^2/\text{g}$) compared to the huge total internal area of the basal surfaces (typically over $1000 \text{ m}^2/\text{g}$) that is available for intercalates. Consequently, most sensitive analytics are required to follow adsorption purely restricted to the OS. Proving modification of OS by 1,2-dihydroxyphenyl functions is further complicated by the fact that terminal aluminol groups at the edges are expected to be more reactive as compared to the μ -hydroxy groups at the OS and will be complexed first (Weiss et al., 1956).

Herein, the modification of the OS of kaolinite using siderophilic ligands (SLs), such as substituted catechols and flavones, containing a 1,2-dihydroxyphenyl group, was investigated. The 1,2-dihydroxyphenyl group is considered as an extremely reactive functional group (compared to the related alcohol or phenols) and forms stable chelate-complexes with Al-cation. The main focus was on optimization of reaction conditions to maximize adsorption capacities and hence grafting density of the surface modifiers. Brazilian kaolinite was used and modified using two different SLs i) 3,4-dihydroxybenzophenone (DBP) and ii) quercetin (Qu). As the adsorption capacities of external surfaces are very small, UV-Visible spectrometry, sedimentation kinetics test, X-ray diffraction and reflectance spectroscopy were applied to characterize and confirm the modification. Optimization and quantification of the absorption then allows that to unequivocally prove that these modifiers are not only adsorbed at the edges but clearly also on the aluminol basal surfaces.

2. Experimental

2.1. Materials and instruments

Kaolinite (Amazone 88/90) from Brazil was provided by Vale International S.A. (Saint-Prex, Switzerland). The mineral was size fractioned by a hydrocyclone but no dispersing agent and no sedimentation agent were added.

The kaolinite was further purified through three steps i) removal of magnesium and calcium carbonate using ethylenediaminetetraacetic acid (EDTA), ii) deferration using dithionite-citrate-bicarbonate method (Mehra and Jackson 1958) and iii) removal of organic impurities by ozonization. This fine-grained kaolinite showed typical dimensions of the ideally hexagonal platelets around 1 μm in diameter and up to 100 nm in height (see SEM in Figure 5). The specific surface area (SA) was calculated using the Brunauer, Emmett, and Teller (BET) method (Quantachrome Nova 2000e analyzer, N_2 -adsorption).

The siderophilic ligands used for the surface modification, 3,4-dihydroxybenzophenone (DBP) and quercetin (Qu); 2-(3,4-dihydroxyphenyl)-3,5,7-trihydroxy-4H-chromen-4-one, were purchased from Alfa Aesar. The organic solvents, tetrahydrofuran (THF) and ethanol (EtOH) were purchased from Sigma Aldrich. Sodium fluoride (NaF) was purchased from Merck. Ethylenediaminetetraacetic acid disodium salt, glacial acetic acid, sodium citrate, sodium dithionite, sodium hydroxide and sodium chloride were purchased from Grüssing GmbH.

2.2. Modification of the OS of kaolinite

In a tightly closed glass vessel, 0.25 g of kaolinite was suspended in 25 mL of a solution of SLs in EtOH (concentration ranging between $0.05 - 0.5 \times 10^{-3}$ mol/L). The reaction mixture was ultrasonified (2 min) and shaken for equilibration using an overhead shaker for two days at temperatures of 25 or 60 $^{\circ}\text{C}$. The suspensions were immediately centrifuged (Heraeus Multifuge 1L) at 9000 rpm for 10 min using closed polypropylene centrifuge tubes. Finally, the supernatants were analyzed using UV-Vis spectrometer (Cary 300 UV-Vis, Varian, cell path length of 1 cm) to determine the remaining amount of the SLs in solution. Kao-Qu and kao-DBP represent the kaolinite modified by Qu and DBP, respectively.

2.3. Quantifying the adsorption capacities of the edges

An estimate of the adsorption capacities of the edges was achieved by monitoring the adsorption isotherm of fluoride ions by potentiometric titration. The determination of fluoride ions in suspension was achieved using a fluoride ion selective electrode (F^- -ISE Ω Metrohm, 905 Titrand). The titration was carried out in a hydrous total ionic strength adjustment buffer (TISAB) in polypropylene beakers. This buffer was prepared by dissolving 58 g of NaCl (1 mol), 4 g of Na_2EDTA (0.01 mol), 57 mL of glacial acetic acid in 0.5 L bi-distilled water.

Anion exchange at the edges works best at the point of zero charge, which was reported to lie between 4.5 - 5.0 (Scroth and Sposito 1997). The pH value of the mixture was therefore adjusted to 5.5 by adding NaOH (10 mol/L) after cooling the mixture in an ice bath. The total volume was adjusted to 1 L by adding bi-distilled water. The potentials of a series of standard concentrations ($0.05 - 1.5 \times 10^{-3}$ mol/L) were measured and a potential vs. concentration curve was obtained. After that, a suspension of 1 g kaolinite was prepared in 100 mL of a 1:1 mixture of TISAB and an aqueous solution of NaF (final NaF concentrations ranging between $0.05 - 1.5 \times 10^{-3}$ mol/L) that was equilibrated for 30 min at room temperature.

2.4. Characterization of surface modified kaolinite

To prove that no intercalation occurred, PXRD patterns were recorded in reflection mode (PANalytical Xpert Pro equipped with a X'Celerator Scientific RTMS detector and using Cu $K\alpha$ radiation). The samples were measured on flat glass holders to foster texture and boost the intensities of the basal reflections.

To compare the stability of different suspension in an organic solvent upon surface modification, suspensions of 0.25 wt% of pristine kaolinite and the surface modified samples, kao-DBP and kao-Qu, were prepared in THF. The semi-quantitative measurement was carried out applying a Lumifuge (Lumifuge 114 stability analyzer) with stepwise increasing centrifugal velocities.

The reflection spectra of the adsorbed SLs on the kaolinite were recorded using UV-Vis spectrometer (Cary 5, Varian) equipped with a Praying Mantis unit. The modified samples were repeatedly (5 times) washed with EtOH (approximately 25 mL) prior to measurement to ensure complete removal of non-bonded SLs. Moreover, the results were compared to the absorption spectra of the SLs in an EtOH solution (Cary 300, Varian).

3. Results and Discussions

3.1. Siderophilic ligands (SLs)

As a result of the small size of the trivalent Al-cation, it is considered as a so-called 'hard Lewis acid'. Therefore, stable complexes are expected to be formed with 'hard Lewis bases' such as carboxylates, catecholates, and phenolates. Furthermore, as stated in the introduction, the complexation behavior of Al-cations located at the surface of a layered inorganic material was found to be similar to a solution (Kummert and Stumm 1980). The most stable complexes of trivalent metal ions are formed by so-called siderophilic ligands (SLs) that are hard chelate

ligands of the catechol type. The two ortho-hydroxy groups are part of a larger conjugated planar π -system which increases the electron density at the coordinating oxygen atoms (Lewis base; electron donor), and hence, improves the reactivity towards metal cations (Lewis acid; electron acceptor). For these reasons, SLs containing the 1,2-dihydroxyphenyl group were chosen as a surface modifier due to their high reactivity towards Al^{3+} . Furthermore, the distance between the two oxygen atoms in 1,2-dihydroxyphenyl group ($\approx 2.8 \text{ \AA}$) is similar to the distance between two adjacent μ -hydroxy groups located at the OS of kaolinite (Figure 1). Therefore, catechols are suitable candidates for modification of this type of nominally neutral basal surfaces.

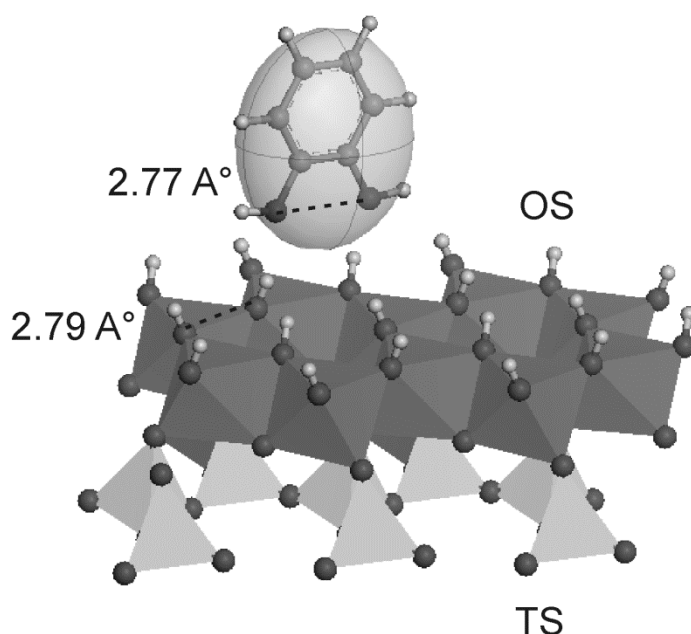


Figure 1. Kaolinite basal surface showing the perfect match between μ -hydroxy groups of the OS and the ortho-oxygen atoms of a simple catechol molecule (1,2-dihydroxybenzene).

When searching for suitable siderophilic ligands and optimal conditions for surface modification, various factors must be considered. First of all, due to the fact that kaolinite tactoids have a rather small surface to volume ratio, and hence, the specific area available for adsorption is small, the molar extinction coefficient of the SLs should be high. This allows for detecting small changes in concentration upon adsorption applying colorimetric analysis by UV-Vis spectrometry. The calculated values of the molar extinction coefficient of the used SLs, DBP and Qu in EtOH were $8000 \text{ L mol}^{-1} \text{ cm}^{-1}$ ($\lambda_{\text{max}} 322 \text{ nm}$) and $23000 \text{ L mol}^{-1} \text{ cm}^{-1}$ ($\lambda_{\text{max}} 373 \text{ nm}$), respectively. Moreover, the solvent should be carefully chosen because it is known that in water auto-oxidation of the catechol function is a severe problem and in some cases might even be promoted by certain minerals (Larson and Hufnal 1980; Talbot et al.,

2003). Therefore, ethanol was used as a reaction medium because the SLs are soluble and, even more important, auto-oxidation is impeded. Finally, the good suspension quality of kaolinite in ethanol makes it an ideal reaction medium.

In addition, the chosen SLs (Figure 2) have extra functional groups allowing for further modification in future work. For instance, the ketone group in DBP allows for cross-linking by UV irradiation (Ohm et al., 2010).

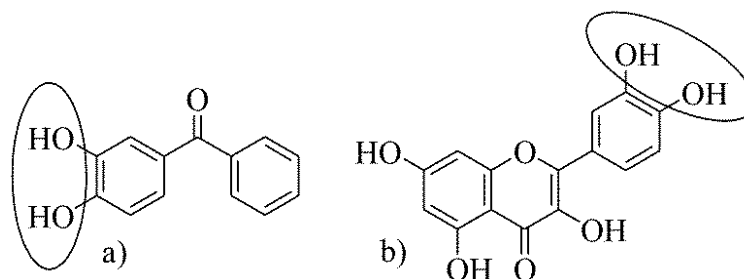


Figure 2. Chemical structures of the used SLs with 1,2-dihydroxyphenyl groups: a) 3,4-dihydroxybenzophenone (DBP) and b) quercetin (Qu)

3.2. Adsorption isotherms/capacities

The hydrogen bonding capability of DBP and Qu are mediocre and therefore it would not be expected that they can directly intercalate into kaolinite. Nevertheless, to check that the observed adsorption capacities of the SLs may be attributed exclusively to the external surfaces of kaolinite and no intercalation occurred, PXRD patterns were recorded before and after adsorption (Figure 3). The PXRD patterns did not indicate any shift in the d-spacing values, and hence, confirmed that the SLs were not adsorbed on the internal surfaces (intercalated), rather they selectively modified the external surfaces.

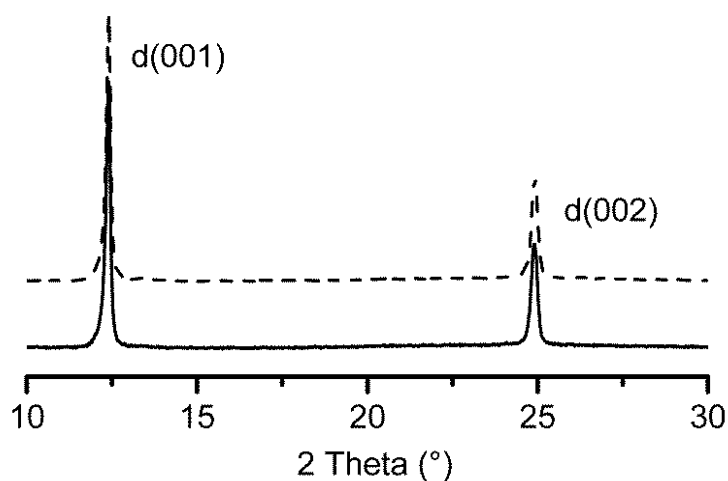


Figure 3. PXRD pattern of the kaolinite (—) and kao-DBP (---)

To optimize reaction parameters allowing for maximizing adsorption capacities, reaction conditions were varied in a systematic way. The adsorption isotherms for both ligands were determined at 25 °C and 60 °C in the concentration range 0.02 - 0.5 × 10⁻³ mol/L. The adsorption capacities were calculated by analyzing the supernatant via UV-Vis spectrometry. Kinetic studies showed that two days were adequate to reach equilibrium of adsorption of SLs on kaolinite (data is not shown). The adsorption isotherms of both, DBP and Qu were of Langmuir type (Figure 4). The adsorption capacity of the smaller DBP was, however, found to be significantly higher than for the bulkier Qu suggesting that the capacities were limited by the maximum grafting density achievable for a given size of the ligand densely packed into a monolayer. Interestingly, the capacities increase significantly at elevated temperatures suggesting that at 60 °C the ligands are more mobile and can be rearranged at the surface into denser (equilibrium) structures. The maxima of the adsorption capacities found at 60 °C were 4.8 × 10⁻⁶ mol/g and 6.7 × 10⁻⁶ mol/g for Qu and DBP, respectively.

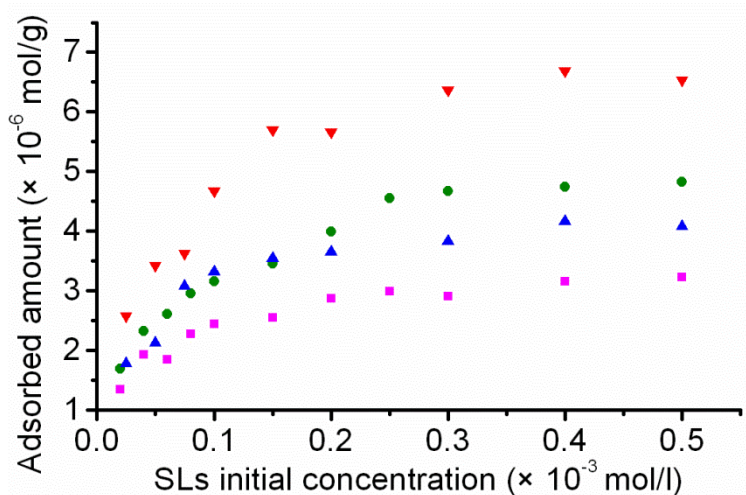


Figure 4. Adsorption isotherms of (■) Qu/25 °C (●) Qu/60 °C (▲) DBP/25 °C (▼) DBP/60 °C

Since the edge surface also contains reactive aluminol sites, in order to derive grafting densities of the modifiers at the OS, we first need to determine the number of reactive sites at the edge surface to be able to estimate the relative contribution of the different external surfaces to the total specific surface.

The total surface area was determined to be 8.9 m²/g by the BET-method. Assuming a uniform and idealized hexagonal morphology of the kaolinite particles (typical morphology: 1 μm diameter and 0.1 μm thickness, compare Figure 5) the total surface area can be calculated from the known density to be 9.5 m²/g of which 40 % would be assigned to the OS, while 20 % would be related to edge surface (SI-1).

Given that the experimentally accessible surface is lowered by some aggregates with parallel overlapping band-like structures the agreement of measured and estimated specific surface area is fair suggesting vice versa that the average aspect ratio assumed in the calculation is sensible.

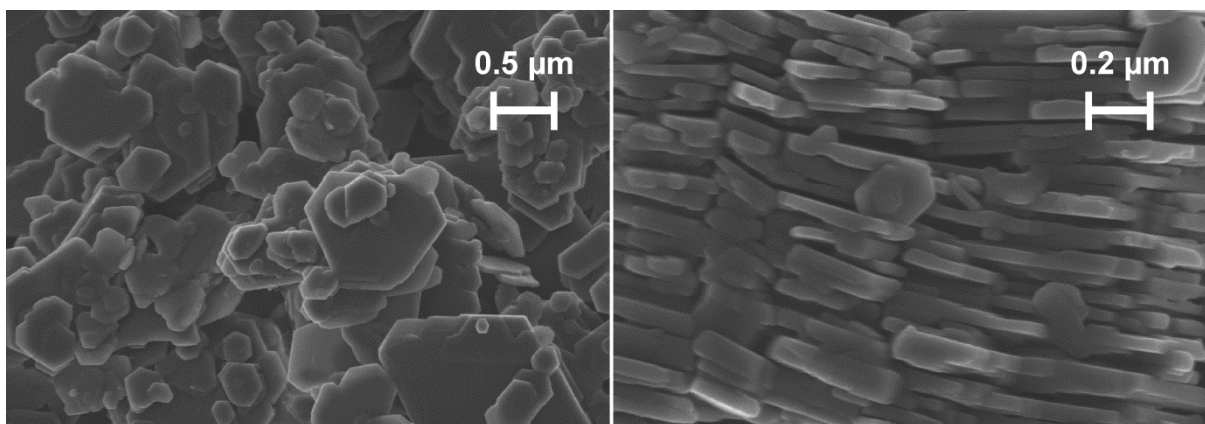


Figure 5. SEM images of the used Brazilian kaolinite

3.3. Adsorption capacity of the edges as determined by adsorption of fluoride ions

The edge surfaces of kaolinite exhibit two different kinds of hydroxy functional groups i) silanols ($\equiv \text{Si-OH}$) and ii) aluminols ($\equiv \text{Al-OH}$), where \equiv represents the edge of the kaolinite. The total adsorption capacity of SLs will be the sum of adsorption at edges and OS. The terminal aluminol groups at the edges are, however, expected to be more reactive as compared to the μ -hydroxy groups at the OS and will be complexed first (Weiss et al., 1956). In order to calculate the grafting density of SLs at the OS, first the adsorption capacity of the edges needs to be estimated and subtracted from the total capacity.

As has been shown by Weiss et al. (1956) these tangling silanol and aluminol groups can be selectively substituted with F^- . This way, the number of hydroxy groups exposed at the edges can be quantified by anion exchange of fluoride ions. Therefore, a potentiometric titration of F^- in a kaolinite suspension using F^- -ISE was carried out in a TISAB buffer solution. Generally, TISAB is used for the fluoride ion analysis to control the total ionic strength, the pH of the solution (pH = 5.5) and to release the fluoride ions from other potential metal complexes in solution. Fluorine adsorption isotherms were determined in the concentration range between 0.1×10^{-3} - 1.5×10^{-3} mol/L (Figure 6). Up to a F^- concentration of 1.2×10^{-3} mol/L the adsorption isotherm is of Langmuir type. As reported by Weiss et al. (1956) beyond this point, additionally the less reactive μ -hydroxy aluminol sites of OS might be replaced by F^- .

The adsorption capacity reached a plateau between 0.8×10^{-3} - 1.2×10^{-3} mol/L corresponding to a total number of more reactive silanol and aluminol sites at the edges of 24×10^{-6} mol/g. The F^- exchange is highly sensitive (detection limit; $< 1 \times 10^{-6}$ mol/L at $pH < 7$) and moreover, access to edges is not restricted at all by band-type aggregation and therefore the adsorption capacity is not affected by aggregation.

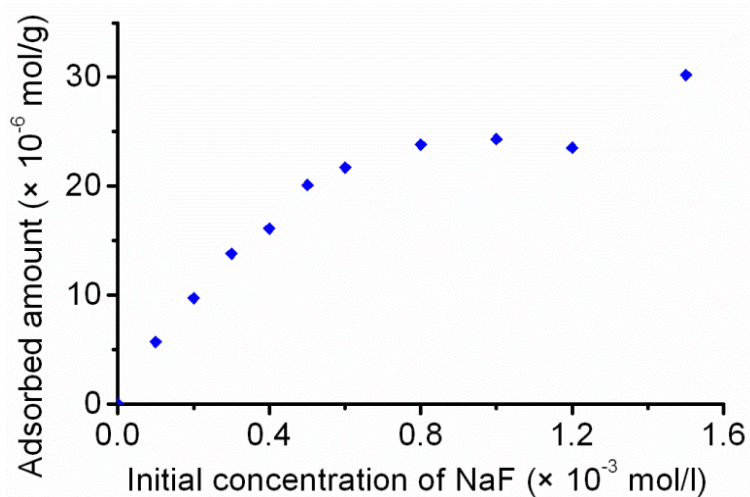


Figure 6. Adsorption isotherm of fluoride ions

From the F^- adsorption capacity, the edge area may be independently estimated to be $1.6 \text{ m}^2/\text{g}$ (for details see SI-2). This calculation was based on two facts: i) each F^- replaces one non- μ -hydroxy and ii) a unit cell side exposed at the edges has six non- μ -hydroxy groups (Figure 7, additional sites occurring at edges of two faces or corners of the crystal are neglected) since the kaolinite structure is pseudo-hexagonal only the bc -face is considered.

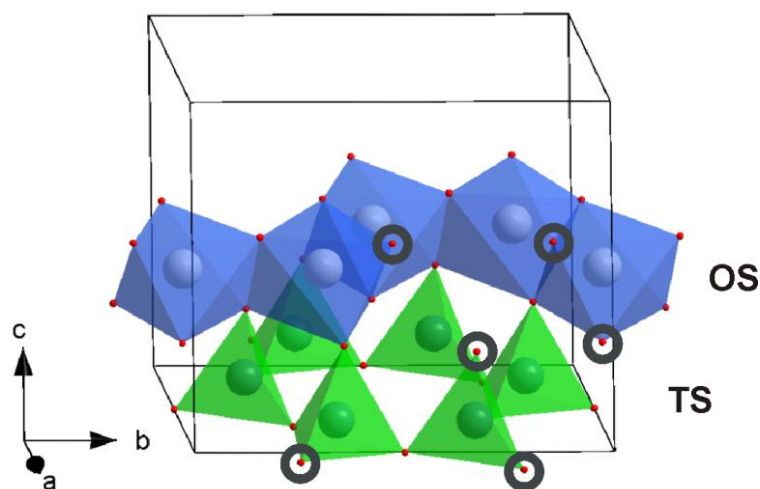


Figure 7. A kaolinite unit cell showing the non- μ -hydroxy groups of the bc -edges

The relative contribution of the edges to the SA calculated this way amounted to 18 %, which is in a good agreement with the value of 20 % estimated by assuming a certain average aspect ratio. The good agreement of the two independently derived values lends confidence. Because of the insensitivity of value based on the F- exchange to possible aggregation, 1.6 m²/g is taken as the edge SA for further considerations.

Obviously not every non- μ -hydroxy group can be replaced by the 1,2-dihydroxyphenyl group because of the sterical demand of rest of the ligand. Molecular models suggest that for DBP a maximum grafting density at the edges of one molecule per one unit cell may be achieved (SI-3). Accordingly, a maximum adsorption capacity at the edges of 4×10^{-6} mol/g can be estimated. By subtracting this result from the total adsorption capacity measured, a minimum adsorption capacity corresponding to the OS of 2.7×10^{-6} mol/g was obtained. This minimum adsorption capacity represents a minimum grafting density to OS of one molecule per five unit cell surfaces ($b \times a$; 46×10^{-20} m², Bish, 1993). Despite possible uncertainties in the determination of the edge surface, this value unequivocally proves that DBP is modifying the basal surface. This statement is even truer for the much bulkier Qu ligand for which the maximum adsorption capacity of the edges will be much smaller.

3.4. Characterization of the modified kaolinite

3.4.1. Suspension stability and sedimentation kinetics

As a result of the surface modification, the hydrophilic nature of the OS and edge surface is rendered more hydrophobic. Consequently, the stability of suspensions of kaolinite in organic solvents is expected to improve upon modification. A Lumifuge was used to compare the suspension qualities of the pristine kaolinite to the modified kao-DBP and kao-Qu in an organic solvent, THF, by centrifugation forced sedimentation. The Lumifuge test provides semi-quantitative information about the sedimentation kinetics by measuring the transmission of light through a horizontal centrifuge cell during centrifugation at different velocities (Figure 8). Generally, stable suspensions have lower transmission values than less stable suspensions.

For more stable suspensions (kao-DBP, Kao-Qu), more absorption/scattering of light was observed at any time by scattering particles kept in suspension. For the least stable suspension of pristine kaolinite, the particles sediment quickly, and hence, more light was transmitted through the sample.

At the beginning of forced sedimentation, only 45 % and 53 % of the light was transmitted through the kao-DBP and kao-Qu suspensions, respectively, while for the pristine kaolinite suspension 66 % of the light was transmitted.

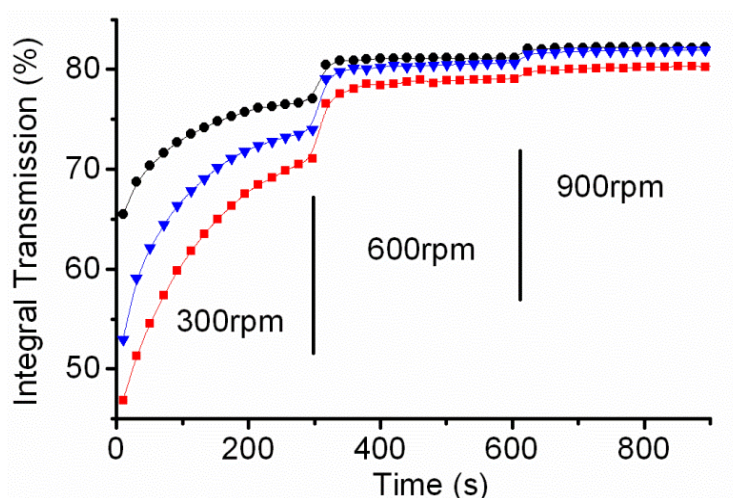


Figure 8. Sedimentation kinetics of pristine kaolinite (●) and the modified; kao-Qu (▼) and kao-DBP (■) in THF as determined by centrifugation forced sedimentation using a Lumifuge. Vertical lines indicate times when the centrifugal velocity was increased stepwise.

By increasing the centrifugal velocities, all suspensions clarify due to forced sedimentation, nevertheless, the modified kao-DBP and kao-Qu clear up much more slowly. Interestingly, the kao-DBP turned out to be significantly more stable than the kao-Qu in THF. The forced sedimentation result showed that even small amounts of SLs adsorbed on kaolinite (in the range of a few $\mu\text{mol/g}$) are capable to improve the suspension quality in hydrophobic environments. This result will be of major impact for the preparation of polymer/kaolinite composite materials.

3.4.2. Reflection spectra

The pristine kaolinite is a white powder while the modified samples turned yellow. Therefore, the adsorption can even be visualized by the naked eye (Figure 9).



Figure 9. Photographs showing the different colors of the pristine kaolinite (middle) and the modified kao-DBP (left) and kao-Qu (right)

The color of the modified kaolinite was governed by two factors: i) the color of the used SLs and ii) the color shift triggered by the surface complex formation of the SLs with the Al-cations of the OS and edges of kaolinite. To characterize the modified sample, UV-Vis reflection spectra of the SLs adsorbed on kaolinite were recorded and then compared to the absorption spectra of the SLs in EtOH solution (Figure 10). The pristine kaolinite was used as baseline measurement with a reflection value of 0.

The characteristic absorption maxima of DBP and Qu in ethanol were at 322 nm and 373 nm, respectively. However, upon adsorption, the characteristic reflection maxima of SLs were shifted towards higher wavelength of 380 nm and 420 nm for kao-DBP and kao-Qu, respectively.

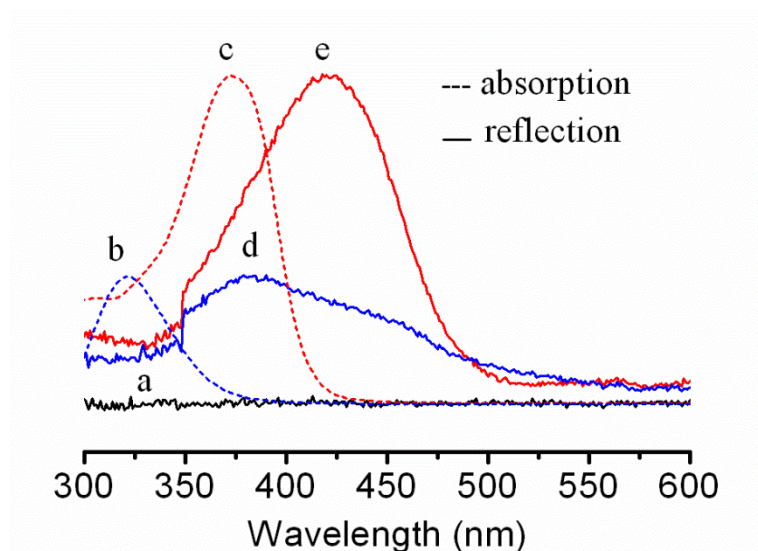


Figure 10. Absorption/reflection UV-Vis spectra (300 - 600 nm) of a) kaolinite (as baseline), b) DBP/EtOH, c) Qu/ETOH, d) kao-DBP and e) kao-Qu

The shift of the characteristic absorption/reflection maxima between the free and the adsorbed SLs (around 50 nm) is explained by the changes of the electrical environment (electronic delocalization) of the SLs upon complexation (Cornard and Lapouge 2004). The bathochromic shift observed upon adsorption onto kaolinite hence confirms the chelate-complex formation of SLs with Al-cations.

4. Conclusions

Comparing maximum adsorption capacities with edge areas as determined by ion exchange of fluoride ions, it can be concluded that ligands with a 1,2-dihydroxyphenyl group are capable to coordinate to the aluminol basal surface of kaolinite. This conclusion is corroborated by

significant bathochromic shifts upon adsorption of the ligands that indicate the formation of a surface complex with exposed Al³⁺.

Even small amounts of adsorbed ligands change the surface tension of kaolinite significantly. Consequently, forced sedimentation experiments showed the modified kaolinite to be rendered hydrophobic enough to form stable suspensions in organic solvents. This kind of surface modification will therefore be applied in future work to organophilize kaolinite for utilization as filler in polymer composite materials. The type of modification by 1,2-dihydroxyphenyl carrying molecules is expected to be generally applicable to all compounds carrying μ -hydroxy groups at external surfaces.

Acknowledgments

The authors thank Dr. B. Biersack, Department of Organic Chemistry I, University of Bayreuth, for long discussions. B. D-B also acknowledges the German Academic Exchange Service (DAAD) for financial support. This work was further supported by the Deutsche Forschungsgemeinschaft (DFG) within the Collaborative Research Center (SFB 840).

References

- Bish, D.L., 1993. Rietveld refinement of the kaolinite structure at 1.5 K. *Clays Clay Miner.* 41, 738-744.
- Blesa, M.A., Weisz, A.D., Morando, P.J., Salfity, J.A., Magaz, G.E., Regazzoni, A.E., 2000. The interaction of metal oxide surfaces with complexing agents dissolved in water. *Coord. Chem. Rev.* 196, 31-63.
- Brady, P.V., Cygan, R.T., Nagy, K.L., 1996. Molecular controls on kaolinite surface charge. *J. Colloid Interface Sci.* 183, 356-364; Weiss A, Russow J., 1963. Uber die Lage der austauschbaren Kationen bei Kaolinit. *Proc. Int. Clay Conf. Stockholm.*1:203-213
- Brigatti, M.F., Galan, E., Theng, B.K.G., 2006. Chapter 2, structures and mineralogy of clay minerals, in: Faiza Bergaya, B.K.G., (Eds.), *Developments in clay science handbook of clay Science*. Elsevier, Amsterdam, pp. 19-86.
- Cornard, J.P., Lapouge, C., 2004. Theoretical and spectroscopic investigations of a complex of Al(III) with caffeic acid. *J. Phys. Chem. A* 108, 4470-4478.

- Diar-Bakerly, B., Beyer, G., Schobert, R., Breu, J., 2012. Significance of aspect ratio on efficiency of layered double hydroxide flame retardants, in: Morgan, A.B., Wilkie, C.A., Nelson, G.L., (Eds.), *Fire and polymers VI: New advances in flame retardant chemistry and science*. American Chemical Society, Washington, DC, pp. 407-425.
- Elbokl, T.A., Detellier, C., 2008. Intercalation of cyclic imides in kaolinite. *J. Colloid Interface Sci.* 323, 338-348.
- Gardolinski, J.E., Carrera, L.C.M., Cantao, M.P., Wypych, F., 2000. Layered polymer-kaolinite nanocomposites. *J. Mater. Sci.* 35, 3113-3119.
- Guez, R., Blesa, M.A., Regazzoni, A.E., 1996. Surface complexation at the TiO₂(anatase)/aqueous solution interface: Chemisorption of catechol. *J. Colloid Interface Sci.* 177, 122-131.
- Haderlein, S.B., Schwarzenbach, R.P., 1993. Adsorption of substituted nitrobenzenes and nitrophenols to mineral surfaces. *Environ. Sci. Technol.* 27, 316-326.
- Hirseman, D., Köster, T.K.J., Wack, J., van Wüllen, L., Breu, J., Senker, J., 2011a. Covalent grafting to μ -Hydroxy-capped surfaces? A kaolinite case study. *Chem. Mater.* 23, 3152-3158.
- Hirseman, D., Shylesh, S., De Souza, R.A., Diar-Bakerly, B., Biersack, B., Müller, D.N., Martin, M., Schobert, R., Breu, J., 2011b. Large-scale, low-Cost fabrication of Janus-type emulsifiers by selective decoration of natural kaolinite platelets. *Angew. Chem. Int. Ed.* 51, 1348-1352.
- Kogure, T., Elzea-Kogel, J., Johnston, C.T., Bish, D.L., 2010. Staking disorder in a sedimentary kaolinite. *Clays Clay Miner.* 58, 62-71.
- Kummert, R., Stumm, W., 1980. The surface complexation of organic acids on hydrous α -Al₂O₃. *J. Colloid Interface Sci.* 75, 373-385.
- Larson, R.A., Hufnal, J.M., 1980. Oxidative polymerization of dissolved phenols by soluble and insoluble inorganic species. *Limonol. Oceanogr.* 25, 505-512.
- Letaief, S., Detellier, C., 2007. Functionalized nanohybrid materials obtained from the interlayer grafting of aminoalcohols on kaolinite. *Chem. Commun.* 2613-2615.
- Mehra, O.P., Jackson, M.L., 1958. Iron oxide removal from soils and clays by a dithionite-citrate system buffered with sodium bicarbonate. *Clays Clay Miner.* 7, 317-327.

Murakami, J., Itagaki, T., Kuroda, K., 2004. Synthesis of kaolinite-organic nanohybrids with butanediols. *Solid State Ionics* 172, 279-282.

Ohm, C., Brehmer, M., Zentel, R., 2010. Liquid crystalline elastomers as actuators and sensors. *Adv. Mater.* 22, 3366-3387.

Perro, A., Reculosa, S., Ravaine, S., Bourgeat-Lami, E., Duguet, E., 2005. Design and synthesis of Janus micro- and nanoparticles. *J. Mater. Chem.* 15, 3745-3760.

Scroth, B.K., Sposito, G., 1997. Surface charge properties of kaolinite. *Clays Clay Miner.* 45, 85-91.

Talbot, D., Bee, A., Treiner, C., 2003. Adsorption of 4-nitrophenol at a kaolinite/water interface as a function of pH and surfactant surface coverage. *J. Colloid Interface Sci.* 258, 20-26.

Tunney, J.J., Detellier, C., 1994. Preparation and characterization of two distinct ethylene glycol derivatives of kaolinite. *Clays Clay Miner.* 42, 552-560.

Walther, A., Müller, A.H.E., 2008. Janus particles. *Soft Matter* 4, 663-668.

Weiss, A., Mehler, A., Koch, G., Hofmann, U., 1956. über das Anionenaustauschvermögen der Tonmineralien. *Z. Anorg. Allg. Chem.* 284, 247-271.

Weiss, S., Hirsemann, D., Biersack, B., Ziadeh, M., Müller, A.H.E., Brey, J., 2013. Hybrid Janus particles based on polymer-modified kaolinite. *Polymer* 54, 1388-1396.

Appendix 1: Modification of Kaolinite by Grafting of Siderophilic Ligands to the External Octahedral Surface

Bashar Diar-Bakerly¹, Dunja Hirsemann¹, Hussein Kalo¹, Rainer Schobert², Josef Breu^{1,*}

¹) Department of Inorganic Chemistry I, University of Bayreuth, Universitaetsstr. 30, 95447 Bayreuth, Germany

²) Department of Organic Chemistry I, University of Bayreuth, Universitaetsstr. 30, 95447 Bayreuth, Germany

Corresponding author: Prof. Dr. Josef Breu, Universitaetsstr. 30, 95440 Bayreuth, Germany

* E-mail: josef.breu@uni-bayreuth.de

Supplementary Information (SI)

1. Estimation of the relative contribution of the different external surfaces to the total surface area (SI-1)

In order to get a reasonable contribution of the OS and the edges to the SA, the following estimation was done. Assuming a uniform and ideal hexagonal morphology for the kaolinite platelets (diameter of 1 μm , height of 0.1 μm , and consequently, an aspect ratio of 10, Figure SI-1) the SA is given by the following equation (1):

$$SA = (2B + S) \times N \quad (1)$$

where B and S are the base and the side areas of a platelet, respectively, and N is the number of platelets/g.

In a regular hexagonal prism (platelet) B and S are given as:

$$B = 3 (\sqrt{3}/2) s^2 \quad (2)$$

$$S = P \times h = 6s \times h \quad (3)$$

where s is the side length, P is the base perimeter and h is the height of a platelet.

N is correlated to the density of kaolinite ($d = 2.6 \times 10^{+6} \text{ g/m}^3$) and is given as:

$$N = 1/m = 1/(V \times d) = 1/(B \times h \times d) \quad (4)$$

where m and V are the mass and the volume of a platelet, respectively.

By replacing (2, 3, 4) in (1), SA = 9.5 m²/g.

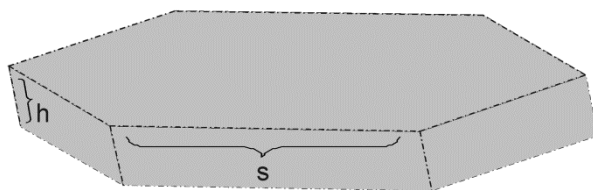


Figure SI-1. An ideal hexagonal morphology of a kaolinite platelet

The OS and the edges are obtained by multiplying B and S by N, respectively:

- OS = B x N = 3.8 m²/g that represents around 40 % of the SA
- Edges = S x N = 1.8 m²/g that represents around 20 % of the SA

Please note that the contribution of the OS and the edges to the SA is strongly correlated to the suggested aspect ratio of 10 (see SEM in Figure 5).

2. Calculation of the edge surfaces from the adsorption capacity of F⁻ (SI-2)

Considering that each F⁻ replaces one non-μ-OH at the bc-edge, the number of non-μ-OH exposed to the edges/g is given as:

$$F^- \text{ adsorption capacity} \times \text{Avogadro constant} \quad (5)$$

where the experimental adsorption capacity of F⁻ = 24 × 10⁻⁶ mol/g and Avogadro constant (NA) = 6.022 × 10⁺²³ mol⁻¹

number of non-μ-OH exposed to the edges = 14.5 × 10⁺¹⁸ OH/g

Each bc-face of a unit cell side has six non-μ-OH exposed to the edges (see Figure 7), as a result, the number of unit cell sides exposed to the edges:

$$(14.5 \times 10^{+18})/6 = 2.4 \times 10^{+18} \text{ unit cell sides/g} \quad (6)$$

Finally the edge surface is calculated from the following equation:

$$\text{number of unit cell sides exposed to the edges} \times (b \times c^*) \quad (7)$$

with $b = 8.94 \times 10^{-10}$ m and $c^* = 7.38 \times 10^{-10}$ m (Bish, 1993).

By replacing (6) in (7) the edge surface are amounts to 1.6 m²/g.

The calculated edge area represents 18 % of the experimentally (BET) measured SA (8.9 m²/g).

3. Estimation of the maximum adsorption capacity of the edges (SI-3)

The maximum adsorption capacity of the edges (mol/g) is given by the following equation:

$$\text{Edge surface}/(\text{minimum area needed for adsorption of one molecule} \times \text{NA}) \quad (8)$$

To determine the sterical requirements for adsorption of DBP at edges, CPK-models with different possible orientations of the DBP molecule on the edges with the 1,2-dihydroxyphenyl groups binding to non- μ -hydroxy groups at the surface were built (Figure SI-2).

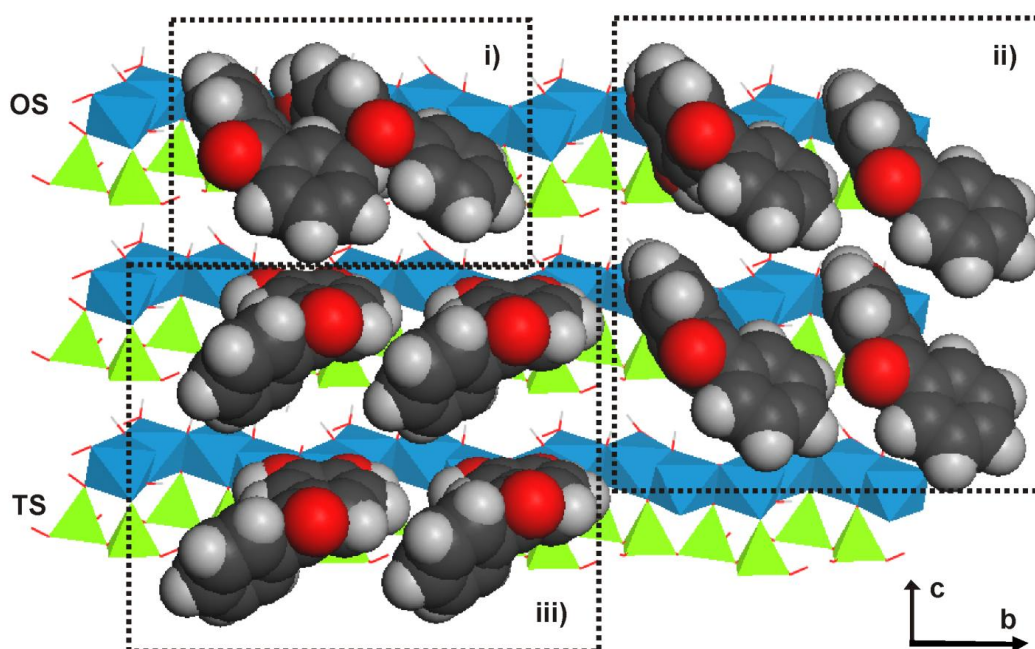


Figure SI-2. CPK-models of different possible orientations of DBP molecules coordinating to Al³⁺ residing at the edges of kaolinite.

In first case (i) we assumed that two molecules coordinate in a bi-dentate mode to adjacent Al³⁺, which turned out to be impossible due to sterical hindrance. Arrangements where the ligands coordinate in a bi-dentate mode to every other Al³⁺ (ii) and where the ligands coordinate in a mono-dentate way to two adjacent Al³⁺ are feasible and represent reasonably maximum grafting densities of one molecule per *bc*-face (1 molecule/66 × 10⁻²⁰ m², Bish, 1993) for both cases ii and iii. This maximum grafting density corresponds to an adsorption capacity of the edges of 4 × 10⁻⁶ mol/g.

5.2. Appendix 2: Significance of Aspect Ratio on Efficiency of Layered Double Hydroxide Flame Retardants

Bashar Diar-Bakerly¹, Günter Beyer², Rainer Schobert³, Josef Breu^{1,*}

¹) Department of Inorganic Chemistry I, University of Bayreuth, Universitaetsstr. 30, 95447 Bayreuth, Germany

²) Kabelwerk Eupen AG, 4700 Eupen, Belgium

³) Department of Organic Chemistry I, University of Bayreuth, Universitaetsstr. 30, 95447 Bayreuth, Germany

Corresponding author: Prof. Dr. Josef Breu, Universitaetsstr. 30, 95440 Bayreuth, Germany

* E-mail: josef.breu@uni-bayreuth.de

Abstract

The effect of specific surface area and aspect ratio of different layered double hydroxides (LDHs) on flame retardant properties of PS/LDH nanocomposites was systematically investigated. Carbonate LDH, with a Mg:Al molar ratio of 2:1, was synthesized by the urea hydrolysis method and external basal surfaces were selectively modified using a siderophilic ligand (3,4-dihydroxybenzo-phenone). The efficiency of this surface modification was investigated by studying the sedimentation kinetics in an organic solvent. PS/LDH nanocomposites were prepared by solution blending in a three roll mill. Cone calorimeter measurements showed little influence of specific surface areas but a pronounced influence of aspect ratio on flame retardancy. Optimizing aspect ratio yielded a significant reduction of the peak of heat release rate (PHRR) of 36 % at 5 wt% loading of LDH. A maximum reduction of PHRR of 51% could be achieved at a loading of 15wt%. Interestingly, at this loading an unusual increase of t_{ign} could be observed.

1. Introduction

Most of the currently used, commercially available flame retardants are halogenated molecular compounds because of their high efficiency allowing for low loadings. However, in the last decade increasing environmental concerns (1, 2) have generated growing interest for non-halogenated and environmentally benign flame retardants. Inorganic flame retardants, such as aluminum trihydroxide (ATH) and magnesium dihydroxide (MDH), in contrast to the organic additives are considered to be immobile and non-toxic.

However, high loadings (40-70 wt%) of these fillers are required to achieve sufficient flame retardancy that, on the other hand, alter the mechanical properties of the polymer crucially and represent a major drawback of these fillers. As alternatives, layered double hydroxides (LDHs), which are structurally and chemically related fillers to ATH and MDH, were intensively studied as flame retardants or synergistic flame retardants (3–12). These LDHs are anionic clays having the same layer structure as brucite. Partial isomorphous substitution of the divalent cation by trivalent cations in the octahedral layer renders the layers to carry a permanent positive charge. The cationic layer charge is balanced by interlayer anions resulting in the general formula of $[M(II)_{1-x}M(III)_x(OH)_2]^{x+}[A^{n-x/n}]^{x-} \cdot mH_2O$, where M(II) and M(III) are divalent and trivalent metal cations, respectively, A^{n-} is the charge balancing interlayer anion, while x ranges between 0.20 and 0.33 and m refers to the number of interlayer water molecules (13).

Whereas the influence of cationic clays, like hectorite and montmorillonite (MMT), on the flame retardant properties of polymer nanocomposites is fairly well understood and the crucial role of the aspect ratio of fillers has been elucidated (14, 15), the mechanism by which LDHs influence flame retardant properties is not yet clear. The individual contributions of the endothermic nature of the thermal degradation of the filler, the specific interface area between the polymer and filler, and the gas barrier or mechanical reinforcement of the char related to the filler's aspect ratio is not obvious.

Additionally, LDHs are highly hydrated and cannot be dispersed effectively in hydrophobic polymer matrices without surface modification. Usually this problem has been solved by intercalation of different organic anions (sulfonates, carboxylates, and phosphonates) containing a hydrophobic aromatic/aliphatic chain (16–20). However, the ion exchange capacity of LDH is considerably higher as compared to montmorillonite and consequently, a lot of readily flammable organic matter is introduced by the ion exchange.

Here, we present a novel approach for organic modification of Mg/Al-CO₃-LDH, which selectively restricts organophilization to external surfaces, using siderophilic ligands, e.g. catechol derivatives like 1,2-dihydroxyphenyl. This functional group is well known to form stable complexes with aluminum cations in solution (21, 22) and even Al immobilized at solid surfaces like external octahedral layers of Mg/Al-LDH or kaolinite (23). Modification of LDH by a suitable siderophile allowed stable suspensions of LDH in organic solvents and assured a better compatibility with the polymer matrix.

Additionally, we systematically investigated the effect of specific surface area and aspect ratio of the filler on the fire properties of PS/LDH nanocomposites in an attempt to elucidate the mechanism of flame retardancy of LDHs.

2. Experimental Section

2.1 Materials

Polystyrene (PS 158K, melt index 3.00 g/10 min (200 °C/5kg, ASTM D1238), density 1.04 g/cm³, ASTM D792, glass transition temperature 100 °C, ISO 11357) was supplied by BASF. For Mg/Al-LDH synthesis, urea and magnesium chloride hexahydrate were purchased from Grüssing GmbH, and aluminum chloride hexahydrate was purchased from Merck. LDH-syntal (density 2 g/cm³, BET-surface 74 m²/g) was provided from Süd-Chemie. The siderophilic ligand (3,4-dihydroxybenzophenone, DBP) used for the surface modification was purchased from Alfa-Aesar. The organic solvents (tetrahydrofuran and ethanol) used for solution blending and surface modification were purchased from Aldrich chemicals.

2.2. Instruments and Characterization

The powder X-ray diffraction (PXRD) patterns of the synthesized LDH and the surface modified LDH were obtained in reflection mode on a PANalytical Xpert Pro equipped with a X'Celerator Scientific RTMS detector and using Cu K α radiation. The samples were measured on flat glass holders.

A 5 wt% aqueous suspension of LDH was milled in a stirred media mill, Netzsch Labstar LS 1 LMZ. Yttrium stabilized zirconia beads were used as grinding media (diameter of 0.6 – 0.8 mm). The volume fraction of the grinding media in the grinding chamber was 80 vol%.

The particle size distribution (PSD) was determined by static light scattering using a Retsch Horiba LA-950 SLS instrument. The Brunauer, Emmett, and Teller (BET) method was used to calculate the specific surface areas of freeze-dried LDH. Measurements were carried out on a Quantachrome Nova 2000e analyzer. The specific surface area was determined using 5 points within the range of $0.05 < p/p_0 < 0.3$ using N₂ as adsorption gas. All samples were degassed overnight at 110 °C under ultra high vacuum.

Scanning electron microscope (SEM) measurements were carried out on a Zeiss 1530 FESEM (acceleration voltage of 3 kV). The samples were freeze-dried then mounted on conductive sample holders and sputtered with carbon.

Transmission electron microscope (TEM) measurements were carried out on a Zeiss EM 922 EFTEM with an acceleration voltage of 200 kV. Specimens were microtomed to obtain 30-70 nm thick pieces, which were placed on a lacey carbon copper grid.

The suspension stability tests were carried out in a Lumifuge 114 stability analyzer. Suspensions of LDH and modified LDH (0.25 wt%) were centrifuged for 900 s with gradually increasing centrifuge velocities (300, 400, 500 rpm).

Solution blending was carried out in a three roll mill (Exakt-80E) at -23 °C. All samples were passed through the mill 7 times. The roller distance was gradually lowered from initially 25 µm in the first cycle to 5 µm in the final cycle.

The cone calorimeter experiments were carried out using an ULTRAMAT 6 instrument from FIRE (35 kW/m² heat flux with horizontal orientation of the samples) according to ASTM E 1354, on 100 x 100 mm² plaques (4 mm thickness) prepared by melt pressing at 190 °C for 8 min. All samples were tested in triplicate and the recorded cone data were reproducible to within ±5 %.

2.3. Synthesis of Magnesium Aluminum Carbonate Layered Double Hydroxides (Mg/Al-CO₃-LDH)

Mg/Al-CO₃-LDH was synthesized applying the urea hydrolysis method (24). An aqueous solution of a mixture of metal salts (1.3 l, 0.5 M total metal concentration, Mg:Al-ratio; 2:1) of MgCl₂.6H₂O (88.1 g, 0.43 mol) and AlCl₃.6H₂O (52.3 g, 0.22 mol) was refluxed in the presence of urea (128.9 g, 2.1 mol) for 36 h. The suspension was then centrifuged and washed with deionized water. The obtained slurry was next re-suspended in a solution of sodium bicarbonate (1 l, 0.4 mol) and aged at 60 °C over night. The resulting white precipitate was centrifuged and repeatedly washed with deionized water until a test for chloride with AgNO₃ was negative. Please note that the obtained LDH was not dried but was rather stored as aqueous suspension.

3.4. Surface Modification and Suspension Stability of LDH

For surface modification, the aqueous LDH-suspension was centrifuged and then re-suspended (5 wt%) in ethanol which contained the siderophilic ligand 3,4-dihydroxybenzophenone (0.5×10^{-3} mol). To complete surface modification, the suspension was ultrasonified for 3 min and was then shaken for 30 min in a rotary shaker.

Finally, the suspension was centrifuged and washed with ethanol and tetrahydrofuran (THF). At last, the surface modified LDH-DBP was re-suspended in THF at a solid content of 5 wt%.

To compare suspension stability, suspensions of 0.25 wt% of the LDH and the surface modified LDH-DBP were prepared in THF. The measurement was carried out using the Lumifuge with increasing centrifuge velocities (300, 400, 500 rpm).

2.5. Preparation of PS/LDH Nanocomposites by Solution Blending

PS/LDH nanocomposites were prepared by adding appropriate amounts of the 5 wt% suspension of LDH-DBP in THF to a solution of 25 wt% of PS in THF to achieve loadings of 5, 10, and 15 wt% in the final nanocomposites. The dispersions were first mixed for 30 min using an overhead stirrer (500 rpm, RT). Afterwards, the dispersion was further homogenized applying a three roll mill. Despite cooling at -23 °C a good share of THF evaporated in the course of three roll milling (1 h) and highly viscous dispersions were obtained which were dried in a vacuum oven (80 °C, 600 mbar, 3 h). For better processability, all samples were ground into a powder in a planetary ball mill (5 min, 350 rpm) and dried again in a vacuum oven (110 °C, 300 mbar, 24 h) to remove remaining traces of THF. Moreover, a blank sample of the virgin polymer was prepared following the same described procedure. Finally, the dried powders were hot pressed for cone calorimetric analysis.

3. Results and Discussions

3.1. Synthesis, Morphology, and Stirred Media Milling of Mg/Al-CO₃ LDH

LDH was synthesized by the urea hydrolysis method with a Mg:Al ratio of 2:1. By raising the temperature to 100 °C, hydrolysis of urea was accelerated and pH rose to 9 - 10, which is a suitable pH to precipitate LDHs. The urea hydrolysis method is also called the homogeneous precipitation method and produces well ordered, crystalline LDHs of high aspect ratio with carbonate (CO₃²⁻) as charge balancing interlayer anions whereas the more frequently used co-precipitation method produces disordered, low crystalline LDHs of comparatively lower aspect ratio but more variable interlayer anions (in particular Cl⁻ or NO₃⁻-LDH are also accessible). Due to the high charge density and the low hydration enthalpy of carbonate, CO₃²⁻-LDHs, however, cannot be directly ion exchanged/intercalated with other organic/inorganic anions, in contrast to the nitrate or chloride containing LDHs obtained by the co-precipitation method.

Although the urea hydrolysis method in principal delivers platelets of larger aspect ratio, the product was obtained as tightly intergrown crystals of so-called rose-like aggregates (Figure 1).

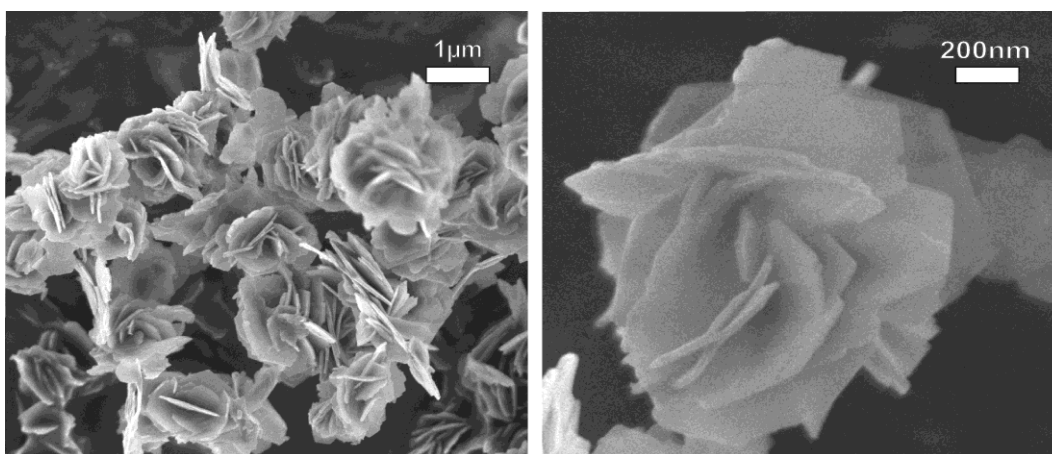


Figure 1. SEM images of LDH synthesized by the urea hydrolysis method showing the rose-like aggregate morphology at low (left) and high (right) magnification.

Disaggregation of rose-like morphologies required strong shearing forces as supplied e.g. by stirred media mills. By stirred media milling of the as-synthesized LDH in an aqueous medium, two crucial features could be significantly improved: i) the aspect ratio, which is the ratio between the diameter and the thickness of the particles, and ii) the interface area between the polymer matrix and the LDHs (filler) because the specific surface area of the LDH increased.

The influence of stirred media milling on the PSDs is presented in Figure 2. Please note that SLS measures the hydrodynamic diameter of the platelets which is closely related to the lateral extension. The thickness can only be determined by the Scherer broadening of basal reflections. However, due to the high layer charge density of LDHs and the low hydration enthalpy of carbonate anions, the electrostatic attraction between positively charged layer and negatively charged interlayer was found to be too strong as to allow for any exfoliation. Although stirred media mills provide considerable shearing forces and are for instance capable to exfoliate hectorite clays (25), we noticed no increase of the full widths of half maximum of the 003 basal reflections (Figure 3). The shearing forces produced in this mill were insufficient to induce any exfoliation. The suspension of non-milled LDH (referred to as LDH) in water had a median particle diameter of $9 \mu\text{m}$ that was attributed to rose-like aggregates of singular platelets.

Stirred media milling for 5 min (LDH-SMM 5min), disaggregated already most of the particles and a bimodal PSD with maxima at 1.2 and 0.4 μm , respectively, was observed. After 20 min (LDH-SMM 20min), all aggregates were destroyed and a median particle diameter of 0.4 μm was observed. At this point the mono-modal size distribution suggested that all rose-like structures are disaggregated.

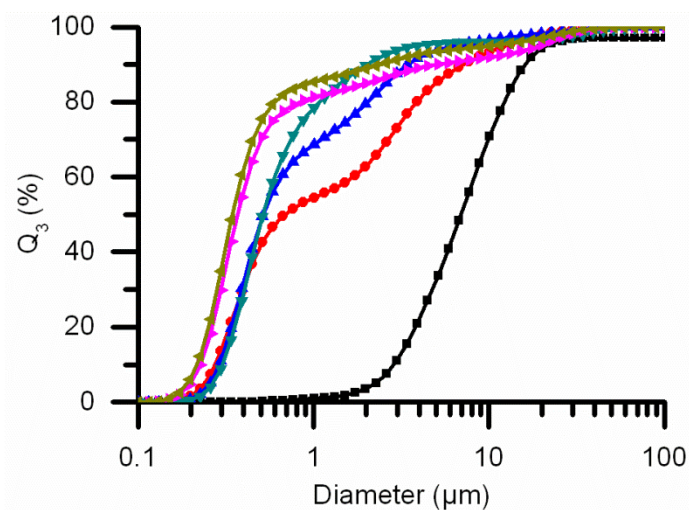


Figure 2. Particle size distributions of (■) LDH (●) LDH-SMM 5min (▲) LDH-SMM 10min (▼) LDH-SMM 20min (◆) LDH-SMM 30min, and (◄) LDH-SMM 60min. All measurements were done in an aqueous suspension.

Further stirred media milling partially breaks the disaggregated singular platelets as indicated by the gradual shift of median particle diameter to 0.3 μm for 60 min (LDH-SMM 60min). Breakage of particles was accompanied by an increase of specific surface area caused by additional edge surface produced. The calculated specific surface areas (BET method) for LDH, LDH-SMM 30min, and LDH-SMM 60min are 45, 64, and 84 m^2/g , respectively.

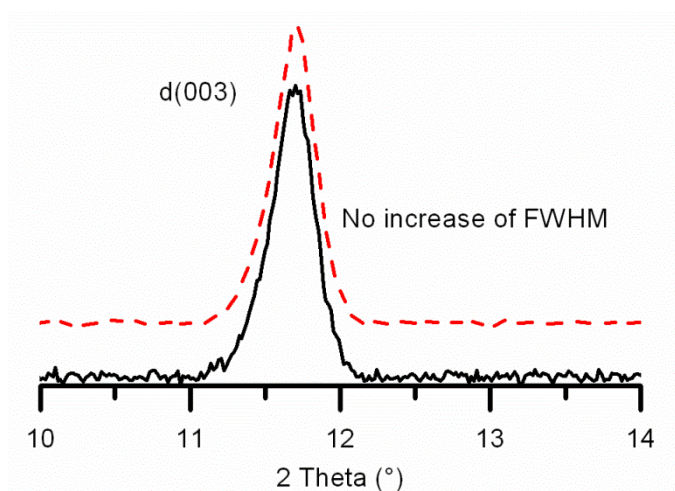


Figure 3. PXRD pattern of the LDH (—) and LDH-SMM 60min (---).

Please note, that, since no exfoliation was observed, this increase of specific surface area was solely related to breakage of platelets and thus concomitantly the aspect ratio was significantly reduced. These LDHs with different specific surface areas and aspect ratios were used for preparation of PS nanocomposite to evaluate the influence of these LDHs features on the flame retardant properties.

3.2. Surface Modification and Suspension Stability of LDHs

Because of strong selective adsorption of carbonate anions, LDH, in contrast to ordinary cationic clays, like MMT (zeta potential typically > -40 mV), have a small zeta potential ($\approx +25$ mV) which moreover is strongly dependant on CO_2 and CO_3^{2-} concentration. In 0.01 M Na_2CO_3 solution the surface was even “umgeladen” and the zeta potential then was -20 mV. Consequently, modification of LDHs by anion exchange at external basal planes was found not to be a particularly robust process. Therefore, based on previous work on kaolinite modification (23, 26), we choose an unconventional modifier for LDHs, siderophilic ligands. These ligands form selectively very stable complexes with trivalent metal cations in solution or at heterogeneous external basal surfaces of LDHs. Since the complexation reaction is independent of Coulomb attraction, the charge status of the surface is irrelevant in a first approximation. The structure of the siderophilic ligand used here for surface modification, 3,4-dihydroxybenzo-phenone, is shown in Figure 4.

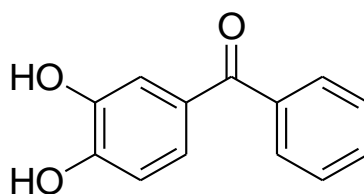


Figure 4. Structure of the organic siderophilic surface modifier; 3,4-dihydroxybenzophenone (DBP).

Appropriate surface modification in the course of preparing PS/LDH nanocomposites via solution blending has to serve two main purposes: i) Stabilization of modified LDH in organic solvents, and ii) compatibilization of the filler with the hydrophobic polymer matrix, which prevents re-aggregation and thus fosters a homogenous dispersion of the filler.

PXRD patterns of LDH-DBP (Figure 5) did not indicate any shift in the d-spacing values and hence confirmed that the modifier is not intercalated but only modified the external basal surface of the octahedral layer by complexation. Success of the surface modification was indicated by the tainted yellow color of the surface modified LDH (Figure 7) inherited by the ligand.

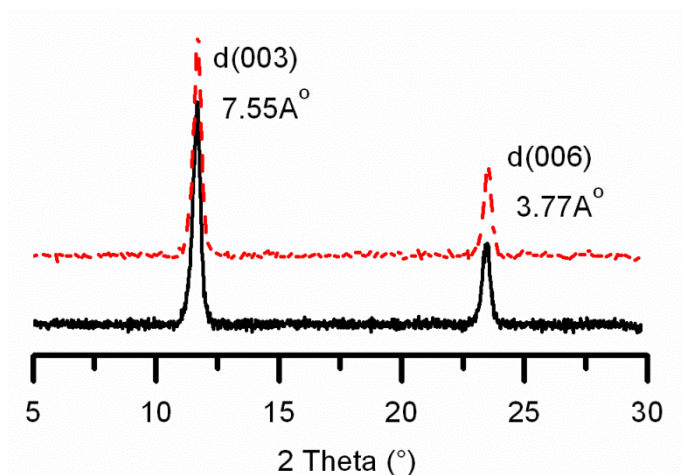


Figure 5. PXR D pattern of the LDH (—) and LDH-DBP (---).

The stability of the suspensions of LDH and LDH-DBP in an organic solvent, THF, was compared by using the Lumifuge. The transmission of light through a horizontal centrifuge cell was measured during centrifugation at different velocities providing important semi-quantitative information about the sedimentation kinetics of these suspensions at low solid concentration (in our case 0.25 wt%). For stable suspensions (LDH-DBP/THF), less transmission is recorded, due to absorption/scattering of light by particles kept in suspension.

On the other hand, for unstable suspensions (LDH/THF), the particles sediment readily, and hence, more light was transmitted through the sample and a higher transmission is recorded as compared to the stable suspensions as shown in Figure 6.

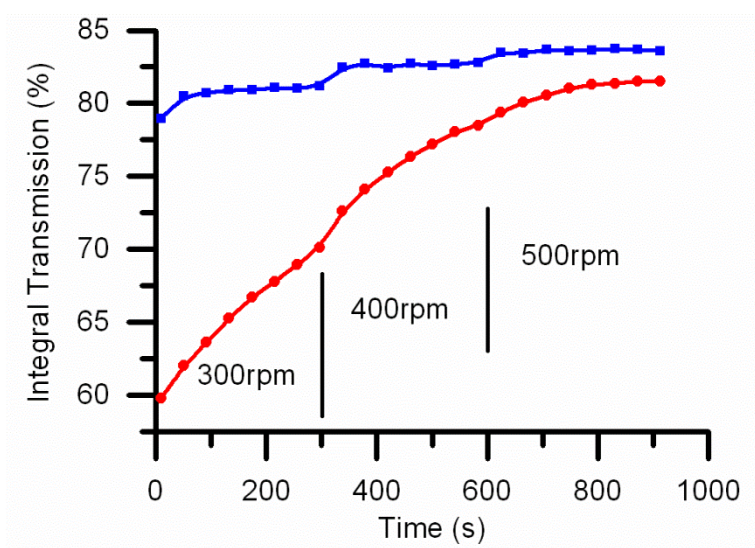


Figure 6. Sedimentation kinetics of LDH (■) and the surface modified LDH-DBP (●) in THF as determined by centrifugation forced sedimentation using a Lumifuge. Vertical lines indicate times when the centrifugation velocity was increased stepwise.

While the instable LDH/THF suspension clarified quickly, the LDH-DBP/THF suspension remained more stable even at high centrifugation velocities. At the beginning of the measurement, only 59 % of the light was transmitted through the LDH-DBP/THF suspension while for the LDH/THF suspension 78 % of the light was transmitted. By centrifugation at higher velocities, both suspensions clarify due to forced sedimentation but the stabilized LDH-DBP/THF did so at much reduced pace. The results of the Lumifuge experiment are confirmed by static sedimentation tests (Figure 7).

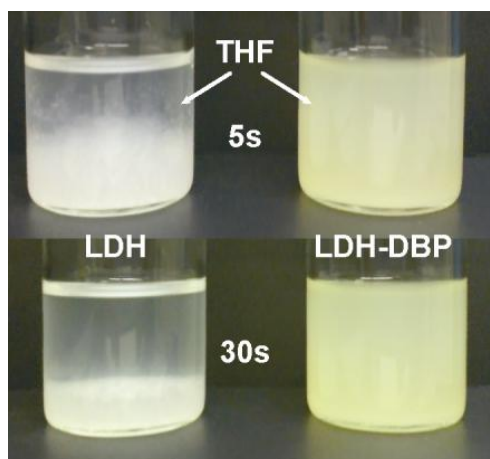


Figure 7. Photographs of THF suspensions of LDH (left) and LDH-DBP (right).

3.3. Compounding by Solution Blending

The specific interface area in a nanocomposite is crucially dependant on the specific surface area of the filler and the quality of the dispersion which defines the share of the surface area being active in the composite. Therefore, the quality of dispersion of fillers is always considered to have an essential effect on fire retardancy of nanocomposites (15). In order to optimize the dispersion and to take advantage of the full potential of the filler, special care was taken in handling the filler.

For instance we avoided drying of LDH throughout all steps, this way electrosteric stabilization helped in minimizing agglomeration/aggregation of the LDH particles. Moreover, solution blending was carried out in two steps to achieve a homogenous dispersion: i) suspension of the surface modified LDH was first mixed with the polymer solution using an overhead stirrer. ii) Then homogenization and disaggregation was pushed by applying high shear forces by milling the dispersions in a three roll mill. Seven cycles were applied at different milling velocities and roller distances (from 25 μm down to 5 μm) at -23 $^{\circ}\text{C}$.

Despite the cooling, due to the energy input and the high surface nevertheless most of the solvent was removed during three roll milling and a highly viscous dispersion was obtained.

To evaluate the efficiency of solution blending and to check the dispersion quality, the resulting highly viscous dispersions were diluted with THF again and then the PSDs were determined by SLS. The results were compared to the PSDs of the pristine suspension of surface modified LDH in THF before solution blending (Figure 8).

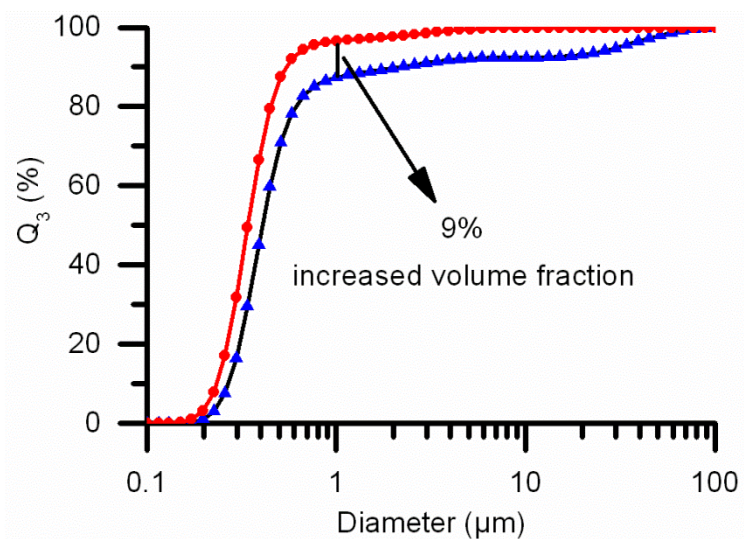


Figure 8. Particle size distributions of (▲) LDH-SMM 60min-DBP and (●) PS/LDH-SMM 60min-DBP-5wt% -7 cycles three roll mill.

Comparison of the PSDs underlines the quality of compatibilization applying the siderophilic ligand and dispersion by three roll milling. The applied shear forces even increased the volume fraction of non-aggregated particles $< 1 \mu\text{m}$ by 9 %, suggesting the solution blending did not induce any aggregation and that the maximum potential interface area could be assured by this type of solution blending affording a three roll mill. This will allow probing the full potential of the different fillers since the specific surface area of the filler was fully converted to specific interface area in the PS/LDH nanocomposites produced by solution blending.

Figure 9 shows TEM images of the PS/LDH-SMM 30min-DBP-5wt% nanocomposite. LDH particles appeared well dispersed and no rose-like aggregates could be observed. Please note that no exfoliation has occurred either by stirred media milling or by solution blending in a three roll mill.

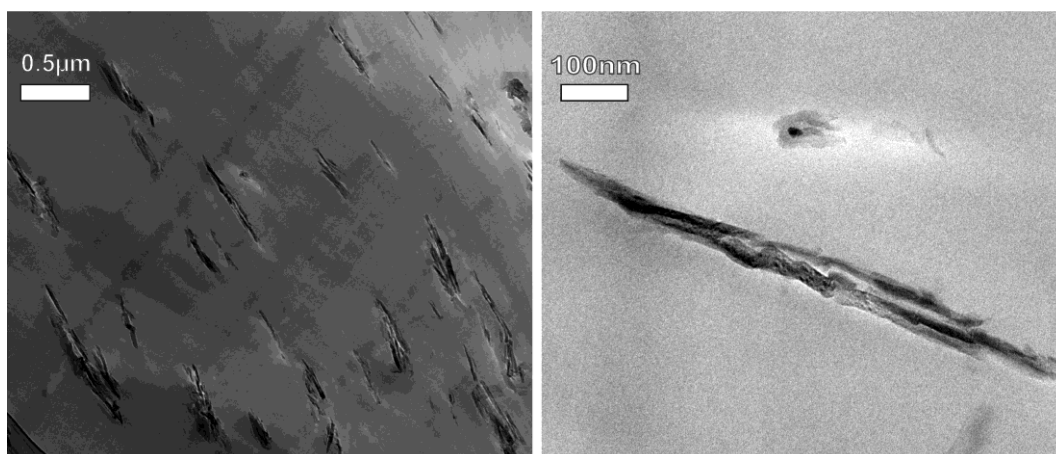


Figure 9. TEM images of PS/LDH-SMM 30min-DBP-5wt% at low (left) and high (right) magnification.

3.4. Thermal Decomposition of LDHs

The flame retardancy effect of inorganic fillers, like ATH and LDHs, is related to heat consumption and release of inert gases (H_2O , CO_2) produced by decomposition of the inorganic filler during combustion of nanocomposites. To quantitatively evaluate the heat consumption by LDH as compared to conventional ATH additives, differential scanning calorimetric (DSC) analysis was applied (Figure 10). Although structurally closely related, the decomposition of ATH and LDH is quite different. As known from literature, the endothermic decomposition of LDH occurred in three separate steps: i) dehydration, ii) dehydroxylation, and iii) decarbonation, whereas the decomposition of ATH occurred in one step.

Please note that the exact temperatures at which the individual steps are observed vary a great deal with the type of octahedral cations and the layer charge of the LDH. In principle these decomposition steps could even be tailored to best fit the particular matrix and its decomposition kinetics. For the particular composition chosen here, the onset temperature for the dehydration of interlayer water of LDH is as low as 146°C . This implies that dehydration will at least partially have occurred during processing.

Remaining interlayer water will, however, induce an early cooling effect that spreads over a wider temperature range as compared to ATH. The heat consumption of ATH is solely related to dehydroxylation which represents a much sharper endothermic event. The heat consumption by ATH (931 J/g) is, however, 47% higher than the total heat consumption by LDH (490 J/g).

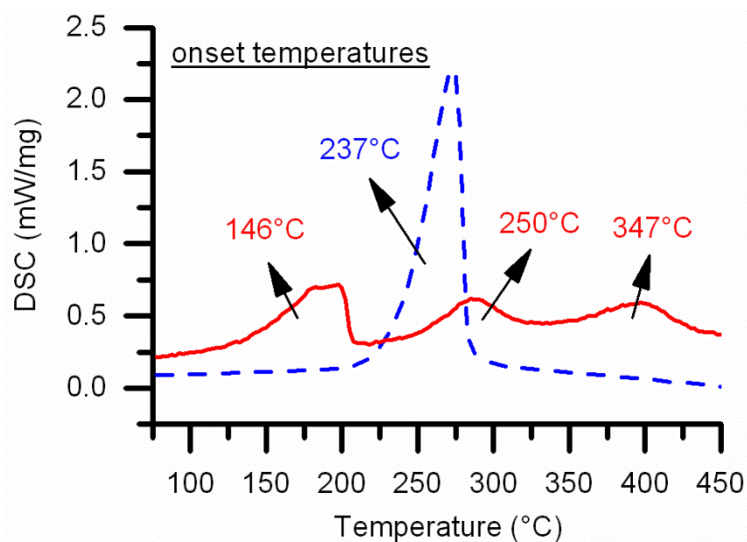


Figure 10. Differential scanning calorimetry curves (DSC) for LDH (—) and ATH (---) measured at a heating rate of 1 °C/1 min.

3.5. Cone Calorimeter Data

In a systematic effort to evaluate the effect of the specific surface area versus the aspect ratio of LDH on the flame retardant properties of PS/LDH nanocomposites, LDH with different specific surface areas obtained with different synthesis routes were prepared. The specific surface area of large aspect ratio LDH obtained by urea hydrolysis was increased to different levels by means of stirred media milling as described before. Furthermore, a commercially available LDH (LDH-syntal supplied by Süd-Chemie) produced by co-precipitation and thus showing low aspect ratio but a high specific surface area of 74 m²/g was included. The LDH as obtained from the urea hydrolysis method has a specific surface area of 45 m²/g. After stirred media milling for 30 and 60 min, the specific surface areas increased to 64 and 84 m²/g, respectively. The different LDHs were surface modified in the same way and PS/LDH nanocomposites with a constant loading of 5 wt% were produced by solution blending while dispersion was assisted by three roll milling. Finally, their flame retardant properties were investigated by cone calorimeter.

Cone calorimetry analysis is an essential analysis to determine the fire properties of polymer nanocomposites. Information is collected about the time to ignition (t_{ign}), the heat release rate (HRR), the peak of heat release rate (PHRR), the total heat release (THR), and burn out time. For perfect flame retardants, as known from literature, it is favorable to increase t_{ign} , decrease PHRR and THR, and increase the burn out time.

Table I summarizes the cone data for LDHs with different surface areas and aspect ratios, while the heat release rate curves obtained at a heat flux of 35 kW/m² are shown in Figure 11. A maximum reduction in the peak of heat release rate of 36 % was obtained by PS/LDH nanocomposite using LDH-SMM 30min. As suggested by the PSD (Figure 2) at this point of stirred media milling, rose aggregates were already destroyed while little breakage of singular platelets had occurred. This filler thus represents the material with the largest aspect ratio. Prolonged stirred media milling further increased the specific surface area but on the cost of reducing the aspect ratio. For these samples, despite the increase of the specific surface areas (Table I), the flame retardancy deteriorated suggesting that the aspect ratio is more important than specific interface area. It is however not clear at this point, whether the main role of the aspect ratio is reduction of gas permeability or reinforcement of the char.

Table I. Cone calorimeter data for PS/LDH nanocomposites

<i>Formulation</i>	<i>PHRR (kW/m²)</i>	<i>PHRR Reduct. (%)</i>	<i>THR (MJ/m²)</i>	<i>T_{ign} (s)</i>	<i>specific surface area (m²/g)</i>
PS	813 ± 29	-	138 ± 2	88 ± 3	-
PS/LDH-DBP - 5wt%	616 ± 13	24	133 ± 3	72 ± 2	45
PS/LDH-SMM 30min-DBP-5wt%	517 ± 17	36	133 ± 3	65 ± 3	64
PS/LDH-SMM 60min-DBP-5wt%	621 ± 25	23	131 ± 4	66 ± 1	84
PS/LDH-syntal-DBP-5wt%	627 ± 8	22	129 ± 1	59 ± 2	74

The time to ignition (ease of ignition) is reduced for all PS/LDH nanocomposites. This reduction ranges between 16 and 33 % for PS nano-composites with LDH and LDH-syntal, respectively. Reduction of t_{ign} commonly is attributed to the content of the easily flammable organic modifier, since most of the organic modifiers have lower onset temperature than the virgin polymer. Alternatively, the filler might act as heterogeneous catalyst in the degradation of the virgin polymer.

With our samples, the surface modification being restricted to outer basal planes considerably reduces the organic content as compared to intercalated LDHs commonly used. Please note that for intercalated LDH, the organic content could reach 30 - 40 wt% of the modified LDHs and reductions of t_{ign} up to 80 % may be observed (4).

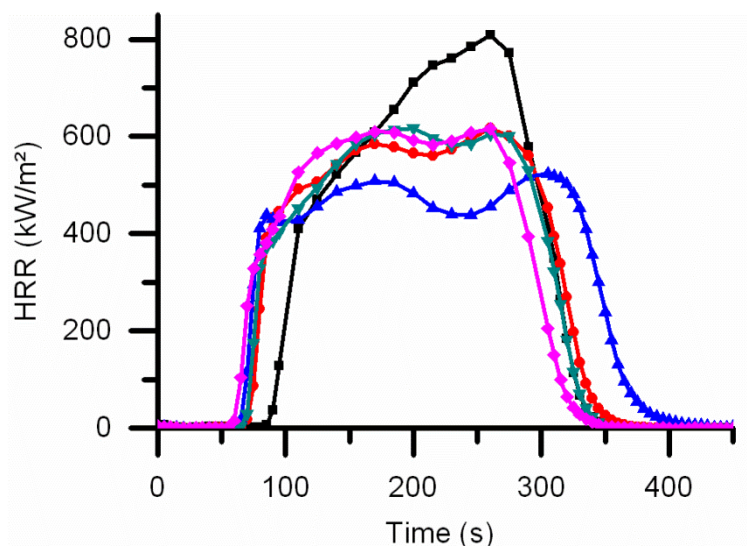


Figure 11. Heat release rate curves for PS/LDH nanocomposites at different surface areas: (■) PS (●) PS/LDH-DBP-5wt% (▼) PS/LDH- syntal-DBP-5wt% (▲) PS/LDH-SMM 30min-DBP-5wt% (◆) PS/LDH-SMM 60min-DBP-5wt%.

The increase of viscosity of nanocomposites as compared to neat polymers is closely related to specific interface area which limits the maximum filler content that can still be processed. If the specific surface, however, plays a minor role in the retardancy mechanism, the lower values of LDH ($45 \text{ m}^2/\text{g}$) as offers the advantage that much higher filler contents (more than 10 wt%) can be explored.

Table II and Figure 12 present the cone calorimeter data and the heat release rate curves for PS nanocomposites with LDH at increasing loadings (5, 10, and 15 wt%) measured at a heat flux of 35 kW/m^2 . For the nanocomposites with higher LDH loadings, the PHRR is significantly decreased which could be the result of the endothermic decomposition of LDH (thermal quenching) that releases water and CO_2 and, hence, cools the surface of the burning polymer and dilutes the combustible gases (inert gas dilution).

A maximum reduction of PHRR of 51 % was achieved at 15 wt% loading. At this loading, the HRR curve was spread over a wide range of time and shifted towards a higher burn out time value (from 370 to 960 s), which indicates a slower transfer of mass and heat during the combustion of the polymer (longer burning time at lower HRR). This spread, which only sets in at higher loadings, may be related by the formation of a thin layer of char and residues of metal oxides that insulate the polymer from heat radiation.

Table II. Cone calorimeter data for PS/LDH nanocomposites

<i>Formulation</i>	<i>PHRR</i> (kW/m ²)	<i>PHRR</i> <i>Reduct.</i> (%)	<i>THR</i> (MJ/m ²)	<i>T_{ign}</i> (s)
PS	813 ± 29	-	138 ± 2	88 ± 3
PS/LDH-DBP-5wt%	616 ± 13	24	133 ± 3	72 ± 2
PS/LDH-DBP-10wt%	444 ± 12	45	127 ± 2	74 ± 2
PS/LDH-DBP-15wt%	402 ± 15	51	125 ± 2	95 ± 2

Surprisingly, contrary to the usual decrease of t_{ign} observed for all lower loadings, for 15 wt% loading instead an increase of 8 % of t_{ign} was observed. We suggest that the PS/LDH nanocomposite at 15 wt% loading released more water during early stages of decomposition and therefore diluted the combustible gases sufficiently to delay the ignition.

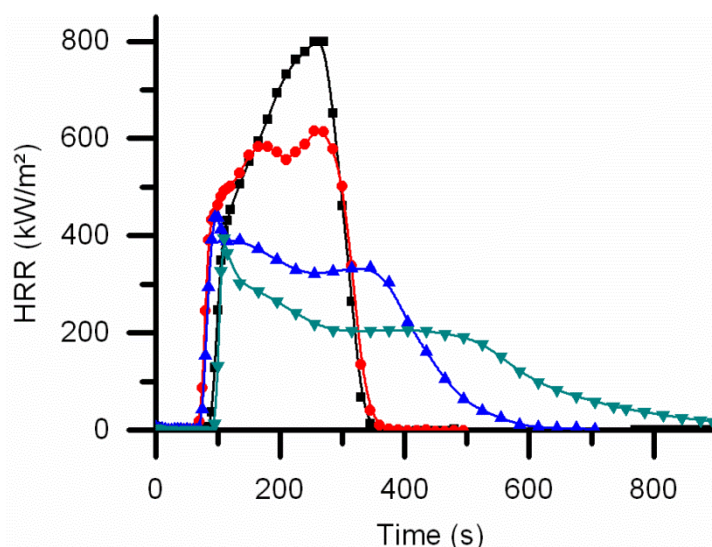


Figure 12. Heat release rate curves for PS/LDH nanocomposites at different loadings; (■) virgin PS (●) 5wt% (▲) 10wt%, and (▼) 15wt%.

Figure 13 shows the total heat release of PS/LDH nanocomposite at different loadings. The total heat release was consistently decreased with increasing LDH loadings (from 138 MJ/m² for virgin PS to 125 MJ/m² for PS/LDH at 15 wt% loading) while at the same time the final value was achieved at increasing time lags. The reduction of total heat release may be explained by first the reduction of the mass of combustible polymer when more LDH is added (reduction of the fuel content) and second the thermal dissipation effect due to the endothermic nature of the decomposition of LDH.

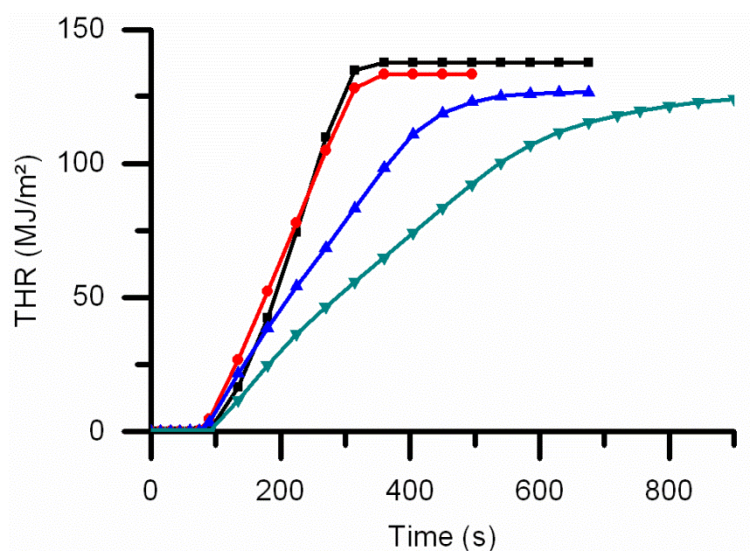


Figure 13. Total heat release curves for PS/LDH nanocomposites at different loadings; (■) virgin PS (●) 5wt% (▲) 10wt%, and (▼) 15wt%.

This effect is comparable to MDH and ATH flame retardants. For intercalated types of LDH-fillers, no appreciable reduction of total heat release was observed (4, 27) which might be attributed to the high organic content which increases the fire load, and consequently counterbalances the cooling effect of the filler on total heat release. The combustion residues of different PS/LDH nanocomposites at different loadings are shown in Figure 14. With increasing LDH loadings more carbonaceous char was formed suggesting that LDHs promoted char formation. Nevertheless, the char surfaces were not continuous but rather had a lot of cracks.

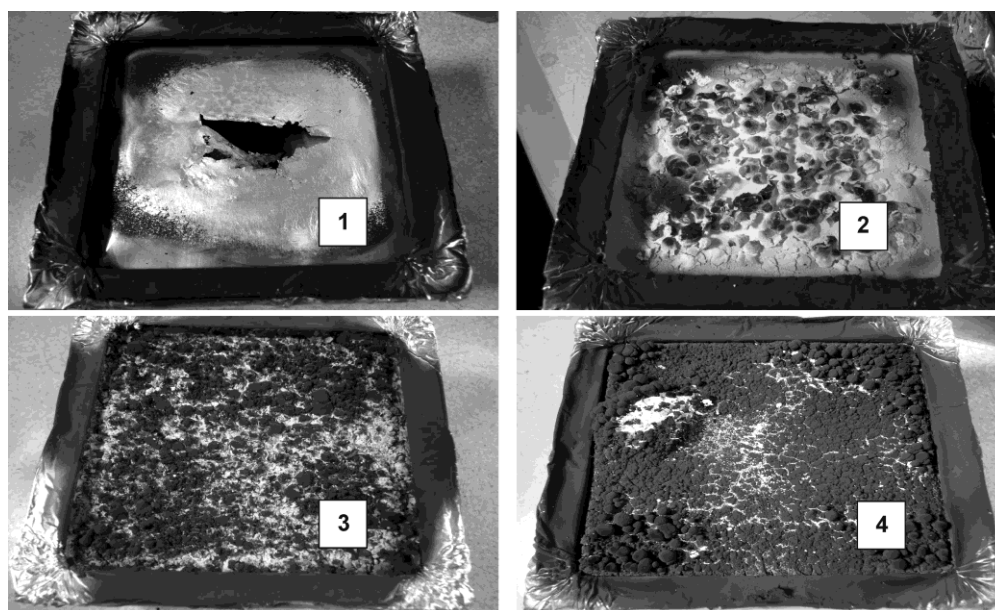


Figure 14. Photographs represent a comparison between the residues of the cone test (1) PS (2) PS/LDH-DBP-5wt% (3) PS/LDH-DBP-10wt% and (4) PS/LDH-DBP-15wt%.

4. Conclusions

We present a new approach for surface modification of LDH selective to external basal surfaces using a siderophilic ligand (3,4-dihydroxybenzophenone). LDHs were synthesized by urea hydrolysis method. This modification provides a stable suspension in organic solvents and a good compatibility with the polystyrene matrix. We systematically investigated the influence of specific surface area and aspect ratio of LDH on flame retardancy of PS nanocomposites prepared by solution blending in a three roll mill. The specific surface area and aspect ratio of LDH were varied by means of stirred media milling. Flame retardant properties were determined by cone calorimeter analysis. Cone calorimeter data suggest that aspect ratio is more important than specific surface area of the fillers investigated. A maximum reduction of PHRR of 51% could be achieved at a loading of 15wt%. Interestingly, at this loading an unusual increase of t_{ign} could be observed. The data underline the potential of large aspect ratio LDH which certainly can be further optimized by applying more sophisticated surface modifiers.

Acknowledgment

The authors thank Prof. Dr. V. Altstädt, Department of Polymer Engineering, University of Bayreuth, for his assistance for the hot pressing of the cone samples. B. D-B. also acknowledges the German Academic Exchange Service (DAAD) for financial support. This work was further supported by the Deutsche Forschungsgemeinschaft (DFG) within the Collaborative Research Center (SFB) 840.

References

1. Law, R. J.; Herzke, D.; Harrad, S.; Morris, S.; Bersuder, P.; Allchin, C. R. *Chemosphere* **2008**, *73*, 223-241.
2. Birnbaum, L. S.; Staskal, D. F. *Environ Health Perspect* **2003**, *112*, 9-17. 3. Nyambo, C.; Chen, D.; Su, S.; Wilkie, C. A. *Polym. Deg. Stab.* **2009**, *94*, 1298-1306.
4. Nyambo, C.; Songtipya, P.; Manias, E.; Jimenez-Gasco, M. M.; Wilkie, C. A. *J. Mater. Chem.* **2008**, *18*, 4827-4838.
5. Nyambo, C.; Kandare, E.; Wang, D.; Wilkie, C. A. *Polym. Deg. Stab.* **2008**, *93*, 1656-1663.
6. Costa, F. R.; Wagenknecht, U.; Heinrich, G. *Polym. Deg. Stab.* **2007**, *92*, 1813-1823.

7. Chen, W.; Qu, B. *J. Mater. Chem.* **2004**, *14*, 1705-1710.
8. Ramaraj, B.; Nayak, S. K.; Yoon, K. R. *J. Appl. Polym. Sci.* **2010**, *116*, 1671-1677.
9. Pereira, C. M. C.; Herrero, M.; Labajos, F. M.; Marques, A. T.; Rives, V. *Polym. Deg. Stab.* **2009**, *94*, 939-946.
10. Sahu, B.; Pugazhenti, G. *J. Appl. Polym. Sci.* **2011**, *120*, 2485-2495.
11. Nogueira, T.; Botan, R.; Wypych, F.; Lona, L. *Composites Part A* **2011**, *42*, 1025-1030.
12. Ding, P.; Qu, B. *J. Colloid Interface Sci.* **2005**, *291*, 13-18.
13. Evans, D.; Slade, R. In *Layered Double Hydroxides*; Duan, X., E; Evans, D. Ed.; Structure and Bonding 119; Springer Berlin / Heidelberg: 2005, Vol. 119, pp. 1-87.
14. Schutz, M. R.; Kalo, H.; Lunkenbein, T.; Breu, J.; Wilkie, C. A. *Polymer* **2011**, *52*, 3288-3294.
15. Schutz, M. R.; Kalo, H.; Lunkenbein, T.; Groschel, A. H.; Muller, A. H. E.; Wilkie, C. A.; Breu, J. *J. Mater. Chem.* **2011**, *21*, 12110-12116.
16. Greenwell, H. C.; Jones, W.; Rugen-Hankey, S. L.; Holliman, P. J.; Thompson, R. L. *Green Chem.* **2010**, *12*, 688-695.
17. Wypych, F.; Satyanarayana, K. G. *J. Colloid Interface Sci.* **2005**, *285*, 532-543.
18. Oh, J. M.; Biswick, T. T.; Choy, J. H. *J. Mater. Chem.* **2009**, *19*, 2553-2563.
19. Costa, F. R.; Leuteritz, A.; Meinel, J.; Wagenknecht, U.; Heinrich, G. *Macromol. Symp.* **2011**, *301*, 46-54.
20. Newman, P.; Jones, W. *New J. Chem.* **1998**, *22*, 105-115.
21. Sancho, M. I.; Jubert, A. H.; Blanco, S. E.; Ferretti, F. H.; Castro, E. A. *Spectrochim. Acta, Part A* **2007**, *68*, 387-393.
22. Golounin, A. V.; Shchedrin, Y.; Fedorov, V. A. *Russ. J. Org. Chem.* **2001**, *37*, 1266-1269.
23. Hirsemann, D.; Shylesh, S.; De Souza, R. A.; Diar-Bakerly, B.; Biersack, B.; Mueller, D. N.; Martin, M.; Schobert, R.; Breu, J. *Angew. Chem. Int. Ed.* **2012**, *51*, 1348-1352.

24. Costantino, U.; Marmottini, F.; Nocchetti, M.; Vivani, R. *Eur. J. Inorg. Chem.* **1998**, 1998, 1439-1446.
25. Ziadeh, M.; Chwalka, B.; Kalo, H.; Schuetz, M. R.; Breu, J. *Clay Miner.* **2012**, in press.
26. Hirsemann, D.; Koester, T. K. J.; Wack, J.; van Wuellen, L.; Breu, J.; Senker, J. *Chem. Mater.* **2011**, 23, 3152-3158.
27. Manzi-Nshuti, C.; Chen, D.; Su, S.; Wilkie, C. A. *Polym. Deg. Stab.* **2009**, 94, 1290-1297.

5.3. Appendix 3: Superior Flame Retardant by Combining High Aspect Ratio Layered Double Hydroxide and Graphene Oxide

Bashar Diar-Bakerly¹, Patrick Feicht, Andreas Edenharter¹, Günter Beyer², Josef Breu^{1,*}

¹) Department of Inorganic Chemistry I, University of Bayreuth, Universitaetsstr. 30, 95447 Bayreuth, Germany

²) Kabelwerk Eupen AG, 4700 Eupen, Belgium

Corresponding author: Prof. Dr. Josef Breu, Universitaetsstr. 30, 95440 Bayreuth, Germany

* E-mail: josef.breu@uni-bayreuth.de

Abstract

By combining two platy nano-additives with high aspect ratio, a layered double hydroxide (LDH) and graphene oxide (GO), a superior flame retardant was obtained showing a tremendous flame retardancy in polystyrene nanocomposite. The nanocomposites were prepared via solution blending from tetrahydrofuran utilizing a three-roll mill for better compounding. Highly stable suspension of a mixture of the two nano-additives in THF afforded a sophisticated surface modifications of LDH and GO using 3,4-dihydroxybenzophenone (DBP) and 1-dodecylamine (DDA), respectively. Forced sedimentation tests and particle size distribution confirmed the good dispersion and suggested that heterocoagulation between the two types of oppositely charged colloids could be prevented by the appropriate combination of surface modifiers. Cone calorimetry revealed a considerable synergism as indicated by a significant reduction of the peak of heat release rate of 47 % at a very low loading (5.5 wt%). Most interestingly, due to formation of a protective layer, the steady combustion occurred at a much reduced heat release rate, and consequently, the related burn out time was prolonged by 154 %.

Keywords: polystyrene nanocomposite, synergistic flame retardant, layered double hydroxide, graphene oxide, surface modification.

1. Introduction

In order to overcome the flammability problems of polymers, flame retardants (FRs) have become an essential part of polymer formulations [1-11] and a wide range of FRs were commercialized during the last decades. On a quantity base the FRs market is dominated by aluminum trihydroxide (ATH) and halogenated FRs [12]. However, high loadings of ATH

(up to 65 wt%) are required to get sufficient flame retardancy, which in turn severely deteriorates the physical properties of the polymer matrices. Besides, halogenated FRs are threatened to be banned due to environmental concerns [13,14]. Thus, an increasing demand for halogen-free and innovative FRs is created.

Recently, an emerging class of FRs represented by inorganic layered materials (nano-additives) were intensively investigated [1,2,7,9]. These FRs include clays of the so-called 2:1 family (e.g., montmorillonite, hectorite), layered double hydroxides (LDHs), and graphite-based compounds (e.g., graphene oxide; GO, expanded graphite).

Various parameters of these nano-additives could be tailored, particularly the aspect ratio (α : particle diameter divided by its thickness). For instance, it was shown that increasing α of hectorite or LDHs lead to a significant enhancement of flame retardancy [1,8].

Moreover, it is well documented in the literature that the dispersion quality of nano-additives in polymer matrices has a crucial effect on their FR efficiency [3,7,8,10,15]. The specific interface between nano-additives and matrix needs to be maximized in order to achieve the best results. The specific interface may be maximized by reducing the surface tension between filler and matrix and thus improving the interaction between filler and matrix, while at the same time the interaction between adjacent filler particles is minimized to avoid aggregation. Commonly, dispersion quality was enhanced by organophilization of nano-additives through surface modification followed by compounding via solution blending [1,7].

The efficiency of such inorganic nano-additives was related to several factors such as i) cooling by endothermic degradation, ii) catalytic formation of a protective layer (char), iii) reinforcement of the char, and iv) increasing viscosity and melt temperature [1,2,8].

Combinations of conventional and new nano-additives were utilized to explore possible synergistic effects [16-19]. Nevertheless, it is still intricate to clearly identify a mechanism of synergism, since generally any given FR could introduce several interactions with the polymer at the same time. The synergism of different FRs is, however, an attractive concept in flame retardancy, which may provide higher efficiency at low loadings, hence, preserving the property characteristics of the polymer matrix. To the best of our knowledge, there are so far no studies that investigated a possible synergism between LDH and graphene oxide which could represent a potential FR system for polymer nanocomposites.

LDHs, also known as hydrotalcite-like compounds, are anionic clays that are structurally related to brucite with edge-sharing layers of octahedrally coordinated cations. Partial isomorphic substitution of the divalent cations by trivalent cations in the octahedral layer renders the layer to be positively charged. A variety of interlayer anions are possible that balance the layer charge resulting in the general formula of $[M(II)_{1-x}M(III)_x(OH)_2]^{x+}[A^{n-}_{x/n}]^{x-} \cdot mH_2O$, where M(II) and M(III) are divalent and trivalent metal cations, respectively, A^{n-} is the charge balancing interlayer anion, while x ranges between 0.2 and 0.33, and m refers to the number of interlayer water molecules [20,21]. These LDHs are i) chemically comparable to ATH as FRs, ii) easy to synthesize, ii) tunable (e.g., particle size, layer charge), and iii) considered as immobile and environmentally friendly FRs. Moreover, in order to enhance FR properties, LDHs were used in combination with conventional FRs that showed synergistic effects such as intumescent FRs (ammonium polyphosphate, melamine polyphosphate) or metal hydroxide/oxide (magnesium hydroxide, zinc oxide) [17-19].

Furthermore, graphite-based compounds with high α (> 10000) such as carbon nanotubes and graphene showed sufficient flame retardancy at relatively low loadings ($\approx 5\text{wt}\%$) in polymer nanocomposites [2,9,22-24]. However, these compounds are difficult to suspend in organic solvents and show a pronounced tendency to aggregate. Conversely, GO used in this study, possesses a large cation exchange capacity, can be easily surface modified by ion exchange and consequently, stable suspension in organic solvents could be obtained. Combining LDH with GO via solution blending, however, is still not trivial due to surface charges of opposite sign of anionic LDH and cationic GO. As a consequence heterocoagulation will arise if failing to reverse (“Umladen”) one of the two nano-additives by appropriate surface modification.

In this work, LDH with relatively high α (20-40) was combined with delaminated GO ($\alpha > 20000$) as FRs in PS nanocomposites. The main focus of this work was i) to achieve good dispersion of these peculiar nano-additives with surface charge of opposite sign in a hydrophobic polymer matrix and ii) to investigate a possible synergism indicated by decreasing the heat release rate (HRR).

2. Experimental

2.1. Materials

Polystyrene (PS 158K, melt index 3.00 g/10 min (200 °C/5kg, ASTM D1238), density 1.04 g/cm³, ASTM D792, glass transition temperature 100 °C, ISO 11357) was supplied by BASF.

For Mg/Al-LDH synthesis, urea and magnesium chloride hexahydrate were purchased from Grüssing GmbH, and aluminum chloride hexahydrate was purchased from Merck. The surface modifiers 1-dodecylamine (DDA) and 3,4-dihydroxybenzophenone (DBP) were purchased from Sigma-Aldrich and Alfa-Aesar, respectively. The organic solvents, ethanol and tetrahydrofuran, used for surface modification and solution blending were purchased from Sigma-Aldrich. Sulfuric acid, sodium nitrate, potassium permanganate, and hydrogen peroxide were purchased from Alfa-Aesar. Graphite flakes (RFL 99.5) were obtained from Kropfmühl AG. All chemicals were used as received.

2.2. Preparation of LDH

The urea hydrolysis method was used to synthesize Mg/Al-CO₃-LDH with Mg:Al-ratio of 2:1 [21]. An aqueous solution of a mixture of metal salts (1.3 l, 0.05 M total metal concentration) of MgCl₂·6H₂O (8.8 g, 0.04 mol) and AlCl₃·6H₂O (5.2 g, 0.02 mol) was refluxed in the presence of urea (12.9 g, 0.21 mol) for 36 h. The suspension was then centrifuged and washed with deionized water. The slurry obtained was next re-suspended in a solution of sodium bicarbonate (1 l, 0.4 mol) and aged at 60 °C over night. The resulting suspension was centrifuged and repeatedly washed with deionized water until a test for chloride with AgNO₃ was negative. The surface modification was achieved following our published procedure [1]. Briefly, the aqueous suspension of LDH was centrifuged and then re-suspended (5 wt%) in an ethanol solution of 3,4-dihydroxybenzophenone (0.5×10^{-3} mol). After 10 min of shaking, the suspension was centrifuged, washed first with ethanol, and then with THF. Finally, the surface modified LDH was stored in suspension (5 wt%, THF) for later solution blending. Please note that the obtained LDH was not dried during the different procedures rather it was stored as aqueous or THF suspension.

2.3. Preparation of graphene oxide

GO was prepared by a modified Hummers/Offeman method [25]. Briefly, 1 g of flake graphite and 1 g NaNO₃ were added to 30 mL of 98 % sulfuric acid aqueous solution. The suspension was mixed in an overhead shaker for 1 h at 25 °C (RT). Subsequently, 4 g of KMnO₄ was slowly added and it was then kept shaking for 12 h at RT. Afterwards, the suspension was diluted with water (1:1) and hydrogen peroxide was added until the suspension turned golden. After centrifugation it was dialyzed until the conductivity of the washing water was below 2 μS/cm. The low ionic strength is essential to achieve delamination of GO by osmotic swelling.

The surface modification of GO was done by a modified method described in the literature [26]. An EtOH solution of the modifier (DDA) was added to a hydrous suspension of delaminated GO (final water:EtOH ratio of 1:1). The concentration of the modifier was adjusted to 125 % of the CEC of GO (625 meq/100g) to ensure complete surface modification. The suspension was then shaken for 2 h at RT. Subsequently, the suspension was filtered, and finally, re-suspended in THF and the remaining water was distilled off azeotropically.

2.4. Compounding via three-roll mill

PS nanocomposites were prepared by adding appropriate amounts of suspension of the nano-additives in THF to a solution (25 wt%) of PS in THF. The dispersions were first mixed for 30 min using an overhead stirrer (500 rpm, RT). Afterwards, the dispersion was further homogenized applying a three-roll mill (Exakt-80E) placed in an exhaust hood. All samples were passed through the mill 6 times. The roller distance was gradually lowered from initially 25 μm in the first cycle to 5 μm in the final cycle. Despite cooling at -23 $^{\circ}\text{C}$ a good share of THF evaporated in the course of three-roll milling (1 h) and highly viscous dispersions were obtained which were pre-dried in a vacuum oven (80 $^{\circ}\text{C}$, 600 mbar, 3 h). For better processability, all samples were then ground into a powder in a planetary ball mill (Retsch PM 100 , 5 min, 350 rpm) and dried again in a vacuum oven (110 $^{\circ}\text{C}$, 300 mbar, 24 h) to remove remaining traces of THF. Moreover, a blank sample of the virgin polymer was prepared following the same described procedure. Finally, the dried powders were hot pressed at 180 $^{\circ}\text{C}$ for 5 min to obtain plaques with dimensions of 100 x 100 x 4 mm^3 for cone calorimetric analysis (Fire, ULTRAMAT 6).

2.5. Characterization

The suspension stability tests were carried out in a Lumifuge 114 stability analyzer. Suspensions of the surface modified additives (0.25 wt%) were centrifuged for 900 s with gradually increasing centrifuge velocities (300, 400, 500 rpm).

The particle size distributions were determined by static light scattering using a Retsch Horiba LA-950 SLS instrument.

Scanning electron microscope (SEM) measurements were carried out on a Zeiss 1530 FESEM (acceleration voltage of 3 kV). The samples were freeze-dried then mounted on conductive sample holders and sputtered with carbon.

Transmission electron microscope (TEM) measurements were carried out on a Zeiss EM 922 EFTEM with an acceleration voltage of 200 kV. Specimens were microtomed to obtain 30-70 nm thick pieces, which were placed on a lacey carbon copper grid.

The cone calorimeter experiments were carried out using an ULTRAMAT 6 instrument from FIRE (35 kW/m² heat flux with horizontal orientation of the samples) according to ASTM E. All samples were tested in triplicate and the recorded cone data were reproducible to within $\pm 5\%$.

3. Results and Discussion

3.1. Synthesis and surface modification of LDH

Several methods are available to synthesize LDHs with desired composition and morphology to best match the application in mind. Among the different methods, the urea hydrolysis method, also called the homogeneous precipitation, is well known to produce highly crystalline LDHs with large lateral dimensions. This method is based on the thermally induced hydrolysis of urea resulting in rising the pH (8 – 9) of a solution of a mixed metal salts, which is suitable to precipitate LDHs [21]. The produced LDHs possess high layer charge and carbonates as charge balancing anions in the interlayer. The carbonate is intercalated due to access of carbonates released during the hydrolysis of urea which have high affinity towards the positively charged layers. In addition to heat consumption by dehydroxylation, the endothermic decarbonation will also contribute to cooling and dilution of the gas phases with an inert gas (CO₂), which is expected to further enhance the FR properties.

In our previous work [1], we proved the significance of α of LDH on the FR properties of PS/LDH nanocomposite. In this previous work, the high- α LDH was produced by a two-step process. The LDH was first synthesized at much higher concentration (0.5 M) where a highly aggregated material was obtained which had to be disaggregated post-synthesis by ball milling to improve the aspect ratio. Recently, we found, that high- α LDHs can be directly synthesized starting from a diluted solution (0.05 M) of mixed metal salts (Figure 1). Typical platelet dimensions as apparent from the TEM images (Figure 1) are 2-4 μm in diameter and 100 nm in thickness yielding an aspect ratio range of 20-40. A comparison of the two types of LDH regarding flame retardancy will be discussed later (section 5, cone results).

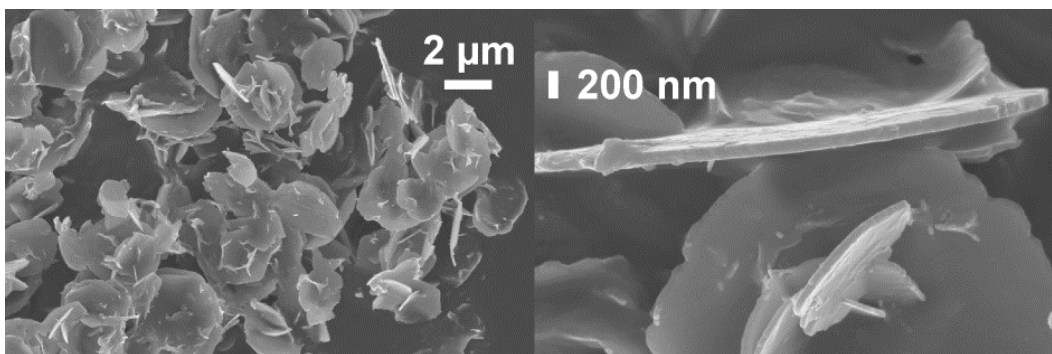


Figure 1. SEM images of high- α LDH synthesized by the urea hydrolysis method (0.05 M) at low (left) and high (right) magnification.

To achieve a stable suspension of LDH in THF and to improve the compatibility with PS, an appropriate surface modification using DBP (Figure 2.a) was applied. This kind of surface modification affects only external surfaces and no intercalation is observed [1]. The organic modifier has a lower onset temperature for decomposition (around 260 °C) than the polymer (around 365 °C), which could deteriorate the FR properties by increasing the fire load. Hence, selective modification of the external surfaces through low molecular weight compounds minimizes the content of the highly flammable organic.

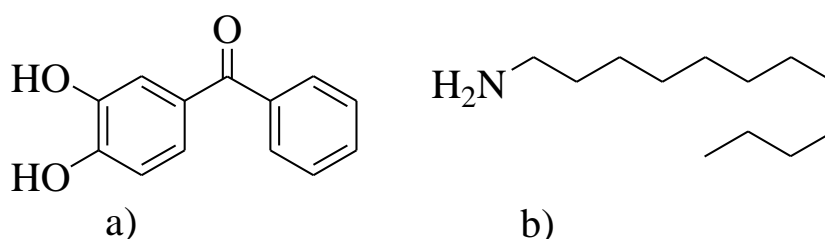


Figure 2. Structures of modifiers applied for LDH and GO, respectively: a) 3,4-dihydroxybenzophenone (DBP) and b) 1-dodecylamine (DDA)

3.2. Synthesis and surface modification of GO

Usually, graphite oxide is prepared by oxidation of graphite using strong oxidation agents in concentrated acids (e.g., $\text{H}_2\text{SO}_4/\text{KMnO}_4$). The oxidation introduces epoxy and hydroxyl functional groups at the surface and carboxyl functional groups at the edges and at defects, yielding hydrophilic GO with a considerable cation exchange capacity (≈ 500 meq/100g [27]). Moreover, due to the interlayer cations, at low ionic strength GO can be delaminated based on osmotic swelling. Depending on the lateral extension of the pristine graphite flakes used, huge α up to 10^4 can be achieved. As mentioned previously, with LDH and hectorite, high α was found to be a key factor to enhance flame retardancy. Delaminated GO was modified via a cation exchange with DDA to obtain hydrophobic GO-DDA which was re-dispersed in THF.

3.3. Sedimentation kinetics in a Lumifuge

The stability of modified LDH and GO was analyzed by forced sedimentation in a Lumifuge. In this device, the transmission of light through a horizontal centrifuge cell is measured during centrifugation at increasing velocities (Figure 3). Thus the Lumifuge test provides important semi-quantitative information about the sedimentation kinetics of these suspensions at low solid concentration. Generally, less transmission is expected for more stable suspensions due to scattering of light by particles kept in suspension. Conversely, more transmission is expected for less stable suspensions due to sedimentation.

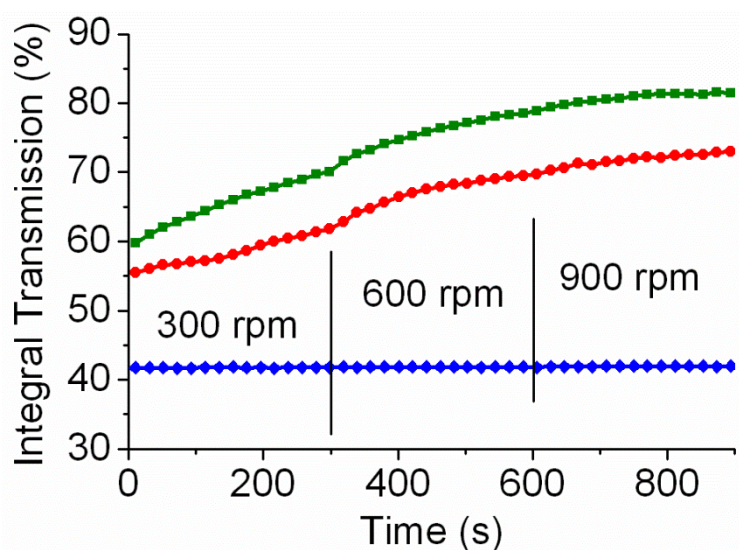


Figure 3. Sedimentation kinetics of GO-DDA (♦), LDH-DBP (■), and a mixture of LDH-DBP/GO-DDA (5:0.5) (●) by centrifugation forced sedimentation using a Lumifuge in THF. Vertical lines indicate times when the centrifugation velocity was increased stepwise.

At the beginning, transmission of light through GO-DDA was 42 %, while for LDH-DBP it was 60 % (0.25 wt%). This difference indicates more scattering/absorption of light by the delaminated GO-DDA. Shortly, increased centrifugation time and velocity resulted in increased transmission of LDH-DBP due to forced sedimentation. Interestingly, even at higher centrifugation velocities (up to 900 rpm), the GO-DDA did not clear indicating a very stable suspension. Moreover, transmission of light through the mixture of both LDH-DBP and GO-DDA was lower at any time than for pure LDH-DBP. Actually one might have expected a pronounced destabilization when mixing the two nano-additives.

Unmodified LDH and GO have surface charges of opposite sign (zeta potential values: LDH $\approx +20$ mV and GO ≈ -40 mV [28,29]). As a consequence heterocoagulation will arise if failing to reverse (“Umladen”) one of the two nano-additives by appropriate surface modification.

Organic cations like DDA are known to have a high selectivity for GO surfaces and thus may be adsorbed in excess of the cation exchange capacity reversing the surface charge (“Umladen”). Although the zeta potential could not be measured in THF suspension, the forced sedimentation results for the mixed suspensions showing suspension stability suggest that the sign of the surface potential of GO might indeed have been reversed upon DDA modification. With both LDH-DBP and GO-DDA ending up positively charged no flocculation is induced and the stability of the mixed suspension in THF can be explained. The beneficial effect of “Umladung” becomes strikingly obvious to the naked eye (Figure 4) when comparing a mixture of unmodified LDH and GO flocculating immediately (in water, left image) and a mixture of the surface modified LDH-DBP and GO-DDA remaining stable (in THF, right image).

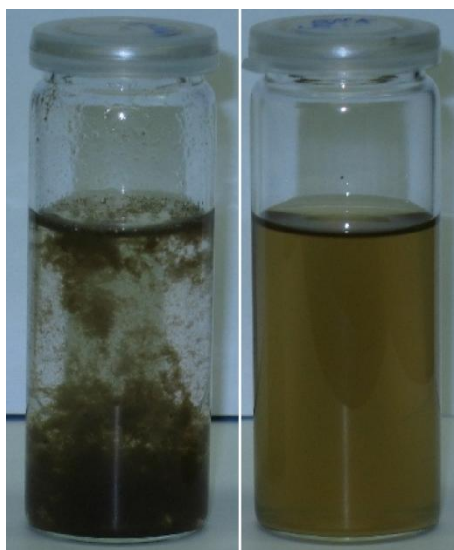


Figure 4. Photograph showing flocculation in mixtures of non-modified (left) and surface modified (right) LDH and GO

To summarize, the understanding of the surface chemistry of the nano-additives is a key factor to establish sufficient dispersion in organic solvents and as will be shown later in polymer matrix. Therefore, appropriate surface modification is always essential to serve several purposes: i) to prevent flocculation of different nano-additives, hence, to preserve effective α , ii) to provide stable suspension in organic solvent (e.g., THF), and iii) to maximize the specific interface in polymer nanocomposites.

3.4. Compounding via solution blending utilizing a three-roll mill

Particular care was taken to achieve good dispersion in PS. Compounding via solution blending was achieved by using an overhead stirrer followed by mixing in a three-roll mill.

Utilizing three-roll mill is expected to break small fractions of remaining aggregates/agglomerates by providing shear forces in the highly viscose polymer dispersion. This will assist in maximizing the specific interface area between the additives and the polymer. Figure 5 shows TEM images of the nanocomposites where the high- α LDH and GO platelets are well dispersed in PS.

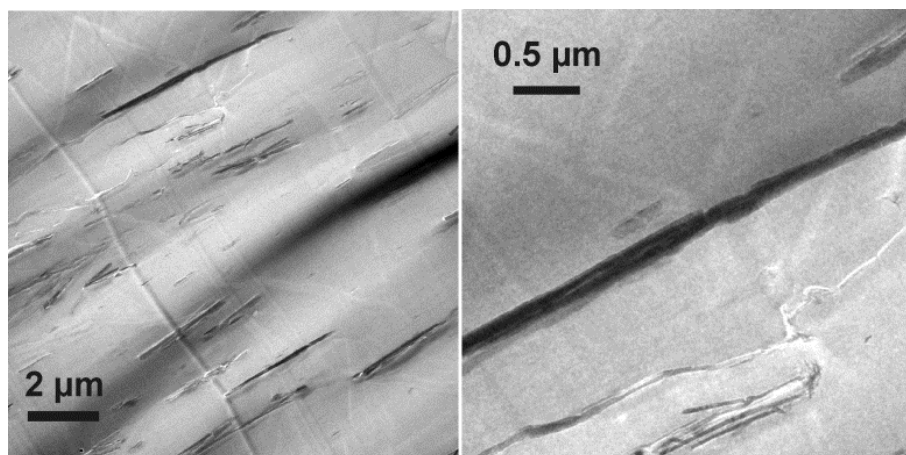


Figure 5. TEM images of PS/LDH-DBP-5wt%-GO-DDA-0.5wt% at low (left) and high (right) magnification.

As TEM is incapable to represent the bulk of the sample, the particle size distribution of the bulk composite was determined. For this, small samples of the composite dispersion after applying 0, 2, 4, and 6 cycles of three-roll milling were collected then diluted by THF to achieve sufficient transmission for allowing the measurement of particle size distribution (PSD) by static light scattering (Figure 6).

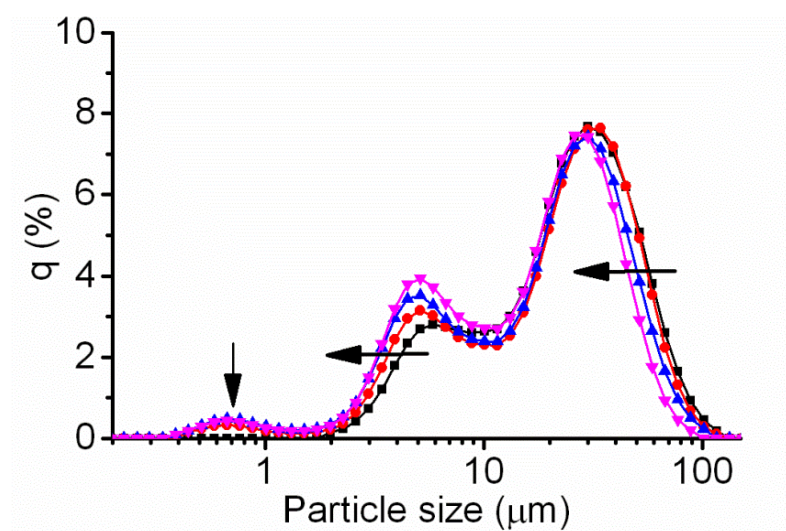


Figure 6. Particle size distributions of PS/LDH-DBP-5wt%-GO-DDA-0.5wt% after increasing numbers of cycles of three-roll milling (■) 0 (●) 2 (▲) 4, and (▼) 6. The static light scattering was done in THF suspension.

As expected, the shear forces provided by three-roll mill resulted in a shift of PSD towards smaller particle size. Hydrous suspensions of unmodified LDH and GO showed maxima in the PSD at $\approx 7 \mu\text{m}$ and $\approx 30 \mu\text{m}$, respectively (Figure SI-1). After the final cycle, the PSD of the mixed composite dispersions represented a superposition of GO-DDA and LDH-DBP distributions with maxima (at $\approx 5 \mu\text{m}$ and $\approx 25 \mu\text{m}$) comparable to what has been found in hydrous suspension. The additional small peak in the PSD at around $0.7 \mu\text{m}$ can be attributed to destruction of a few existing rose-like LDH aggregates. These aggregates can also be seen in the SEM images (Figure 1). Results of both PSD and TEM corroborate an efficient surface modification and consequently good dispersion in PS.

3.5. Cone calorimeter data of PS nanocomposites

The flame retardant behavior of PS nanocomposites was investigated using cone calorimetry. Cone calorimetry mimics the early stages of a fire scenario and provides information on the time to ignition (t_{ig}), the heat release rate (HRR) and its related peak of heat release rate (PHRR), the total heat release (THR), and burn out time. A perfect FR should decrease PHRR and THR, while t_{ig} and burn out time should be increased. Figure 7 compares HRR curves (heat flux of 35 kW/m^2) of PS nanocomposites made with LDHs (5 wt%) with α enhanced through: i) the two-step process including disaggregation by ball milling (LDH-2-DBP) [1], and ii) the direct synthesis in a diluted regime (LDH-DBP). The HRR curve of both types of LDH are almost identical suggesting that the effective α is similar and that the mechanical disaggregation may indeed be avoided by modifying the synthesis concentration.

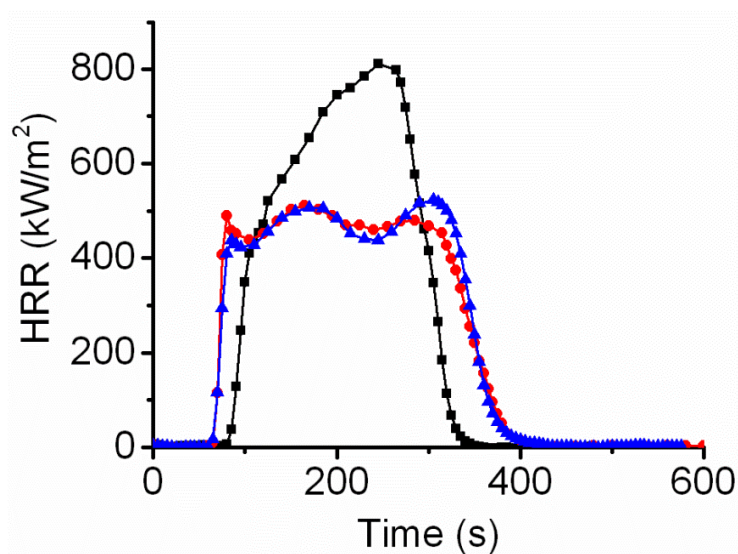


Figure 7. Heat release rate curves for PS/LDH nanocomposites (5wt%) with (■) PS (●) PS/LDH-DBP (▲) PS/LDH-2-DBP.

As a result of dilution by inert gases (CO_2 , H_2O) together with the good dispersion and high α , a reduction of PHRR of $\approx 36\%$ was obtained for both LDHs. In the literature, PS/LDH nanocomposites, prepared either by melt blending or by bulk polymerization achieved typical reductions of PHRR of 20-25% at 5 wt% loading [3,15]. Few studies reported a reduction of PHRR comparable to our value: Nyambo et al. [4] observed a reduction of PHRR of 39% of PS nanocomposite filled by 5 wt% LDH. This LDH was intercalated with a linear alkyl carboxylate (C10) where the intercalation process had to be repeated several times to assure complete exchange. Moreover, the intercalation was carried out under a steady flow of nitrogen to exclude CO_2 . Anyhow, the efficiency of the LDH used in this work is comparable to Nyambo's work, while less effort was needed for the preparation.

This pronounced reduction in PHRR (Table I) highlights the importance of α on the flame retardancy of LDHs. The t_{ig} was slightly reduced for PS/LDH nanocomposites which might be attributed to the additive acting as heterogeneous catalyst in the degradation of the pristine polymer.

In order to explore a possible synergism, the PS nanocomposites containing just a single additive; 0.5 wt% of GO-DDA (PS/GO-DDA-0.5wt%), 1.0 wt% of GO-DDA (PS/GO-DDA-1.0wt%), or 5 wt% of LDH-DBP (PS/LDH-DBP-5wt%) were compared with formulations containing a combination of both fillers; 5 wt% of LDH-DBP and 0.5 wt% or 1.0 wt% of GO-DDA (PS/LDH-DBP-5wt%/GO-DDA-0.5wt% or 1.0wt%). Table 1 summarizes the cone data for the various PS nanocomposites, while the HRR curves obtained at a heat flux of 35 kW/m^2 are shown in Figure 8.

Table I. Cone calorimeter data for PS nanocomposites

<i>Formulation</i>	<i>PHRR</i> (kW/m^2)	<i>PHRR</i> <i>Reduct.</i> (%)	<i>THR</i> (MJ/m^2)	t_{ig} (s)
PS	813 ± 29	-	138 ± 2	88 ± 3
PS/GO-DDA-0.5wt%	564 ± 18	31	138 ± 1	70 ± 2
PS/GO-DDA-1.0wt%	$564 \pm$	42	$133 \pm$	$69 \pm$
PS/LDH-DBP-5wt%	521 ± 11	36	135 ± 4	71 ± 3
PS/LDH-DBP-5wt%/GO-DDA-0.5wt%	434 ± 13	47	135 ± 3	61 ± 1
PS/LDH-DBP-5wt%/GO-DDA-1.0wt%	$480 \pm$	41	$124 \pm$	$65 \pm$

Reductions in the PHRR of 31 % and 42 % were obtained by PS/GO-DDA-0.5wt% and PS/GO-DDA-1.0wt% respectively. Dittrich et al. [2] recently reported a high reduction of the PHRR of 74 % by filling polypropylene with 5 wt% of thermally reduced graphite oxide. They related the FR-efficiency to the increase of viscosity of the melt at constant filler content of 5 wt% of several carbon nano-materials which they claimed is an indirect measure of the quality of dispersion. Please note that reduction of PHRR of different polymer matrices cannot be directly comparable where the observed reduction of PHRR for PS is much more lower as compared to PP [2,30]. Since we see significantly higher reductions of the PHRR at much smaller loadings than previously reported for 5 wt% GO in PS nanocomposite prepared by melt blending (37 %) [30], this would indicate that the careful reduction of ionic strength by dialysis might have resulted in a better delamination and consequently a higher specific interface of GO-DDA with the PS matrix. Uhl and Wilkie [22], reported a similar reduction of PHRR for PS nanocomposites of 42 % at 1.0 wt% GO-content. These authors achieved an excellent dispersion by in-situ polymerization of styrene monomer with 1 wt% of GO intercalated with 4-vinylbenzyl-ammonium chloride. Contrary to this well dispersed nanocomposite, Uhl and Wilkie found a much lower reduction of PHRR of 17 % for a melt blended sample. In summary, these authors concluded that the dispersion of GO in the polymer matrix is a key parameter for the reduction of PHRR. Comparing their results with the PHRR observed for PS/GO-DDA-1.0wt% would suggest that delamination by osmotic swelling followed by an appropriate surface modification is capable of producing the same excellent specific interface areas as in situ polymerization.

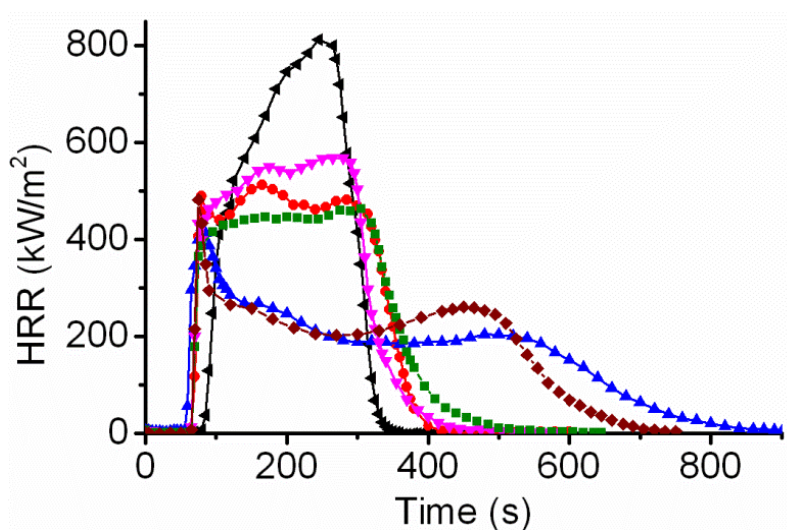


Figure 8. Heat release rate curves for PS nanocomposites with (◄) PS (▼) PS/GO-DDA-0.5wt% (●) PS/LDH-DBP-5wt%, (■) PS/GO-DDA-1.0wt%, (▲) PS/LDH-DBP-5wt%/GO-DDA-0.5wt%, and (◆)PS/LDH-DBP-5wt%/GO-DDA-1.0wt%.

Most interestingly, when combining the two nano-additives, LDH-DBP and GO-DDA, a maximum reduction in PHRR of 47 % was obtained with PS/LDH-DBP-5wt%/GO-DDA-0.5wt%. While only a mediocre reduction of the PHRR is observed for the combination, the maximum clearly undervalues the real benefit in respect to FR-efficiency. The full profile of the HRR curve offers a more detailed understanding of the fire scenario and the possible mechanism of flame retardancy: The PHRR is observed shortly after ignition, but the maximum is a narrow spike and the HRR decreased in a big step immediately after passing through the PHRR. Consequently, the polymer continued to burn at much lower HRR values.

The so-called steady HRR is reduced by as much as 75 %. It seems like the flame retardancy required a kind of activation process at early stages of burning. The time lag (≈ 10 s) associated with this activation could be related to the time needed for migration of active nano-additives to the surface and/or ablation of the polymer from the surface. Furthermore, the steep reduction shortly after the PHRR indicated the formation of a protective ceramic-like layer of the residual metal oxides and carbonaceous char. This layer acts as a thermal insulator which slows down mass and heat transfer and separates the burning polymer from the flame [31]. Consequently, a severely prolonged burn out time (154 %) was recorded. This behavior is typical for combustion of thick-charring composites [32].

While the PHRR for composites filled with GO-DDA as singular nano-additive decreased further when increasing the content from 0.5 wt% to 1.0 wt% from 31 % to 42 %, respectively, for the combined system the optimum was observed with 0.5 wt% of GO-DDA. We have no explanation for this observation of this plateau at very low GO-DDA content.

The formation of a protective layer is corroborated by the THR curves (Figure 9). Clearly, with the combination of GO-DDA and LDH-DBP additives the THR was spread over much longer time, which will provide significantly more time for potential victims to escape from a fire. Nevertheless, at the end of the combustion the entire polymer was consumed and the total fire load is released for most samples. A small reduction of the THR in the range $< 2\%$ for formulations containing LDH-DBP most likely is related to the reduction of the sample's fire load by replacing PS by the filler rather than being indicative of a passive cooling effect.

For PS/LDH-DBP-5wt%/GO-DDA-1.0wt%, however, a significant lower THR value was recorded. The char appears more compact and some polymer might not have been entirely combusted.

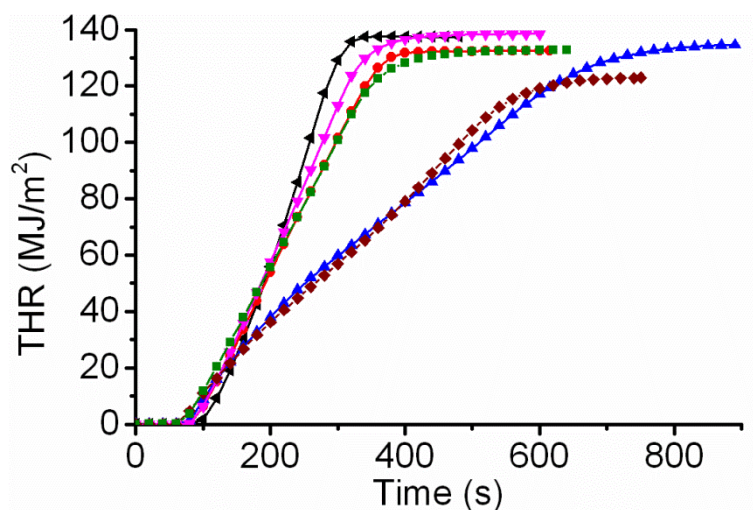


Figure 9. Total heat release curves for PS nanocomposites with (▲) PS (▼) PS/GO-DDA-0.5wt% (●) PS/LDH-DBP-5wt%, (■) PS/GO-DDA-1.0wt% Sand (▲) PS/LDH-DBP-5wt%/GO-DDA-0.5wt%, and (◆) PS/LDH-DBP-5wt%/GO-DDA-1.0wt%.

Figure 10 shows the residual char of the cone calorimetry analysis. More carbonaceous char was obtained for both combinations of LDH-DBP and GO-DDA (c, d), as compared to the sample containing just LDH-DBP (b).

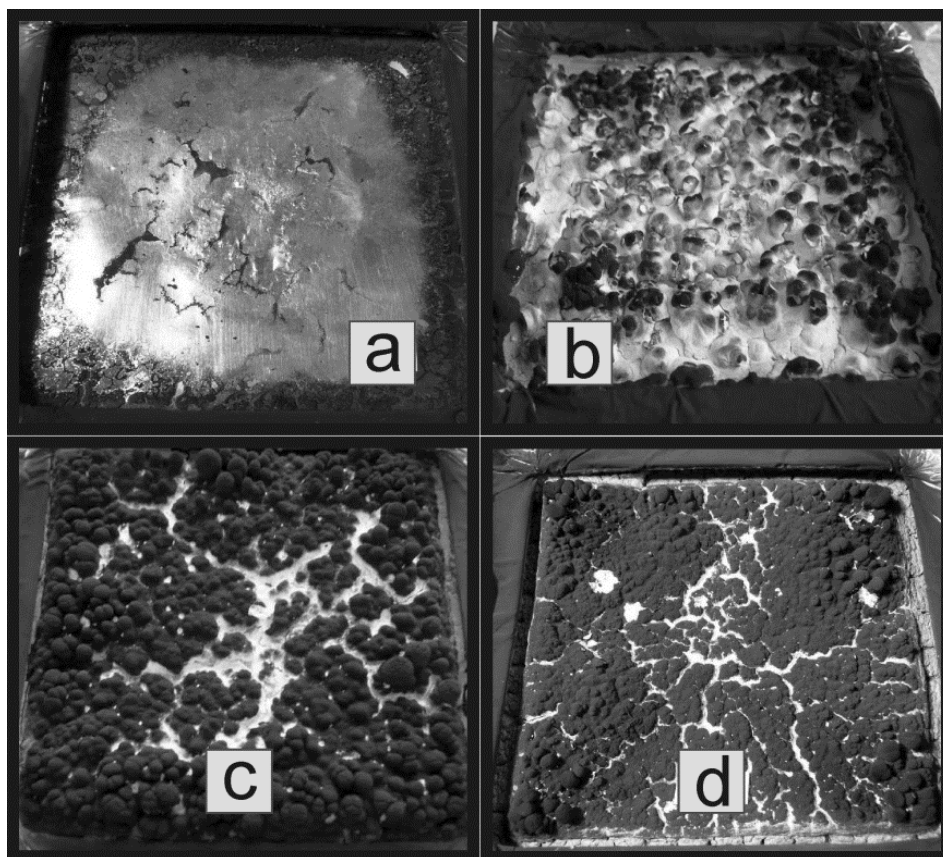


Figure 10. Photographs represent a comparison between the residues of the cone test of (a) PS/GO-DDA-1.0wt, (b) PS/LDH-DBP-5wt%, (c) PS/LDH-DBP-5wt%/GO-DDA-0.5 wt%, and (d) PS/LDH-DBP-5wt%/GO-DDA-1.0wt%.

This observation is in line with the superior flame retardancy described above. In line with earlier literature reports [30], for the two PS/GO-DDA nanocomposites, almost no residual char was obtained (< 1 %). Interestingly, a minor intumescent effect could be observed for the PS/LDH-DBP-5wt%/GO-DDA-0.5wt% sample. This might have been caused by the ‘blowing effect’ of gases released upon LDH decomposition (CO₂ and H₂O) while the large aspect ratio GO filler provided a good gas barrier in the melt which synergistically expanded the char-layer formed.

4. Conclusions

A novel flame retardant combination of LDH-DBP and GO-DDA was tested. Appropriate surface modification provided stable suspensions of the two nano-additives in an organic solvent. This surface modification hinders heterocoagulation of nano-additives of surface charge of different sign as confirmed by TEM and PSD measurements.

Cone calorimeter results showed a significant reduction of PHRR of 47 % at relatively low loading of a combination of 5 wt% LDH-DBP and 0.5 wt% GO-DDA. The formation of protective layer isolating the burning polymer from the flame lead to a steady combustion at much lower HRR resulting in dramatically prolonged burn out time (154 %). This superior flame retardancy stress the potential of utilizing LDHs with graphite-based compounds as synergistic FRs in polymer nanocomposites.

While this work is a proof of principle demonstrating the pronounced synergism of combinations of nano-additives, further investigations should be carried out helping to establish a more detailed understanding of the mechanism of flame retardancy in this system.

Acknowledgments

The authors thank Kropfmühl AG, for providing graphite. B. D-B. also acknowledges the German Academic Exchange Service (DAAD) for financial support. This work was further supported by the Deutsche Forschungsgemeinschaft (DFG) within the Collaborative Research Center (SFB 840).

References

[1.] Diar-Bakerly B, Beyer G, Schobert R, Breu J. Significance of Aspect Ratio on Efficiency of Layered Double Hydroxide Flame Retardants. In: Morgan AB, Wilkie CA, Nelson GL,

editors. Fire and Polymers VI: New Advances in Flame Retardant Chemistry and Science, American Chemical Society: Washington, DC, 2012, pp. 407-425.

[2.] Dittrich B, Wartig KA, Hofmann D, Mülhaupt R, Scharrel B. Polym Deg Stab 2013;98(8):1495-1505.

[3.] Matusinovic Z, Lu H, Wilkie CA. Polym Deg Stab 2012;97(9):1563-1568.

[4.] Nyambo C, Songtipya P, Manias E, Jimenez-Gasco MM, Wilkie CA. J Mater Chem 2008;18(40):4827-4838.

[5.] Nyambo C, Chen D, Su S, Wilkie CA. Polym Deg Stab 2009;94(8):1298-1306.

[6.] Scharrel B, Hull TR. Fire Mater 2007;31(5):327-354.

[7.] Schütz MR, Kalo H, Lunkenbein T, Groschel AH, Müller AHE, Wilkie CA, Breu J. J Mater Chem 2011;21(32):12110-12116.

[8.] Schütz MR, Kalo H, Lunkenbein T, Breu J, Wilkie CA. Polymer 2011;52(15):3288-3294.

[9.] Uhl FM, Yao Q, Wilkie CA. Polym Adv Technol 2005;16(7):533-540.

[10.] Wang L, Su S, Chen D, Wilkie CA. Polym Deg Stab 2009;94(5):770-781.

[11.] Wang L, Xie X, Su S, Feng J, Wilkie CA. Polym Deg Stab 2010;95(4):572-578.

[12.] Edward DW, Sergei VL. Flame Retardants in Commercial Use or Development for Polyolefins., editors. Flame Retardants for Plastics and Textiles, Carl Hanser Verlag GmbH & Co. KG: Munich, 2009, pp. 3-34.

[13.] Birnbaum LS, Staskal DF. Environ Health Perspect 2003;112(1):9-17.

[14.] Law RJ, Herzke D, Harrad S, Morris S, Bersuder P, Allchin CR. Chemosphere 2008;73(2):223-241.

[15.] Manzi-Nshuti C, Chen D, Su S, Wilkie CA. Polym Deg Stab 2009;94(8):1290-1297.

[16.] Nyambo C, Kandare E, Wang D, Wilkie CA. Polym Deg Stab 2008;93(9):1656-1663.

[17.] Zhao CX, Liu Y, Wang DY, Wang DL, Wang YZ. Polym Deg Stab 2008;93(7):1323-1331.

[18.] Zhang G, Ding P, Zhang M, Qu B. Polym Deg Stab 2007;92(9):1715-1720.

- [19.] Jiao C, Chen X. *J Therm Anal Calorim* 2009;98(3):813-818.
- [20.] Evans D, Slade R. *Structural Aspects of Layered Double Hydroxides*. In: Duan X, Evans D, editors. *Layered Double Hydroxides*, Springer: Berlin / Heidelberg, 2006, pp. 1-87.
- [21.] Costantino U, Marmottini F, Nocchetti M, Vivani R. *Eur J Inorg Chem* 1998;1998(10):1439-1446. 15
- [22.] Uhl FM, Wilkie CA. *Polym Deg Stab* 2004;84(2):215-226.
- [23.] Higginbotham AL, Lomeda JR, Morgan AB, Tour JM. *ACS Appl Mater Interfaces* 2009;1(10):2256-2261.
- [24.] Han Y, Wu Y, Shen M, Huang X, Zhu J, Zhang X. *J Mater Sci* 2013;48(12):4214-4222.
- [25.] Hummers WS, Offeman RE. *J Am Chem Soc* 1958;80(6):1339.
- [26.] Dekany I, Krüger-Grasser R, Weiss A. *Colloid Polym Sci* 1998;276(7):570-576.
- [27.] Hofmann U, Holst R. *Ber dtsh Chem Ges A/B* 1939;72(4):754-771.
- [28.] Li D, Muller MB, Gilje S, Kaner RB, Wallace GG. *Nat Nano* 2008;3(2):101-105.
- [29.] Zhang Y, Evans JRG. *Colloids Surf A* 2012;408(1):71-78.
- [30.] Han Y, Wu Y, Shen M, Huang X, Zhu J, Zhang X. *J Mater Sci* 2013;48(12):4214-4222.
- [31.] Edward DW, Sergei VL. *Overview of Modes of Action and Interaction of Flame Retardants.*, editors. *Flame Retardants for Plastics and Textiles*, Carl Hanser Verlag GmbH & Co. KG: Munich, 2009, pp. 241-251.
- [32.] ScharTEL B, Hull TR. *Fire Mater* 2007;31(5):327-354.

Appendix 3: Superior Flame Retardant by Combining High Aspect Ratio Layered Double Hydroxide and Graphene Oxide

Bashar Diar-Bakerly¹, Patrick Feicht, Andreas Edenharter¹, Günter Beyer², Josef Breu^{1,*}

¹) Department of Inorganic Chemistry I, University of Bayreuth, Universitaetsstr. 30, 95447 Bayreuth, Germany

²) Kabelwerk Eupen AG, 4700 Eupen, Belgium

Corresponding author: Prof. Dr. Josef Breu, Universitaetsstr. 30, 95440 Bayreuth, Germany

* E-mail: josef.breu@uni-bayreuth.de

Supplementary Information (SI)

1. Particle size distribution of GO and LDH in hydrous suspensions (Figure SI-1)

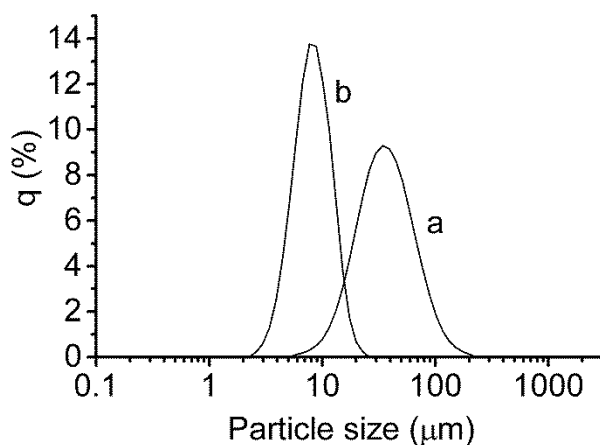


Figure SI-1. Particle size distributions in aqueous suspensions of GO (a) and LDH (b).

2. Influence of three-roll milling on the PSD in THF suspensions: The appearance of small fraction around 0.7 µm (Figure SI-2)

While the particle size fraction at around 5 µm (attributed to LDH) was shifted toward a smaller PSD after 2 cycles of three roll milling, the particle size fraction at around 25 µm (attributed to GO) remained constant. At the same time, a fraction of smaller particles (0.7 µm) had appeared (Figure SI-2). This evidence supports the argument that this fraction is resulting from destruction of a few existing rose-like LDH aggregates.

After 4 and 6 cycles of three roll milling, the GO fraction was also slightly shifted towards a smaller PSD, which could possibly be explained by some breakage of the GO platelets

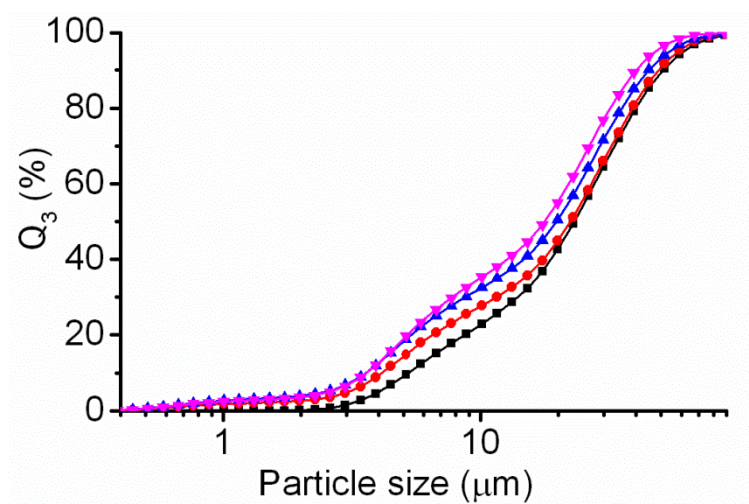


Figure SI-2. Cumulative particle size distributions of PS/LDH-DBP-5wt%-GO-DDA-0.5wt% after increasing numbers of cycles of three roll milling (■) 0 (●) 2 (▲) 4, and (▼) 6. The static light scattering was done in THF suspension.

5.4. Appendix 4: Multi-Component Flame Retardants: Combining Anionic and Cationic Clays as Trojan Horses for Molecular Flame Retardants

Bashar Diar-Bakerly¹, Josef Hausner¹, Hussein Kalo¹, Andreas Edenharter¹, Mazen Ziadeh¹,
Günter Beyer², Josef Breu^{1,*}

¹) Department of Inorganic Chemistry I, University of Bayreuth, Universitaetsstr. 30, 95447
Bayreuth, Germany

²) Kabelwerk Eupen AG, 4700 Eupen, Belgium

Corresponding author: Prof. Dr. Josef Breu, Universitaetsstr. 30, 95440 Bayreuth, Germany

* E-mail: josef.breu@uni-bayreuth.de

Abstract

A multi-component flame retardant (FR) was established by combining two synthetic clays; high aspect ratio hectorite (cationic-type) and layered double hydroxides (LDHs, anionic-type) in polystyrene nanocomposites. Both LDH and hectorite were organophilized with thermally stable molecular FR such as phenyl phosphate and melaminium, respectively.

PS nanocomposites were prepared via solution blending utilizing a three-roll mill. A large portion of the aggregates were destroyed upon mechanical agitation as indicated by recording the particle size distributions. The obtained PS nanocomposites showed enhanced thermal stability and flame retardancy. Cone calorimetry proved a synergism between these two nano-additives where a reduction of peak of heat release of 51 % at low loadings of 5 wt% was recorded. For this combination of nano-additives the reduction of the peak of heat release is some 10 % higher as compared to the average reduction by a singular nano-additive. Furthermore, an intumescent effect was observed for PS nanocomposite with this multi-component FR.

Keywords: polystyrene nanocomposite, flame retardant, synergism, layered double hydroxide, hectorite, clays modification.

1. Introduction

The interest in both anionic (smectite like montmorillonite or hectorite) and cationic (layered double hydroxides, LDHs) clays as innovative flame retardants (FRs) for polymer nanocomposites has been steadily increasing over the last decades [1,2].

Small amounts (3 wt%) of clays were shown sufficient to introduce significant flame retardancy compared to the pristine polymer [3]. The suggested mechanisms of flame retardancy are primarily through thermal insulation subsequent to formation of a protective ceramic/glass-like layer, reinforcement of char, and dilution of the volatiles during the endothermic degradation [4-6]. The intrinsic ion exchange capacities of both types of clays renders them potential hosts/carriers for molecular flame retardants like phosphorus-containing anions or melaminium cations.

The maximum FR efficiency can be achieved when these nano-additives are perfectly dispersed in the polymer matrix yielding a maximum specific interface area. Good dispersion is most efficiently achieved by appropriate surface modification lowering the surface tension. In addition to the dispersion quality, a good correlation has been established between the morphology (particles size and shape) of clays and the FR observed. In particular the aspect ratio (α : lateral extension of a platelet divided by its thickness) where high- α , synthetic Li- or K-hectorite (K-hect) showed a superior flame retardancy compared to the low- α , natural montmorillonite frequently used as standard filler [3,7].

For further enhancement of the flame retardancy of polymer nanocomposites, clays were used in combination with conventional FRs such as aluminum trihydroxide [8] or ammonium polyphosphate [9] to create a synergistic FR system. Consequently, higher FR efficiency was gained at low loading. Such synergism of combined FR systems is of highest importance, because it has the potential to assure FR requirements while preserving physical properties of the polymer and ease of processing.

The focus of this work was to explore a possible synergism of a combination of two synthetic clays, LDH and hect. Moreover, instead of a conventional surface modification, organic ions with FR properties such as melaminium (Me) and phenyl phosphate (PP) were applied. It is expected that flame retardancy of such multi-component system to be maximized.

2. Experimental

2.1. Materials

Polystyrene (PS 158K, melt index 3.00 g/10 min (200 °C/5kg, ASTM D1238), glass transition temperature 100 °C, ISO 11357, density 1.04 g/cm³, ASTM D792) was supplied by BASF. For LDH synthesis, urea, magnesium nitrate hexahydrate, and ammonium nitrate were purchased from Grüssing GmbH, while aluminum nitrate nonahydrate was purchased from

Sigma-Aldrich. Melamine and phosphoric acid were purchased from Merck. Phenyl phosphate disodium salt (Na_2PP) and the organic solvents (ethanol and tetrahydrofuran) were purchased from Sigma-Aldrich. All chemicals were used as received.

2.2. Preparation and anion exchange of LDH

Modified urea hydrolysis method [10,11] was used for the direct synthesis of $\text{Mg}/\text{Al}-\text{NO}_3^-$ -LDH with $\text{Mg}:\text{Al}$ -ratio of 2:1. Briefly, an aqueous solution of a mixture of metal salts (1.0 l, 0.5 M total metal concentration) of $\text{Mg}(\text{NO}_3)_2 \cdot 6\text{H}_2\text{O}$ (85.5 g, 0.33 mol) and $\text{Al}(\text{NO}_3)_3 \cdot 9\text{H}_2\text{O}$ (62.5 g, 0.17 mol) was refluxed in the presence of urea (99.0 g, 1.65 mol) and ammonium nitrate (80.1 g, 1 mol) for 36 h. Later on, the suspension was centrifuged and washed repeatedly with ethanol. The obtained LDH was stored in an ethanol suspension.

For the anion exchange, suspension of LDH in ethanol was centrifuged and then re-suspended (5 g/ 100ml) in an aqueous solution of Na_2PP (2.8 g, 11.3 mmol). The suspension was ultrasonified for 2 min followed by shaking in an overhead shaker for 10 min. The suspension of the anion exchanged LDH (LDH-PP) was washed two times with water to remove the remaining traces of the salt. Finally, the aqueous suspension was centrifuged, washed two times with THF, and re-suspended in THF (3 wt%). Please note that for washing deionized and degassed water was used to prevent intercalation of carbonate.

2.3. Preparation and modification of hectorite

The K-lect was tailored following a reported procedure [12] from a pristine synthetic Na-lect prepared from a melt synthesis [13].

For the surface modification, an aqueous solution of melaminium orthophosphate (prepared following [14], 0.36 g, 1.6 mmol) was added to a suspension of K-lect (8 g/ 200 ml). The suspension was put on an overhead shaker for 5 min. Afterwards the suspension was washed with water, two times with THF, and finally re-suspended in THF at 3 wt%. The modified K-lect with melaminium was referred to hereafter as lect-Me.

2.4. Compounding via solution blending in a three-roll mill

PS nanocomposites were prepared by adding appropriate amounts of suspension of the nano-additives in THF to a solution (25 wt%) of PS in THF. The dispersions were first mixed for 30 min using an overhead stirrer (500 rpm, RT). Afterwards, the dispersion was further homogenized applying a three-roll mill (Exakt-80E) placed in an exhaust hood.

All samples were passed through the mill six times. The roller distance was gradually lowered from initially 25 μm in the first cycle to 5 μm in the final cycle. Despite cooling at $-23\text{ }^{\circ}\text{C}$ a good share of THF evaporated in the course of three-roll milling (1 h) and highly viscous dispersions were obtained which were pre-dried in a vacuum oven ($80\text{ }^{\circ}\text{C}$, 600 mbar, 3 h). For better processability, all samples were then ground into a powder in a planetary ball mill (Retsch PM 100, 5 min, 350 rpm) and dried again in a vacuum oven ($110\text{ }^{\circ}\text{C}$, 300 mbar, 24 h) to remove remaining traces of THF. Moreover, a blank sample of the virgin polymer was prepared following the same described procedure. Finally, the dried powders were hot pressed at $180\text{ }^{\circ}\text{C}$ for 5 min to obtain plaques with dimensions of $100 \times 100 \times 4\text{ mm}^3$ for cone calorimetric analysis (Fire, ULTRAMAT 6).

PS nanocomposites containing 5 wt% of hect-Me, 5 wt% of LDH-PP, or a combination of 2.5 wt% of hect-Me/2.5 wt% of LDH-PP were referred to as PS/hect-Me, PS/LDH-PP, or PS/LDH-PP/hect-Me, respectively.

2.5. Methods and instruments

PXRD patterns were recorded in reflection mode (PANalytical Xpert Pro equipped with a X'Celerator Scientific RTMS detector and using $\text{Cu K}\alpha$ radiation). All samples were measured on flat glass holders to foster texture and boost the intensities of the basal reflections.

Scanning electron microscope (SEM) measurements were carried out on a Zeiss 1530 FESEM (acceleration voltage of 3 kV). The samples were freeze-dried then mounted on conductive sample holders and sputtered with carbon.

Transmission electron microscope (TEM) measurements were carried out on a Zeiss EM 922 EFTEM with an acceleration voltage of 200 kV. Specimens were microtomed to obtain 30-70 nm thick pieces, which were placed on a lacey carbon copper grid.

Thermogravimetric analyses (TGA) were conducted with a Netzsch TG209 F1 thermoanalyzer instrument. Specimens with a mass of around 15 mg were heated up from $30\text{ }^{\circ}\text{C}$ to $600\text{ }^{\circ}\text{C}$ ($10\text{ }^{\circ}\text{C}/\text{min}$) in a nitrogen atmosphere ($20\text{ ml}/\text{min}$).

The particle size distributions (PSDs) were determined by static light scattering using a Retsch Horiba LA-950 SLS instrument.

The cone calorimeter experiments were carried out using an ULTRAMAT 6 instrument from FIRE ($35\text{ kW}/\text{m}^2$ heat flux with horizontal orientation of the samples) according to ASTM E.

All samples were tested in triplicate and the recorded cone data were reproducible to within $\pm 5\%$.

3. Results and discussion

3.1. Designing multi-component clays

The employment of synthetic clays instead of natural clays for the preparation of novel polymer/clay nanocomposites with enhanced flame retardancy has already been explored [7,15]. Synthetic clays exhibit a high degree of purity and charge homogeneity while the type and number of interlayer ions and crucial morphological factors like the aspect ratio (α) can be tailored.

On the first hand, both anionic- and cationic-types of clays are capable of anion/cation exchange. As a result, charged organic molecules can easily be incorporated between the charged layers or at the external surfaces. The charge density of LDH is much higher as compared to smectites. Typical anion exchange capacities (AEC) of LDHs are in the range ≈ 300 - 400 meq/100g [16] while the total cation exchange capacity (CEC) of hect is approximately 120 meq/100g [13]. Here we take advantage of the anion exchange capacity of LDH to encapsulate anions with FR properties such as organic-phosphates into the nano-additive (Figure 1.a). Organic compounds containing phosphates are established flame retardants acting as precursors for phosphoric acid which acts as thermal shield and radical scavenger by the PO and HPO radicals [6].

On the other hand, K-hect has much higher α ($\alpha \approx 500$) than LDH [12]. The interlayer space is, however, cross-linked by the perfect fit of K-ions and therefore only the external cations can be replaced by organic cations allowing the surface tension to be modified. Conventionally utilized surface modifiers like alkylammonium cations have lower decomposition temperatures than the polymer (onset temperature; $T_{0.1} \approx 180$ °C for ammonium salts) and additionally increase the fire load. Therefore, we used melaminium ($T_{0.1} = 322$ °C) as a thermally stable modifier. Since the CEC of the external surfaces is low (18 mmol/100 g), only small amounts of the rather expensive FR are needed to organophilize the K-hect (Figure 1.b). Moreover, melamine is known as a FR that dilutes the volatiles by releasing N_2 upon endothermic degradation.

Combining four different FR elements is expected to maximize the FR efficiency; melamine as nitrogen rich compounds together with organic-phosphate could create an intumescent

system. In such system, an acid generator and N_2 source are required, whereas the acid promotes char formation for non-charring polymers and N_2 acts as blowing agent [5].

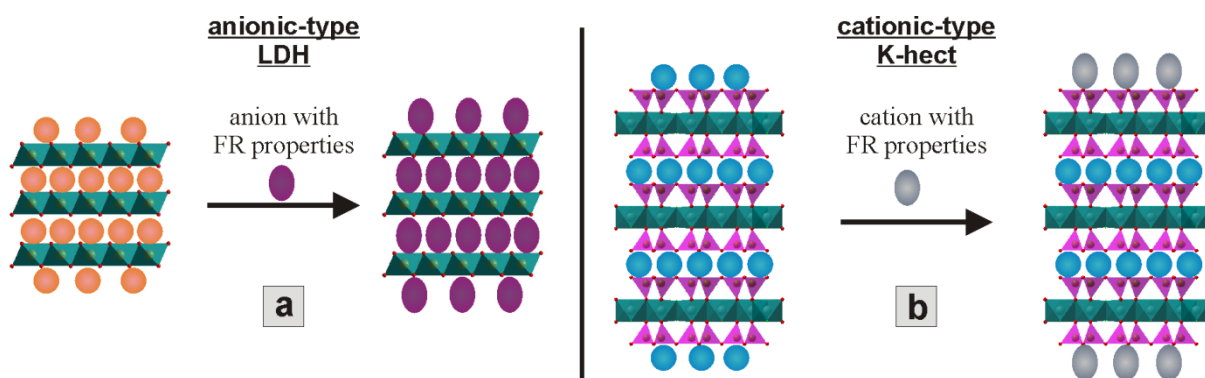


Figure 1. Schematic presentation of the multi-component FR system of both (a) anionic-type (fully intercalated) and (b) cationic-type (the modification is selective to only external surfaces)

3.2. Preparation and modification of LDH

In general, several methods are established for synthesis of LDHs such as co-precipitation and homogeneous precipitation. For reasons of convenience, most studies of polymer nanocomposites apply LDHs synthesized via co-precipitation. While Cl^- or NO_3^- containing LDHs, which could be accessible for anion exchange, can be directly obtained by co-precipitation, LDHs produced by this route are poorly crystalline, have low α , and possess an inhomogeneous layer charge density [11]. In addition, probable due to lattice strain, anion exchange of these LDHs requires a large excess of intercalate, longer reaction time, and should be repeated several times to establish complete intercalation.

Contrary to co-precipitation, precipitation from homogeneous solution, also called the urea hydrolysis method, is well known to produce high charge density, well ordered, and well crystalline CO_3^{2-} containing LDHs [11]. Due to the high charge density and the low hydration enthalpy of carbonate, CO_3^{2-} -LDHs, however, cannot be directly anion exchanged with other organic/inorganic anions, in contrast to the Cl^- or NO_3^- containing LDHs obtained by the co-precipitation method. Recently, the urea hydrolysis method was successfully extended for the direct synthesis of well crystallized $Zn/Al-NO_3^-$ -LDH [10]. In this work, we modified this method to directly produce $Mg/Al-NO_3^-$ -LDH (Figure 2.left).

While this modified urea method still yields large- α , the intercrystalline reactivity is good and this $Mg/Al-NO_3^-$ -LDH can be easily and completely ion-exchanged with PP (Figure 3.a) in one step and in very quick process (10 min) to give LDH-PP.

For the anion exchange, only 125 % of AEC (360 meq/100 g, for more information please see SI-1) had to be applied to assure complete exchange.

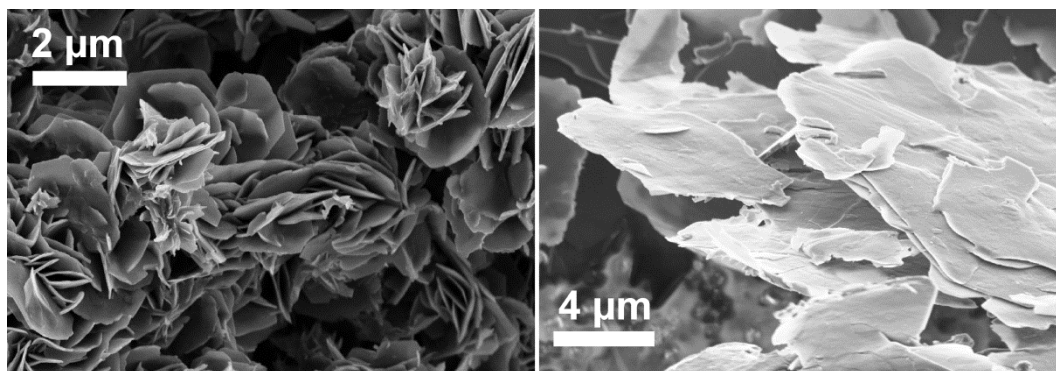


Figure 2. SEM images of (left) directly synthesized NO_3^- -LDH by the modified urea method and (right) high- α K-het

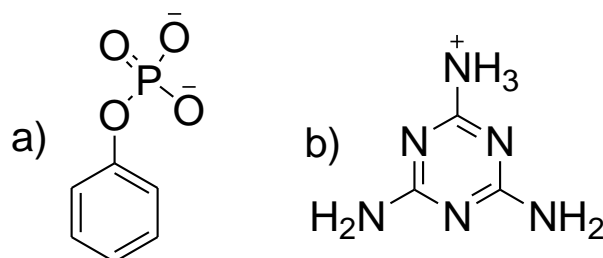


Figure 3. Structures of organic ions used for the exchange: a) phenyl phosphate and b) melaminium

3.3. Maximizing of the aspect ratio and modification of hectorite

Synthesis and processing of K-het was described in detail in the literature [12,13]. The α of K-het was estimated to be around 500 by correlating the platelet thickness as calculated by the Scherer equation (≈ 14 lamella) [17] and the lateral extension of the platelet measured by SLS ($\approx 7\mu\text{m}$, Figure SI-1).

The organophilization of K-het was done by adding a hydrous solution of Me (Figure 3.b) corresponding to the CEC of the external basal surfaces of K-het (18 meq /100 g). This CEC was determined by using the copper complex method [12]. Upon organophilization, the clay flocculates and can be centrifuged and re-suspended in organic solvent (THF).

3.4. Characterization of the modified clays

XRD patterns were recorded before and after organophilization of the clays. In the case of K-het (Figure SI-2), as expected no shift in the d_{001} reflection was observed confirming that Me modified only the external basal surfaces while the internal basal surfaces were not accessible.

Conversely, a significant shift towards lower 2 theta was recorded for LDH after intercalation with PP (Figure 4). Upon intercalation, the d_{003} reflection (8.9 Å) attributed to the basal spacing of NO_3^- -LDH completely disappeared while a new reflection attributed to LDH-PP (d_{003} of 15.4 Å) appeared which confirms complete intercalation. Needless to be mentioned, the external basal surfaces were also modified by anion exchange. As a consequence of this organophilization, the LDH-PP flocculates and can be centrifuged and re-suspended in THF.

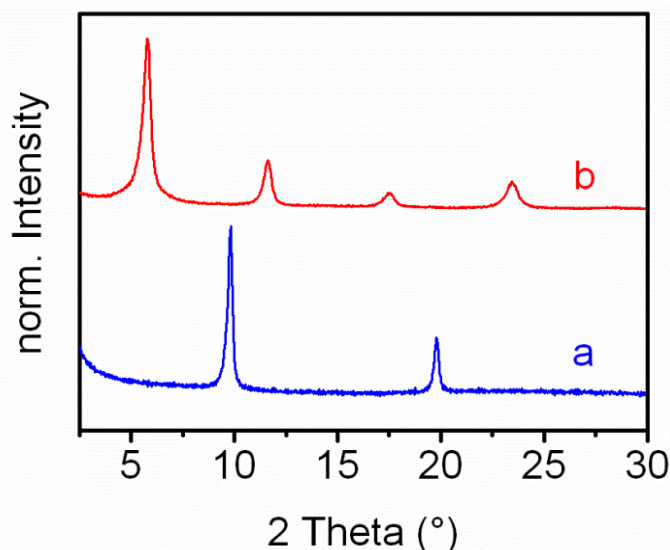


Figure 4. XRD patterns of (a) NO_3^- -LDH and (b) LDH-PP

3.5. Solution blending

Neither LDH-PP nor hect-Me formed stable suspensions in THF rather they tended to aggregate. In an attempt to nevertheless achieve the best possible dispersion of the tow clays in the PS matrix, compounding utilizing a three-roll mill was applied. This process is expected to break aggregates by providing shear forces in the highly viscose polymer dispersion. Hence, this will assist in maximizing the specific interface area between the nano-additives and the polymer to get the maximum flame retardancy. The efficiency of three-roll milling on breaking aggregates was followed by measuring the particle size distributions (PSDs) as determined for diluted samples after 0, 2, 4, and 6 cycles of three-roll milling. Prior to three-roll milling, aggregates of $\approx 20 \mu\text{m}$ and $\approx 8 \mu\text{m}$ were dominating for PS suspensions with hect-Me and LDH-PP, respectively (Figure 5). The shear forces provided by three-roll mill resulted in a shift of the PSDs towards smaller particle size and after the final cycle maxima of $\approx 8 \mu\text{m}$ and $\approx 5 \mu\text{m}$ were obtained, for hect-Me and LDH-PP, respectively. These PSD are comparable to the PSDs observed for hydrous suspensions of K-hect $\approx 7 \mu\text{m}$ and of LDH $\approx 6 \mu\text{m}$ (Figure SI-1).

Consequently, by means of PSD, it can be concluded that three-roll mill provides sufficient shear forces to establish a decent dispersion of these clays in the PS matrix.

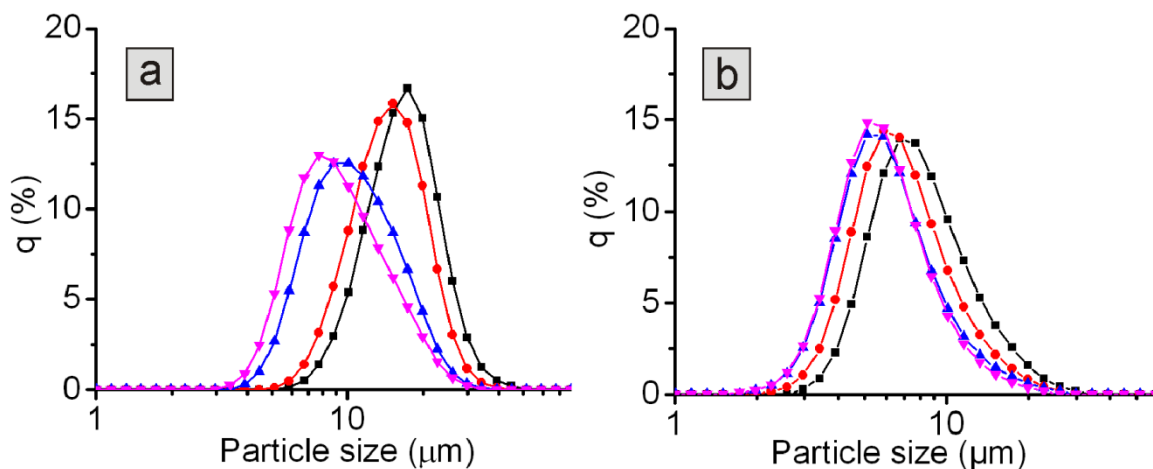


Figure 5. Particle size distributions of (a) PS/hect-Me and (b) PS/LDH-PP after increasing number of cycles of three-roll milling (■) 0 (●) 2 (▲) 4, and (▼) 6. All measurements were done in THF suspension.

PSDs were also recorded for PS/nano-additives suspensions containing a combination of hect-Me and LDH-PP (Figure 6). The PSDs are pronouncedly different than a superposition of the two PSDs of the suspensions containing only a singular nano-additive. Additional aggregation is actually expected because the two types of clays have surface charges of opposite sign and heterocoagulation will be triggered. As a consequence, a very broad PSD with a maximum $\approx 18 \mu\text{m}$ was recorded prior to three-roll milling.

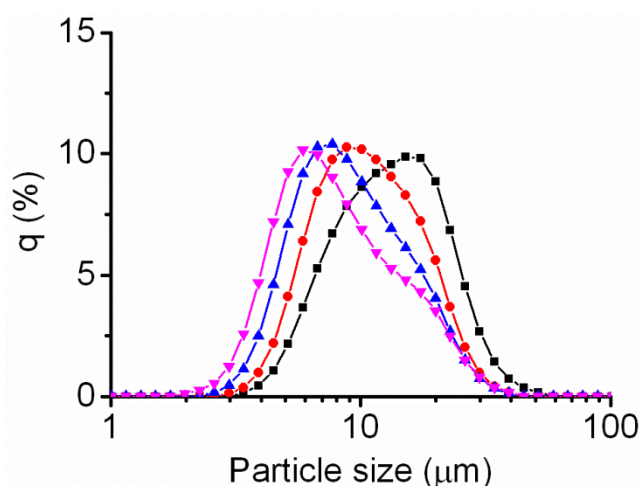


Figure 6. Particle size distributions of PS/LDH-PP/hect-Me after increasing number of cycles of three-roll milling (■) 0 (●) 2 (▲) 4, and (▼) 6. All measurements were done in THF suspension.

But again, a large portion of the aggregates were destroyed upon mechanical agitation as indicated by a shift of the maxima of PSDs towards smaller particle size ($\approx 6 \mu\text{m}$) after the

final cycle of three-roll milling. Nevertheless, the shear forces provided were insufficient to break all aggregates and a bimodal distribution was obtained with a small fraction of $\approx 20 \mu\text{m}$ remaining.

Clearly, the dispersion efficiency of these clays is still sub-optimal as indicated by TEM images (Figure 7). Neither the singular nor the combined nano-additives are dispersed as single platelets rather aggregates persist in the final composite. This is somewhat surprising since the PSDs measured for the singular component systems indicated good dispersion. In the case of K-lect parallel arrangements of the platelets forming band-like structures dominate while for LDH-PP the rose-like aggregates produced in the synthesis persist in the nanocomposites. In any case, the aggregation will reduce the specific interface area between the nano-additives and the PS matrix.

On one hand, based on previous experience this will limit the achievable of the best FR effect [7]. On the other hand, it leaves room for further optimization in future work. Furthermore, despite the aggregation, the nano-additives are homogeneously distributed in the polymer matrix.

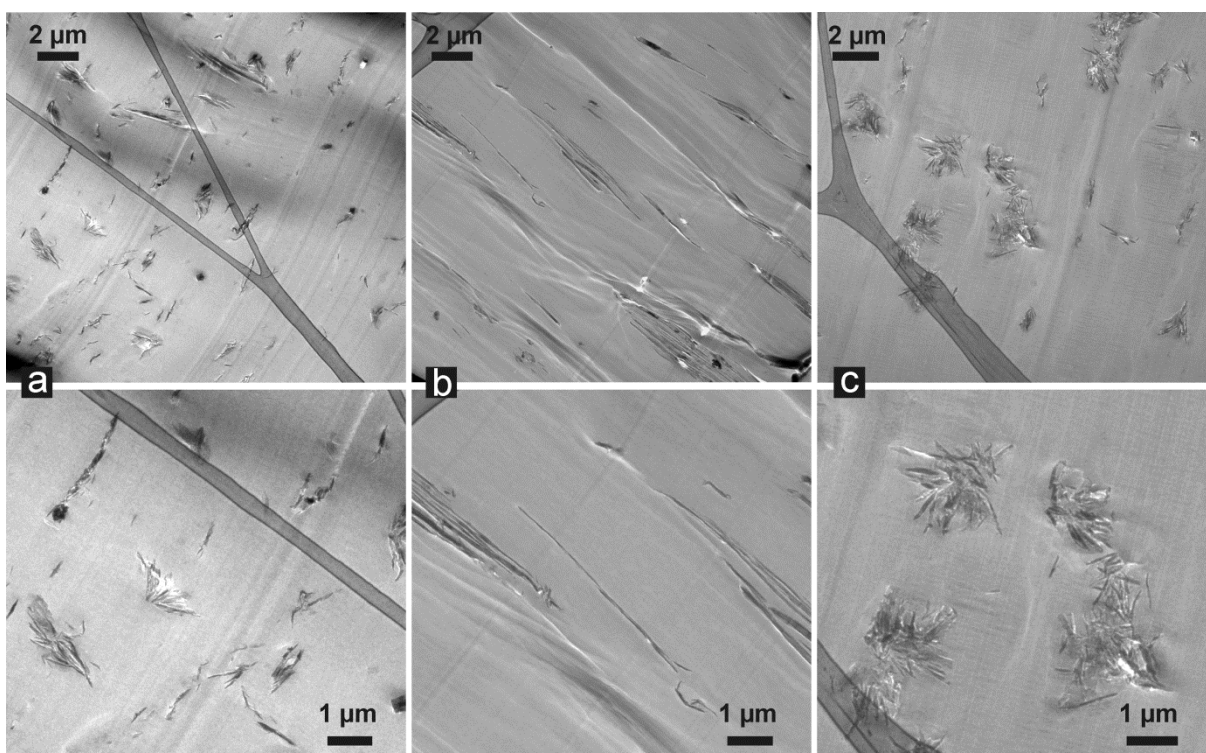


Figure 7. TEM images of PS nanocomposites with (a) LDH-PP/hect-Me, (b) hect-Me, and (c) LDH-PP

3.6. Thermal properties and flammability test

The thermal properties were determined by a thermogravimetric analysis under N₂ atmosphere. Table I and Figure 8 show TGA data of PS nanocomposites where T_{0.1} and T_{0.5} represent the temperatures at 10 % and 50 % mass loss, respectively.

For PS/LDH-PP and PS/hect-Me, T_{0.1} and T_{0.5} were both shifted towards higher temperature by ≈ 37 °C and ≈ 42 °C, respectively. The shifts confirmed the enhanced thermal stability of the prepared PS nanocomposites. Interestingly, an even larger shift by 46 °C was observed for PS/LDH-PP-/hect-Me

Table I. TGA data for PS nanocomposites

<i>Formulation</i>	<i>T_{0.1} (°C)</i>	<i>T_{0.5} (°C)</i>
PS	366	390
PS/LDH-PP	403	433
PS/hect-Me	402	432
PS/LDH-PP-/hect-Me	403	436

This could be seen as a first indicator of synergism between the two clays. The recorded shifts observed for our PS nanocomposites are significantly higher than results reported in the literature (typically 20-30 °C [18], some see no enhancement at all [9]).

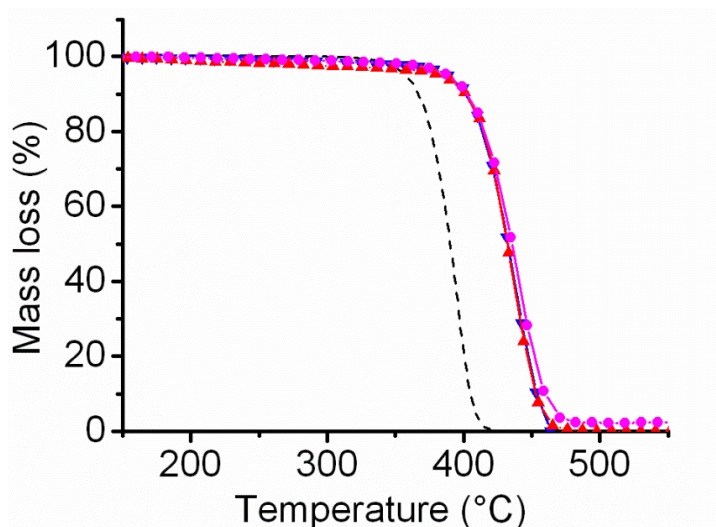


Figure 8. TGA of (---) PS, (\blacktriangledown) PS/LDH-PP, (\blacktriangle) PS/hect-Me, and (\bullet) PS/LDH-PP/hect-Me

We suggest that the modifiers, Me and PP with $T_{0.1}$ of 322 °C and 400 °C, respectively, (TGA shown in Figure SI-3) passed on their thermal stability to the nanocomposites.

Cone calorimeter analysis is one of the most meaningful methods to evaluate the flammability of polymer composite materials. It requires a relatively small sample size, short time, and provides a wide range of key data, which allow a deeper understanding of the mechanism of flame retardancy. These data include time to ignition (t_{ig}), the heat release rate (HRR) and its peak of heat release rate (PHRR), the total heat release (THR), and burn out time. An ideal FR should decrease PHRR and THR, while increasing t_{ig} and burn out time.

Table II summarizes the cone data for PS nanocomposite, while the HRR curves obtained at a heat flux of 35 kW/m² are shown in Figure 9.

Table II. Cone calorimeter data for PS nanocomposites

<i>Formulation</i>	<i>PHRR</i> (kW/m ²)	<i>PHRR</i> <i>Reduct. (%)</i>	<i>THR</i> (MJ/m ²)	<i>t_{ig}</i> (s)
PS	813 ± 29	-	138 ± 2	88 ± 3
PS/LDH-PP	467 ± 11	43	132 ± 1	70 ± 2
PS/hect-Me	491 ± 18	40	126 ± 4	61 ± 3
PS/LDH-PP/hect-Me	398 ± 13	51	131 ± 2	66 ± 1

The flame retardancy of LDH was commonly related to the endothermic degradation and dilution of volatiles by inert gases. Besides, the residual metal oxide forms a protective ceramic-like layer that acts as barrier for mass and heat transfer [2]. For PS/LDH-PP, an additional FR effect is expected to be provided by means of PP, which generally includes endothermic degradation and radical quenching. Moreover, a homogeneous distribution of LDH platelets in the polymer matrix leads logically to a homogeneous distribution of PP. The sum of these effects may explain the enhanced flame retardancy indicated by a reduction of PHRR of 43 % at 5 wt% loading. This synergism between LDH and PP is significant as compared to related results described in the literature. Wang et al. [18] also prepared PS nanocomposite with LDH intercalated with bis-(2-ethylhexyl) phosphate. At 5 wt % loading, reductions of PHRR of 33 % and 6 % were obtained for melt blending and bulk polymerization, respectively. Nyambo et al. [9] observed a synergistic effect between LDH and ammonium polyphosphate when combined in a PS matrix via melt blending.

They recorded a reduction of PHRR of 25 % at 5 wt% loading, while a reduction of PHRR of 42 % was recorded, however, at higher 10 wt% loading. Interestingly, they recorded a significant reduction of t_{ign} of around 60 %, while in our case it was reduced by only 20 %. As described in the literature, the thermal decomposition of LDH is closely related to the type of interlayer anion and the layer charge [19]. For instance, thermal stability of NO_3^- -LDH increased by increasing the layer charge and this was attributed to the different orientation of the NO_3^- in the interlayer space. Moreover, grafting of sulfate to LDH resulted in enhanced thermal stability of sulfate-LDH as compared to carbonate-LDH [20]. We therefore speculate that a possible grafting of PP to LDH as a result of evaluated temperature during combustion may also enhance the thermal stability of LDH-PP leading to a significantly smaller reduction of the t_{ign} .

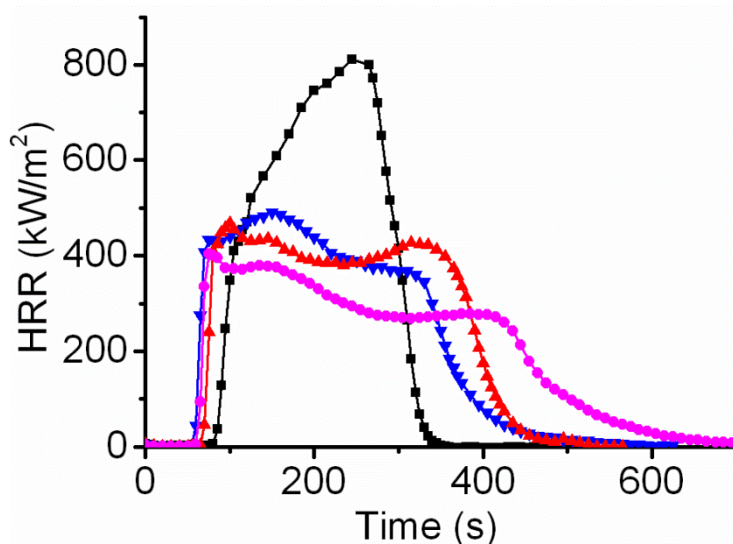


Figure 9. Heat release rate curves for PS nanocomposites with (■) PS (▲) LDH-PP (▼) PS/hect-Me and (●) LDH-PP/hect-Me.

For PS/hect-Me, we observed a reduction of the PHRR of 40 %. Schütz et al. [7] observed a higher reduction of the PHRR of 47 % at 3 wt% loading of PS nanocomposites with K-hect modified with a cationic oligomer ($T_{0.1} = 277$ °C) prepared via solution blending. Please note, that this modification provided a much more stable dispersion but on the expense of a reduced t_{ig} of 35 % as compared to 30% observed with melaminium modification. The more efficient interface management succeeded in preserving the effective aspect ratio of K-hect and thus increased the specific interface area. The formation of band-like aggregates as observed by the TEM likely contributed to deterioration of FR in the final nanocomposite. Moreover, some discrepancy might be due to the fact that the HRR were recorded on different cone calorimeters.

Most interestingly, the maximum reduction of PHRR of 51 % was obtained by PS/LDH-PP/hect-Me. This reduction is much higher ($\approx 10\%$) as compared to the reductions observed for both PS nanocomposites with singular clay additives and again corroborates a synergistic effect. This synergism may be explained by the intumescent effect as resulting from the combination of the two organic modifiers; Me and PP. The formation of a protective layer of the clays residual also resulted in a prolonged burn out time which is typical for thick-charring polymer [6]. For similar reductions of the PHRR for PS/LDH nanocomposites, typical loadings of 10 wt % were required [21].

THR curves (Figure 10) corroborate the formation of a protective layer, where THR spread over longer time as compared to the pristine PS for all Ps nanocomposites. For PS/LDH-PP, at the end of the combustion the entire polymer was consumed. The small reduction of the THR (- 2 %) observed most likely was related to the reduction of the fire load by replacing PS by the LDH rather than being indicative of a passive cooling effect. For PS/LDH-PP/hect-Me, THR showed the most prolonged burn out time indicating the formation of the most effective ceramic/glass-like protective layer. Interestingly, the lowest THR (- 8 %) was nevertheless recorded for PS/hect-Me. This reduction could be explained by promotion of char formation by the hectorite that lead to an incomplete combustion of the polymer and the conversion of a portion of the polymer to residual char.

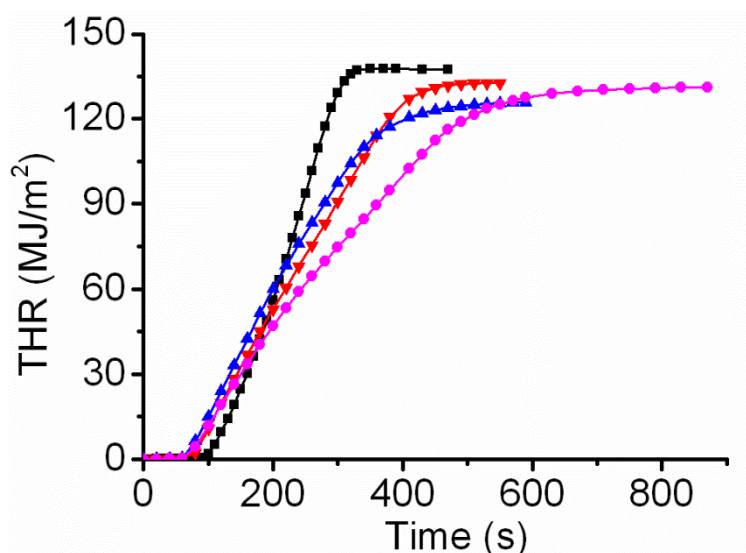


Figure 10. Total heat release curves for PS nanocomposites with (■) PS (▼) LDH-PP (▲) hect-Me (●) LDH-PP/hect-Me

Figure 11 shows the residual char subsequent to the cone calorimeter analysis. For all samples, carbonaceous char was obtained. The PS/LDH-PP (Figure 11.a) resulted in much more carbonaceous char as compared to typical LDH filler [15].

The formation of the char could be explained by the presence of PP, which is already known as a char-promoting agent. Moreover, a small intumescent effect can also be observed which is in line with the fact that more char was formed. The char acts as barrier for H₂O released upon degradation of LDH resulting in an expansion of the char layer. For PS/hect-Me (Figure 11.b), a cracked char surface was observed. Since for composites based on K-hect modified with a cationic oligomer no cracks were observed, this again is in line with an inferior dispersion of the hectorite platelets with melaminium modification.

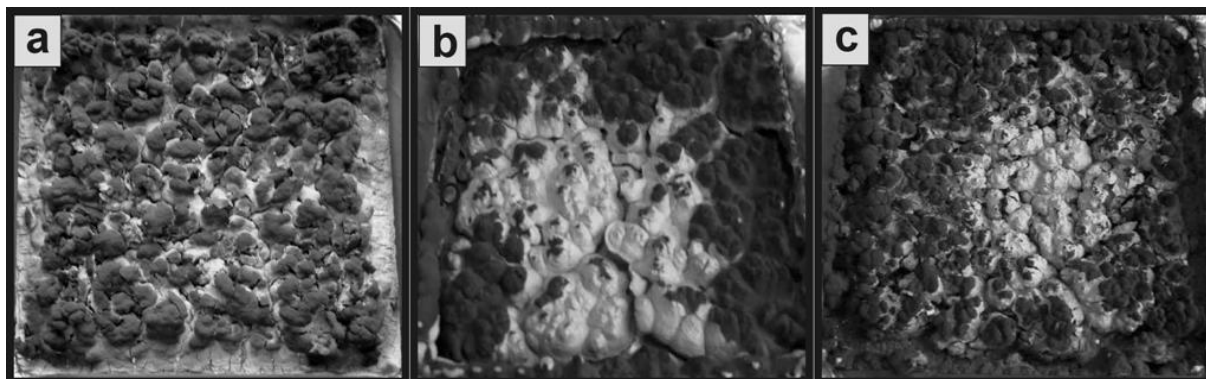


Figure 11. Photographs represent a comparison between the residues of the cone test of (a) PS/LDH-PP (b) PS/Hec-Me and (c) PS/LDH-PP/Hec-Me

For PS/LDH-PP/hect-Me (Figure 11.b) a more compact char can be observed with a small intumescent effect. This intumescent effect resulted in some expansion of the char layer, caused by an effective barrier provided by both clays to the permeation of flammable gases.

4. Conclusion

A multi-component FR system was tested using a combination of two synthetic clays; LDH and high- α K-hect. The intrinsic ion exchange properties of these nano-additives were employed for organophilization with thermally stable molecular FRs.

As clear synergistic effect was observed by combining LDH-PP and hect-Me: With cone calorimetry a reduction of PHRR of 51 % at low loadings of 5 wt% was recorded. Interestingly, for the combined FR, a slight intumescent effect was obtained as result of the effect provided by Me and PP.

Despite organophilization, however, we failed to achieve stable suspensions in THF. Aggregates observed in the TEM images, clearly suggest that the specific interface area between matrix and nano-additives is by far not maximized. Further work is needed to optimize the stability of these clays in organic solvents and by this maximize the flame

retardancy. For the combined clay system the problem is even worsened because aggregation was pushed by heterocoagulation between the two types of clays that carry surface charges of opposite sign. Organophilization should be done in a way to reverse the surface charge of one component to circumvent this problem.

While the maximum reduction of the PHRR of 51 % obtained by PS/LDH-PP/hect-Me is among the best results reported, there is obviously room for future optimization.

Acknowledgments

B. D-B. acknowledges the German Academic Exchange Service (DAAD) for financial support. This work was further supported by the Deutsche Forschungsgemeinschaft (DFG) within the Collaborative Research Center (SFB 840).

References

- [1.] Gordon LN, Alexander BM, Charles AW. Fire Retardancy in 2012, editors. Fire and Polymers VI: New Advances in Flame Retardant Chemistry and Science, American Chemical Society, Washington, DC, 2012, pp. 1-13.
- [2.] Matusinovic Z, Wilkie CA. J Mater Chem 2012;22(36):18701-18704.
- [3.] Schütz MR, Kalo H, Lunkenbein T, Breu J, Wilkie CA. Polymer 2011;52(15):3288-3294.
- [4.] Gilman, J. W. Flame Retardant Mechanism of Polymer-Clay Nanocomposites, Morgan AB, Wilkie CA editors. Flame Retardant Polymer Nanocomposites, John Wiley & Sons, Inc., Hoboken, NJ, USA, 2006, pp. 67-88.
- [5.] Bourbigot S, Duquesne S. J Mater Chem 2007;17(22):2283-2300.
- [6.] Edward DW, Sergei VL. Overview of Modes of Action and Interaction of Flame Retardants., editors. Flame Retardants for Plastics and Textiles, Carl Hanser Verlag GmbH & Co. KG, Munich, 2009, pp. 241-251.
- [7.] Schütz MR, Kalo H, Lunkenbein T, Groschel AH, Muller AHE, Wilkie CA, Breu J. J Mater Chem 2011;21(32):12110-12116.
- [8.] Edward DW, Sergei VL. Flame Retardants in Commercial Use or Development for Polyolefins., editors. Flame Retardants for Plastics and Textiles, Carl Hanser Verlag GmbH & Co. KG, Munich, 2009, pp. 3-34.

- [9.] Nyambo C, Kandare E, Wang D, Wilkie CA. *Polym Deg Stab* 2008;93(9):1656-1663.
- [10.] Inayat A, Klumpp M, Schwieger W. *Appl Clay Sci* 2011;51(4):452-459.
- [11.] Costantino U, Marmottini F, Nocchetti M, Vivani R. *Eur J Inorg Chem* 1998;1998(10):1439-1446.
- [12.] Ziadeh M, Chwalka B, Kalo H, Schütz MR, Breu J. *Clay Miner* 2012;47(3):341-353.
- [13.] Kalo H, Möller MW, Ziadeh M, Dolejs D, Breu J. *Appl Clay Sci* 2010;48(1-2):39-45.
- [14.] De Ridder DJA, Goubitz K, Brodski V, Peschar R, Schenk H. *Helv Chim Acta* 2004;87(7):1894-1905.
- [15.] Diar-Bakerly B, Beyer G, Schobert R, Breu J. Significance of Aspect Ratio on Efficiency of Layered Double Hydroxide Flame Retardants. In: Morgan AB, Wilkie CA, Nelson GL, editors. *Fire and Polymers VI: New Advances in Flame Retardant Chemistry and Science* American Chemical Society, Washington, DC, 2012, pp. 407-425.
- [16.] Forano C, Hibino T, Leroux F, Taviot-Gueho C. Chapter 13.1 Layered Double Hydroxides. In: Faiza Bergaya BKG, editors. *Developments in Clay Science Handbook of Clay Science* Elsevier, Amsterdam, 2006, pp. 1021-1095.
- [17.] Burton AW, Ong K, Rea T, Chan IY. *Microporous and Mesoporous Mater* 2009;117(1-2):75-90.
- [18.] Wang L, Su S, Chen D, Wilkie CA. *Polym Deg Stab* 2009;94(5):770-781.
- [19.] Xu ZP, Zeng HC. *Chem Mater* 2001;13(12):4564-4572.
- [20.] Constantino VRL, Pinnavaia TJ. *Inorg Chem* 1995;34(4):883-892.
- [21.] Nyambo C, Songtipya P, Manias E, Jimenez-Gasco MM, Wilkie CA. *J Mater Chem* 2008;18(40):4827-4838.

Appendix 4: Multi-Component Flame Retardants: Combining Anionic and Cationic Clays as Trojan Horses for Molecular Flame Retardants

Bashar Diar-Bakerly¹, Josef Hausner¹, Hussein Kalo¹, Andreas Edenharter¹, Mazen Ziadeh¹,
Günter Beyer², Josef Breu^{1,*}

¹) Department of Inorganic Chemistry I, University of Bayreuth, Universitaetsstr. 30, 95447
Bayreuth, Germany

²) Kabelwerk Eupen AG, 4700 Eupen, Belgium

Corresponding author: Prof. Dr. Josef Breu, Universitaetsstr. 30, 95440 Bayreuth, Germany

* E-mail: josef.breu@uni-bayreuth.de

Supplementary Information (SI)

1. AEC of LDHs

The general formula of LDH is: $[M(II)_{1-x} M(III)_x (OH)_2]^{x+} [A^{n-}_{x/n}]^{x-} \cdot mH_2O$, where M(II) and M(III) are divalent and trivalent metal cations, respectively, A^{n-} is the charge balancing interlayer anion, while x is the stoichiometric value of the trivalent cation (0.2 x 0.33) and m refers to the number of interlayer water molecules.

The anion exchange capacity is given as:

$AEC = (x/M_w) \times 105$ (meq/100g), where M_w is the weight of the chemical formula for each octahedral unit [1].

$Mg_2Al(OH)_6(NO_3) \cdot 1.8H_2O$; $M_w = 278$ g/mol and $x = 1$, hence, $AEC = 360$ meq/100 g.

2. Particle size distribution of LDH and hectorite in hydrous suspensions (Figure SI-1)

In water for K-lect a narrow PSD is observed with a maximum of $\approx 7 \mu m$. Conversely, hydrous suspensions of LDH show a wide PSD between 2-10 μm with a maximum of $\approx 6 \mu m$.

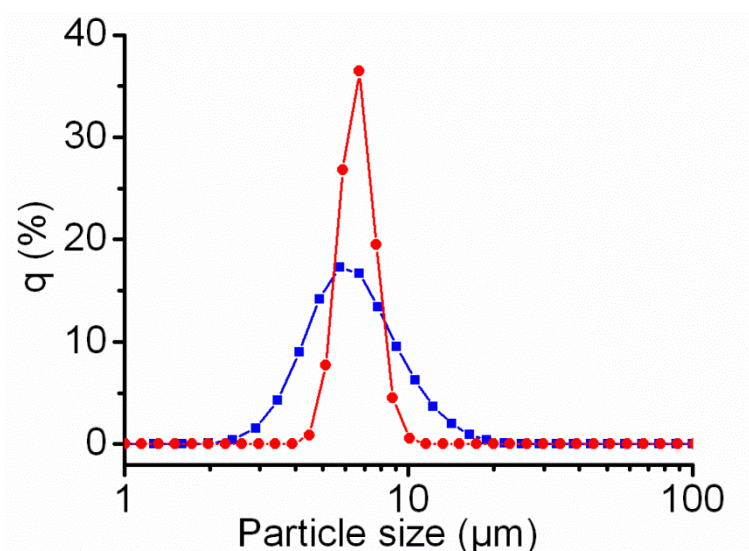


Figure SI-1. Particle size distributions in aqueous suspensions of (■) LDH and (●) K-hect.

3. Success of Selective modification of the external basal surfaces of K-hect (Figure SI-2)

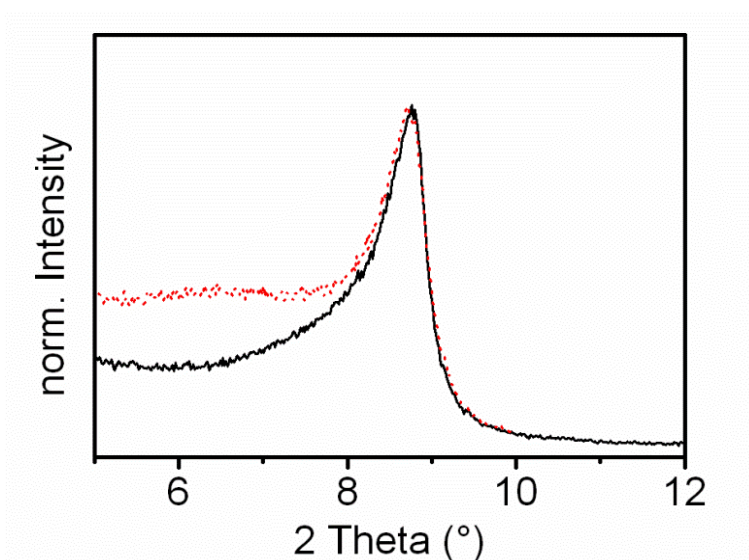


Figure SI-2. XRD patterns of K-hect (—) and hect-Me (…)

4. Thermal stability of the salt of organic ions used for functionalization (Figure SI-3)

The mass loss of ≈ 13 wt% for Na_2PP at 100 °C is corresponding to the loss of structural water molecules that represent ≈ 14 % of the M_w (254.2 g/mol with two water molecules) of the hydrated salt. Therefore, for the calculation of $T_{0.1}$ the baseline reached after the water loss was taken yielding a $T_{0.1}$ of 400 °C.

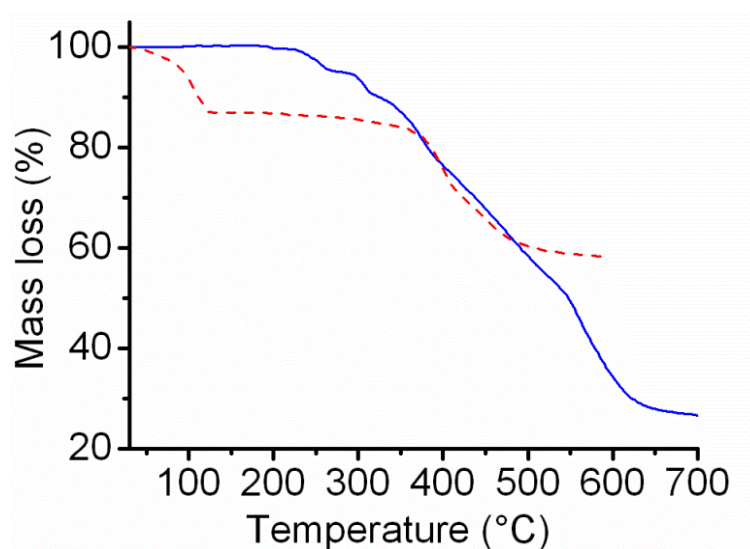


Figure SI-3. TGA curves of (—) melamine ortho phosphate and (---) phenyl phosphates disodium salts

Reference

[1.] Forano C, Hibino T, Leroux F, Taviot-Gueho C. Chapter 13.1 Layered Double Hydroxides, Faiza Bergaya BKG, editors. Developments in Clay Science Handbook of Clay Science, Elsevier: Amsterdam, 2006, pp. 1021-1095.

6. List of publications/manuscripts

6.1. Publications/manuscripts

Diar-Bakerly, B.; Beyer, G.; Schobert, R.; Breu, J. *Significance of Aspect Ratio on Efficiency of Layered Double Hydroxide Flame Retardants*. American Chemical Society Symposium Series, **2012**, Chapter 26, 407 - 425.

Diar-Bakerly, B.; Hirsemann, D.; Kalo, H.; Schobert, R.; Breu, J. *Modification of Kaolinite by Grafting of Siderophilic Ligands to the External Octahedral Surface*. Applied Clays Science, Submitted, **2013**.

Diar-Bakerly, B.; Feicht, P.; Edenharter, A.; Beyer, G.; Breu, J. *Superior Flame Retardant by Combining High Aspect Ratio Layered Double Hydroxide and Graphene Oxide*. To be submitted, **2013**.

Diar-Bakerly, B.; Hausner, J.; Kalo, H.; Edenharter, A.; Ziadeh, M.; Beyer, G.; Breu, J. *Multi-Component Flame Retardants: Combining Anionic and Cationic Clays as Trojan Horses for Molecular Flame Retardants*. To be submitted, **2013**.

Further publication

Hirsemann, D.; Shylesh, S.; deSouza, R.; Diar-Bakerly, B.; Biersack, B.; Mueller, D.N.; Martin, M.; Schobert, R.; Breu, J. *Large-scale, Low-cost Fabrication of Janus-type Emulsifiers by Selective Decoration of Natural Kaolinite Platelets*. Angewandte Chemie International Edition, **2011**, 51, 1348 - 1352.

6.2. Conferences

2011: 16th International symposium on intercalation compounds.

Seč-Ústupy - Czech Republic.

2012: 24th Annual conference: Recent advances in flame retardancy of polymeric materials.

Stamford - United States of America.

2013: 14th European meeting on fire retardancy and protection of materials.

Lille - France.

7. Acknowledgment

I would like to thank my supervisor Prof. Dr. Josef Breu for giving me the opportunity to join his research group, for encouraging me when things went wrong, and for his support and guidance during the course of this research, not only regarding the scientific level but also the personal level.

During my academic study period I was lucky to meet many people who helped me in different ways, in particular my previous coworkers; Dr. Michael Schütz and Dr. Dunja Hirsemann for their patience and guidance that facilitated me a smooth start in the research.

I would like to extend my thanks to the entire ACI group, especially; Dr. Hussien Kalo, Andreas Edenharter, Matthias Stöter, Mazen Ziadeh, Patrick Feicht, Josef Hausner, Sebastian Koch, Thomas Martin, Martin Schieder, Manuela Stirner, and Jasmin Schmid.

My sincere gratitude goes to Dr. Wolfgang Milius for all the scientific discussions whenever I needed.

The technical staff, in particular Lena Geiling, did so many measurements included in this thesis, so I would like to thank all of them. Also many thanks go to the secretaries of the ACI department; Iris Raithel and Petra Seidler.

I would also like to express my thanks to my professors back home at the University of Aleppo; Ousama Dabbit and all my colleges there.

My great appreciation goes also to Dr. Günter Beyer for doing all the cone measurements and for his support and time for scientific discussions and to Prof. Dr. Rainer Schobert for the scientific discussions regarding the organic modifiers.

I would like to convey thanks to the German Academic Exchange Service (Deutscher Akademischer Austausch Dienst; DAAD) for sponsoring my graduate studies, and the international office members of the University of Bayreuth represented by Dr. Arnim Heinemann and Fakhra Heinrich.

Finally, I want to express my gratitude to my family for the support and encouragement. I am grateful for the endless love and support I received from my parents, my sister, my brother, and my girlfriend.

8. Declaration – Erklärung

Hiermit erkläre ich, dass keine Tatsachen vorliegen, die mich nach den gesetzlichen Bestimmungen über die Führung akademischer Grade zur Führung eines Doktorgrades unwürdig erscheinen lassen.

Hiermit erkläre ich mich damit einverstanden, dass die elektronische Fassung meiner Dissertation unter Wahrung meiner Urheberrechte und des Datenschutzes einer gesonderten Überprüfung hinsichtlich der eigenständigen Anfertigung der Dissertation unterzogen werden kann.

Hiermit erkläre ich eidesstattlich, dass ich die Dissertation selbstständig verfasst und keine anderen als die von mir angegebenen Quellen und Hilfsmittel benutzt habe.

Ich habe die Dissertation nicht bereits zur Erlangung eines akademischen Grades anderweitig eingereicht und habe auch nicht bereits diese oder eine gleichartige Doktorprüfung endgültig nicht bestanden.

Hiermit erkläre ich, dass ich keine Hilfe von gewerblichen Promotionsberatern bzw. –vermittlern in Anspruch genommen habe und auch künftig nicht nehmen werde.

Bayreuth, 09.10.2013,

Ort, Datum, Unterschrift